Experimental and Theoretical Investigations of the Dielectric Barrier Electrospray in Respect to μ-Chip Development

Faculty of Electrical Engineering and Information Technology
Technical University of Dortmund

Dissertation

submitted to meet the requirements

for obtaining the Doctor of Engineering academic degree

by

M.Sc. Irina Reginskaya

Tag der mündlichen Prüfung: 05. September 2013

1. Gutachter: Prof. Dr.-Ing. Andreas Neyer

2. Gutachter: PD. Dr. Joachim Franzke

Dortmund 2013

Abstract

The electrospray ionization source is an interface between the separation techniques and mass spectrometry. With the help of electrospray the analyte ions of the liquid phase are transferred to the gas phase, which is necessary for the mass spectrometry detection method. The spraying of the analyte occurs in the high electric field applied between the emitter tip and mass spectrometer inlet.

In the conventional electrospray the high electric field is produced by the application of the high potential to the analyte with a direct contact electrode. In an alternative method the high potential is applied to the analyte through a thin dielectric barrier. The displacement current in the dielectric material is utilized to transfer the charge to the analyte.

The goal of current research is the further development by DB-ESI source, the detailed analysis of advantages of the ionization technique and possible issues comparing to the conventional electrospray ionization systems.

The electrospray formation process is investigated with the experimental work and physical modeling. The effects discovered in the DB-ESI capillary system allow the optimization of the electrospray system parameters for the effective control and improvement of the mass spectrometer absolute signal intensity.

The DB-ESI source integration in a μ-Chip is demonstrated. In contrast to the common nozzle-type emitter shapes, the electrospray out of the flat-surface outlet is discussed. The proposed μ-Chip structure opens vast opportunities for further development, including the manufacturing of the μ-Chips with multiple channels and emitters.

The DB-ESI technique has been successfully integrated in the multiple-emitter electrospray system. The usage of the DB-ESI technique in combination with the multiple-emitter system shows significant improvement of the electrospray ionization efficiency.

Contents

Abstract....3
Contents....5
List of abbreviations....9
List of Symbols....11
Introduction....13

Chapter 1 Electrospray Technique as an Ion Source for Mass Spectrometry....19

1.1. Ionization sources in mass spectrometry....19
1.2. Electrospray history background....23
1.3. Basic principles of the electrospray ionization process....25
1.4. Electrospray as an electrolytic cell....28
1.5. Problems and assumptions of the electrospray ionization....30
1.6. Conclusions....34

Chapter 2 Effects of Various Electrolyte and Capillary Properties in Dielectric Barrier Electrospray Ionization....37

2.1. Motivation....37
2.2. Experimental setup general description....37
2.2.1. Setup components....38
2.3. Charge transfer process in the capillary system....39
2.3.1. Experimental setup and chemicals....39
2.3.2. Physical mechanism of charge transfer....40
2.3.3. EMT signal....41
2.3.4. Ion current signal....42
2.4. Parameter influence on charge transfer process....47
2.4.1. Applied voltage amplitude....47
2.4.2. Electrolyte concentration and ion properties....48
2.5. Conclusions....55

Chapter 3 DB-ESI Electric Model....57

3.1. Introduction....57
3.2. Principles and assumptions in the model....58

3.3. Basic elements calculation....58
3.3.1. Capillary unit length....59
3.3.2. Displacement current in injection electrode....62
3.3.3. Emitter geometry and counter electrode....62
3.4. Closed emitter model....63
3.4.1. Ion current in the capillary system....64
3.4.2. Charge and potential formation at the emitter tip....65
3.4.3. Model and experiment results comparison....67
3.4.4. Supply capillary influence on potential formation....68
3.5. ESI – DC voltage-current characteristic....69
3.5.1. Measurement of electrospray voltage-current characteristic....69
3.5.2. Consideration of voltage drop at electrolyte resistance....72
3.6. Final DB – ESI model 73
3.6.1. Current source implementation in the circuit model....73
3.6.2. Potential formation in the system with the electrospray....76
3.6.3. Model and experiment results comparison....79
3.7. DB-ESI-MS: the signal intensity control....82
3.7.1. Model-based optimizations of the DB-ESI setup....82
3.7.2. Positive and negative ions generation for MS analysis....83
3.7.3. Experimental investigation of triggering effectiveness....84
3.8. Conclusions....89
Chapter 4 Electrospray μ-Chip Development....91
4.1. Introduction....91
4.2. Available approaches for electrospray μ-Chips manufacturing....91
4.2.1. Capillary outlet as electrospray emitter....92
4.2.2. Nozzle-type emitter formation techniques....92
4.2.3. Flat-surface emitter formation techniques....94
4.2.4. Improvement of PDMS hydrophobic properties....95
4.2.4.1.PDMS surface with specific roughness pattern....96
4.2.4.2.High-temperature processing of PDMS surfaces....97
4.3. DB-ESI μ-Chip development....98
4.3.1. μ-Chip structure....98
4.3.2. Glass base with coupling electrode....99
4.3.3. PDMS casting for the structure formation....100
4.3.4. Simple top structure with the mechanically formed channel ….100

4.3.5. Advanced top structure with wafer-casting channel formation…102
4.3.5.1.The master wafer mask design.....103
4.3.5.2.Master wafer manufacturing.....103
4.3.5.3.Thin PDMS film as a dielectric barrier.....107
4.3.5.4.Thin film manufacturing using the spin-coating procedure.....108
4.3.5.5.Plasma surface activation.....109
4.3.5.6.Assembly of the top structure.....109
4.3.6. Final μ-Chip assembling procedure.....110
4.3.6.1.Capillaries connection.....111
4.3.6.2.Nozzle formation.....112
4.4. DB-ESI μ-Chip characterization.....112
4.4.1. DB-ESI μ-Chip with the mechanically – formed channel 113
4.4.2. DB-ESI μ-Chip with wafer-casting based rectangle channels.....114
4.5. Conclusions.....118
Chapter 5 DB-ESI application for multiple-emitter systems.....121
5.1. Free-flow electrophoresis.....121
5.2. Multi-nozzle emitters.....122
5.3. Effects of nozzle interaction.....123
5.4. Experimental validation of multiple-emitter DB-ES system.....124
5.5. Analytical application example.....127
5.6. Conclusions.....129
Conclusions.....131
Literature.....137
Acknowledgments.....142

List of abbreviations

AA	acetic acid
APCI	atmospheric pressure chemical ionization
CI	chemical ionization
CRM	charge residue model
DB	dielectric barrier
DB	dielectric barrier
DB-ESI	dielectric barrier electrospray ionization
DC	direct current
EI	electron ionization
EMT	electromagnetic transfer signal
ESI	electrospray ionization
FA	formic acid
FAB	fast atom bombarding
HPLC	high-performance liquid chromatography
HV	high voltage
IC	ion current
IEM	ion evaporation model
LTQ	linear trap quadrupole
MALDI	matrix-assisted laser desorption ionization
MS	mass spectrometer
OsA	octansulfonic acid
PA	propionic acid
PDMS	polydimethylsiloxan
QIT	quadrupole ion trap
RSD	relative standard deviation
TIC	total intensity current
TTL	transistor-transistor logic

List of Symbols

$[A_-]$	concentration of completely dissociated cations, $mol \cdot L^{-1}$
$[HA]$, $[HA]_{AA}$	concentration of non-dissociated ions in the solution, $mol \cdot L^{-1}$
a	inner capillary diameter, m
A	area of internal cross section of the capillary, m^2
C_{CPL}	coupling electrode capacitance, F
C_{H+}	concentration of completely dissociated ions, $mol \cdot L^{-1}$
C_{LOAD}	load capacitance, F
C_m	capacitance of the cylindrical capacitor, F
C_{TIP}	capacitance of the capillary at the tip, F
C_{unit}	self capacitance of the capillary unit, F
d	distance from the emitter tip to the counter electrode, m
D	diffusion coefficient, $m^2 \cdot s^{-1}$
E	electric field, $V \cdot m^{-1}$
E_{ES}	electric field at the emitter (capillary) tip, $V \cdot m^{-1}$
f	friction coefficient
I	current, A
I_{ES}, i_{ES}	electrospray current, A
j	current density, A/m^2
$[H^+]$	concentration of completely dissociated anions, $mol \cdot L^{-1}$
K_S	dissociation constant
l	length, m
L_m	capillary length under the metal layer, m
M	molar mass
M_0	neutral molecule
M^+	positive ion
$n-$, $n+$	concentration of charges
$_pK_S$	logarithmic constant
$q-$, $q+$	unit charges if the charge carries, Q
Q_R	droplet charge, C
R	droplet radius, m

R_1	outer capillary radius, m
r, R_2	inner capillary radius, m
R_{CPL}	coupling electrode resistance, Ω
R_H	stokes radius, m
R_{LOAD}	load resistance, Ω
R_S	solution resistance, Ω
R_{TIP}	resistance of the capillary at the emitter tip, Ω
R_{unit}	capillary unit resistance, Ω
T	absolute temperature, K
U	voltage, V
U_{APP}, U_{APP_DC}	applied voltage, V
U_{CE}	electrochemical contact voltage, V
U_{CN}	charge neutralization voltage at the counter electrode, V
U_{GAP}	gap voltage, V
V	volume, L
V_{ES-}	minimum potential value required for electrospray, V
V_{ES+}	minimum potential value required for electrospray, V
V_{INT}	potential under the coupling electrode, V
V_{ON}	required electric potential to electrospray, V
V_{TIP}	potential at the emitter tip, V
γ	liquid surface tension, $N \cdot m^{-1}$
ε_r	dielectric constant
μ_-, μ_+	Mobility, $m^2 \cdot V^{-1} \cdot s$
ν_-, ν_+	drift velocities, $m \cdot s^{-1}$
ν_f	volumetric flow rate, $m^3 \cdot s^{-1}$
ρ	resistivity, Ω·m
σ, σ_n	electrolyte conductivity, $S \cdot m^{-1}$

Constants

e^-	elementary charge, 1.6×10^{-19} C
ε_0	permittivity of free space, 8.854×10^{-12} $C^2 \cdot N^{-1} \cdot m^{-2}$
k_B	Boltzmann constant, 1.38×10^{-23} $m^2 \cdot kg \cdot s^{-2} \cdot K^{-1}$

Introduction

The concept of bridging several different techniques together and combining to yield a device that delivers more than one sum of the individuals lies right at the heart of the micro total analytical system idea. Microchip based separation techniques are essential elements in the development of fully integrated micro total analytical systems, which are envisioned to become powerful instruments for obtaining and assessing analytical data in research, industry and everyday life. For micro analytical systems a good detection method is required, while the low component amount is used for analysis. One of the most versatile detection methods is the mass spectrometry. It is a nearly universal detection method, which offers structural information for identification purposes. This detector type could be beneficial for many microchip systems. However, the most analyzed components are commonly present as solutions, while the mass spectrometer instrument requires gas-phase ions for analysis.

Electrospray ionization source is the interface between separation technique (for example, liquid chromatography) and mass spectrometry. Electrospray is the tool to create an aerosol from the solution. With the electrospray source the liquid analyte is ionized and transferred to the gas phase, which is appropriate for the mass spectrometry detection method. Electrospray ionization technique allows to analyze biological molecules, especially peptides and proteins or other organic molecules. Electrospray ionization have been securely involved in the every day life of analytical laboratories. Other analytical techniques can not provide the same level of detailed information regarding molecular weights and structures from extremely small quantities of the material. The ability to produce highly charged ions and the absence of ion fragmentation are the main advantages of the electrospray technique. A combination of analyte separation and the electrospray ionization is a powerful tool for the analytical proposes.

The electrospray ionization technique utilizes the electric field for the spray formation. The electric field is created by the potential difference between the tip of the electrospray capillary and the mass spectrometer inlet. In the conventional electrospray the high potential is applied directly to the liquid in the capillary. The liquid flow in the capillary is managed by pump, and a small charged liquid droplet is formed at the capillary orifice. This droplet is affected by the strong

electric field, which changes its shape to the cone. The small aerosol droplets are generated from the formed apex of the droplet cone in the direction of the applied electric field. The gas phase ions are produced from the charged liquid droplets and reach the mass spectrometer inlet.

In the conventional electrospray system, the high potential is applied to the liquid with a direct contact electrode. This contact is often achieved by simple metal wire insertion into the capillary. Due to redox reactions at the electrode surface, the gas bubbles formation takes place in the capillary volume. The gas bubbles generated in the capillary volume influence the liquid flow. Alternatively, fused silica capillaries coated with a metal layer either at the tip or the back side to ensure a direct electric contact to the electrolyte solution are used. The electrospray quality depends strongly on the uniformity and stability of this coating layers during the electrospray process. A part of the metal layer, necessary for the electric contact to the analyte solution, is eroded during the electrolysis procedure. This erosion is affected by the kind of electrolyte solution and by the electric current. This leads to the reduction of the electrospray efficiency and life time of the capillaries and hence leads to the signal reduction in the mass spectrometer.

Therefore, it is attractive to have no direct contact to the analyte in order to avoid the electrolysis. An attractive method to omit the direct contact in the electrospray ionization was offered by M. Schilling. This method utilizes the displacement current in the dielectric material to transfer the charges to the analyte in the capillary. The displacement current takes place due to the change of the dipole orientation in the dielectric when the external potential is applied. With this displacement current the charge is transferred to the electrolyte.

The mechanism described above is used to transfer the charge from the external electrode at the outer surface of the fused silica capillary to the electrolyte. The high potential obtained at the capillary tip results in the electrospray. This ionization technique is named “Dielectric Barrier Electrospray Ionization” (DB-ESI). The analytical efficiency of the method was demonstrated by A.-K. Stark.

In the DB-ESI source a series of complex physical and chemical phenomena take place. The goal of current research is the further development of the DB-ESI

source, the detailed analysis of advantages of the ionization technique and possible issues comparing to the conventional electrospray ionization systems.

First, the electrospray formation process must be investigated with the experimental work and physical modeling. The influence of various parameters on the electrospray formation process and, more importantly, on the stability of the output signal, should be investigated in details. The parameters responsible for the formation of stable and high intensity signal in mass spectrometer should be obtained.

Second, the DB-ESI source should be integrated in the microchip (μ-Chip) design. The peculiarities of the electrospray generation using the different μ-Chip configurations must be compared to those of a common electrospray.

In capillary electrophoresis the electrophoretic separation occurs due to the different velocities of the analyte components in the applied electrical field and takes place in one channel. The different analyte components can be detected one by one at the end of the channel. In contrast to the capillary electrophoresis, free flow electrophoresis system uses a chamber, where the hydrodynamic flow of the analyte and electric field created two orthogonally acting vectors. The resulting velocity vector deviates by a specific angle from the flow direction. For different analytes with different size and charge and therefore different electrophoretic mobilities, the angles are different and thus the analytes are separated continuously in a two-dimensional manner at the outlet of the separation chamber. For such kind of a system, the multiple-emitter electrospray systems are necessary. Therefore, the functionality of DB-ESI should be investigated for multiple-emitter systems.

The steps performed to reach the sub-goals and the corresponding results are consistently presented in the five chapters of the current research.

In the first chapter the history of the electrospray development and the physical background of electrospray ionization are presented. The main advantages of the electrospray ionization technique among the other techniques are discussed. The preconditions and limitations of the electrospray ionization are shown. The electrospray ionization method based on the dielectric barrier technique is presented in order to solve the commercial electrospray limitations.

In the second chapter the physical mechanisms behind the DB-ESI are studied in details. The basic DB-ESI capillary setup is presented. The physical mechanism

of the charge transfer process in the capillary volume and the ions behavior under the applied high potential are discussed. The output signal formation in the DB-ESI capillary setup is discussed for different properties of setup components. Various side effects in the DB-ESI capillary system are investigated, and the main factors that influences the output signal formation are discussed based on experimental investigations.

In the third chapter, in order to learn more about the charge transfer process and to study the internal processes in the DB-ESI capillary system, the electrical circuit model of the DB-ESI system is developed. The DB-ESI physical setup is separated to the different components with the unique properties. The main properties of each component and its contribution to the total current formation is discussed. Such electrical model allows analyzing the entire DB-ESI system under different stimuli and conditions and extracting different current components from the output signal. This investigation step helps to manage the output mass spectrometric signal intensity and to improve the signal response using the optimal conditions for the DB-ESI capillary system.

In the fourth chapter the design process of a μ-Chip with the integrated DB-ESI source is presented. Integration of DB-ESI technology in the available manufacturing process of μ-Chips offers significant advantages, since long lasting non contacting electrospray ionization technique and existing separation technologies can be fabricated as powerful combination in a single device. The μ-Chip manufacturing procedure is based on a soft lithography technique in combination with the silicon casting. This combination of techniques presents very attractive results for the μ-Chip channel formation on tens-of-nanometers scale. Significant part of the investigation is devoted to the specific capillary orifice formation procedures. For the stable electrospray signal the smallest surface surrounding the emitter tip is required. The aim can be achieved by the sharp emitter tip creation or with using of the hydrophobic material for the surrounded surface creation. The creation of the the hydrophobic surface surrounding the channel outlet is discussed in the chapter. The verification procedure of the designed μ-Chip is shown, and the stable MS signal comparable to that of an original DB-ESI capillary setup is shown and analyzed.

In the fifth chapter the multiple-emiiter DB-ESI capillary systems and it's advantages and possible issues comparing to single-emitter electrospray sources are discussed. A sample system is assembled and investigated. The issues

occurring due to electrical interaction between the channels, especially at the emitter tips, are shown. The parameters of input signals necessary for successful operation of multiple-emitter system and the corresponding output electrospray signal levels at multiple emitters are shown.

The advanced knowledge on the physical processes in DB-ESI capillary system, the successful implementation of DB-ESI source in a μ-Chip, and the development of a multiple-emitter DB-ESI system opens wide possibilities for further development of electrospray system based on the dielectric barrier technique and it's application for analytical purposes.

Chapter 1 Electrospray Technique as an Ion Source for Mass Spectrometry

1.1. Ionization sources in mass spectrometry

The qualitative and quantitative analysis as well as a structural characterization of ionized molecules can nowadays be performed by mass spectrometry technique. Mass spectrometry is an analytical technique for the determination of molecular weight-to-charge relation of free ions in the high vacuum, which is technically performed with an instrument called a mass spectrometer (MS). A common mass spectrometer device consists of an ion source, a mass analyzer and a detector. These components can be of various types and use various physical mechanisms. The mass analyzer can be a quadrupole, an ion trap or a time of flight (TOF) type. The detector can be an electron multiplier, a microchannel plate detector, a Faraday cup or a scintillation counter [1]. The structure of a common MS device is presented in figure 1.1.

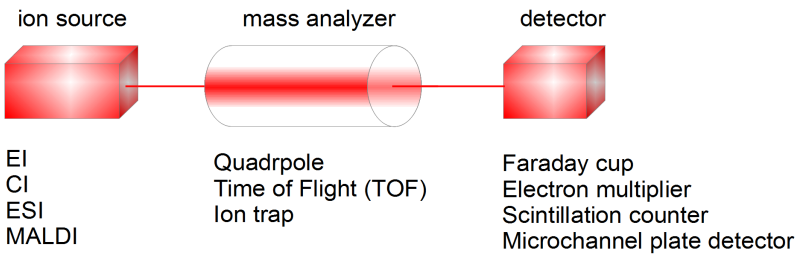

Figure 1.1 Main components of a mass spectrometer (MS): an ion source, a mass analyzer and a detector.

Sample molecules are subjected to ionization in the ionization source. Different source types with different physical ionization methods exist. Among the most common methods, an electron ionization (EI), a chemical ionization (CI), a matrix assisted laser desorption ionization (MALDI), and an electrospray ionization (ESI), can be named. The choice of

the ionization method depends on the nature of the sample and on the type of the required information. Ions are formed in the source, acquire some kinetic energy and leave the source. A calibrated mass analyzer then analyzes the passing ions as a function of their mass to charge ratios (m/z). The detector records either the charge induced or the current produced when an ion passes by.

The oldest and well-studied ionization method for gas molecules is the EI. The EI principle is schematically presented in figure 1.2 a. To prevent the atmospheric gases influence, EI usually takes place in the high vacuum (10^{-4} to 10^{-7} Torr). Molecules in the vaporized state are bombarded by an electron beam. One electron from the highest orbital energy is dislodged, and as a consequence molecular positive ions are formed:

$$M_0 + e^- \rightarrow M^+ + 2e^- \qquad 1.1$$

During EI process some of the new-formed ions M^+ are further decomposed and ion fragments appear. This process is called fragmentation and occurs due to the fact, that an excessive energy is available during the ionization process. Altogether, EI mass spectra contains intense fragment ion peaks and much less intense molecular ion peaks. Formation of the gas-phase ions accompanied by extensive fragmentation is called hard ionization. When the molecular ion peak is not observed in the mass spectrum, CI can be used instead of EI in order to obtain molecular ion information.

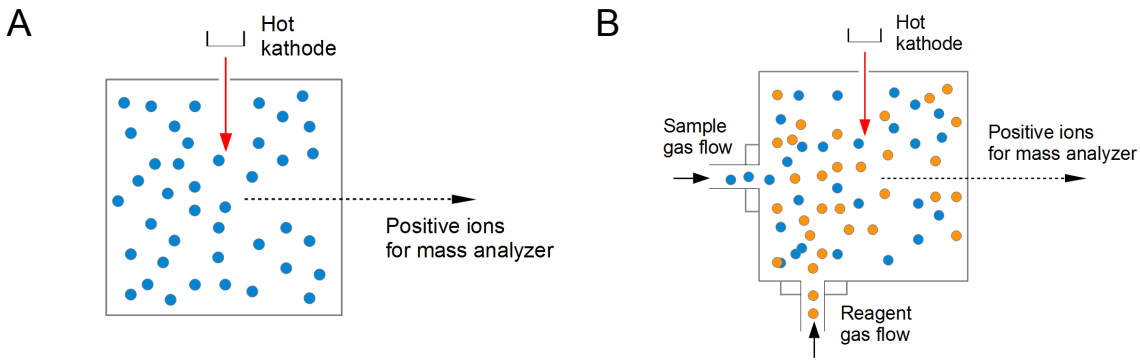

Figure 1.2 a) Electron ionization (EI) source main principle: molecules in the vaporized state are bombarded by an electron beam in the high vacuum; b) Chemical ionization (CI) source main principle: an additional reagent gas is added in the chamber.

With the CI technique the ions are formed by the interaction of an additional reagent gas ions, such as e.g. methane or ammonia, and sample molecules (figure 1.2 b). Inside the ion source, the reagent gas is present in excessive concentration compared to the analyte

(1000:1). Electrons are entering the source and first ionize the reagent gas. Ionized gas molecules have collisions with the non-ionized gas molecules and secondary reagent gases appear. The proton from the secondary gas is transferred to the analyte molecule. One of the possible reaction chain is presented in 1.2.

$$\begin{aligned} CH_4 + e^- &\rightarrow CH_4^+ + 2e^- \\ CH_4 + CH_4^+ &\rightarrow CH_5^+ + CH_3 \\ M_0 + CH_5^+ &\rightarrow CH_4 + [M_0 + H]^+ + H_2 \end{aligned} \qquad 1.2$$

In comparison with the EI method, CI allows to reduce the amount of produced fragments on the one hand, on the other hand the necessity to use an additional gas phase is the CI method limitation [2].

For the fast atom bombardment (FAB) ionization technique, the analyte is dissolved in a liquid matrix, usually glycerol, thioglycerol, m-nitrobenzyl alcohol, or diethanolamine. A small amount (about 1 microliter) is placed on a target. The target is bombarded with a fast atom beam that desorbs the ions and the ion fragments from the analyte. This very rapid and simple technique allows to work with a relatively wide range of samples. However, FAB gives the high chemical background and does not allow to obtain high-charged ions.

Laser desorption ionization method utilizes a pulsed laser to desorb particles from a target surface. The MALDI relies on the absorption of laser energy by a matrix compound. MALDI soft ionization technique typically employs the UV lasers such as nitrogen lasers (337 nm) and frequency-tripled and quadrupled Nd:YAG lasers (355 nm and 266 nm respectively). Matrix sample is the homogenous layer of small matrix crystals (e.g. sinapinic acid or dihydroxybenzoic acid) containing a solid solution of the analyte. It is considered, that primarily the matrix is desorbed and ionized by addition of a proton. The matrix is then considered to transfer proton to the analyte molecules (e.g., protein molecules), thus charging the analyte. Ions observed after this process consist of a neutral molecule [M] and an added or removed ion. The time of flight (TOF) mass analyzer is suited best for the MALDI process. The TOF is proportional to the mass/charge ratio of each single analyte component, the mass of the component can thus be calculated. The MALDI-TOF system is equipped with an ion reflector that reflects ions using an electric field, thereby doubling the ion flight path and increasing the resolution.

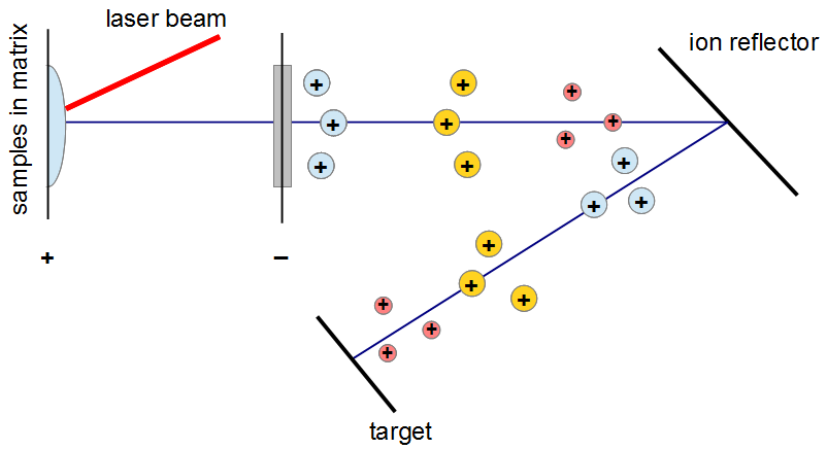

Figure 1.3 MALDI-TOF main principle demonstration.

The ionization methods capable of operating under the atmospheric pressure are usually coupled with the high performance liquid chromatography (HPLC). In these methods, a solution containing the analyte is sprayed at atmospheric pressure into an interface to the vacuum of the mass spectrometer inlet. In atmospheric pressure chemical ionization (APCI), a corona discharge is used to ionize the analyte in the atmospheric pressure region. APCI is a soft ionization technique, because it generates small amount of fragments. An advantage of APCI is the possibility to use a nonpolar instead of a polar solvent as a mobile phase solution, because the solvent and molecules of interest are converted to a gaseous state before reaching the corona discharge pin. Another ionization technique operated in the atmospheric pressure is the electrospray ionization (ESI). The development of ESI has opened new possibilities for mass spectrometric analysis of high molecular weight compounds including proteins, nucleotides and synthetic polymers. The electrospray ion source is comprised of two electrodes, namely the metal electrospray capillary and the atmospheric sampling aperture plate of MS, that are connected together via a high voltage supply. A solution with the analyte is pumped through the capillary system, held at high voltage and sprayed forward the aperture plate (or counter electrode). Under the influence of an applied electric field, ions of the same polarity as the applied voltage migrate from the bulk liquid toward the liquid at the emitter tip. The ions of the opposite polarity migrate in the opposite direction back to the capillary. When the concentration of an excess ions of the same polarity at the surface of the liquid reaches the threshold, where the Coloumbic forces are sufficient to overcome the liquid surface tension, the droplets enriched with ions of this

polarity are emitted (“sprayed”) from the tip. This results in a continuous ion flow at the counter electrode.

Electrospray ionization source is often combined with the quadruple ion trap (QIT) mass spectrometer. The whole scan time consists of a preliminary scan time (“prescan”) and an analytical injection time. A short prescan (less than 10 ms) precedes the analytical scan and is used for determination of proper analytical injection time to avoid the effects of space charge resulting from too many injected ions. The prescan includes all steps related to the analytical scan. QIT operates on the ions over an ion injection, ion isolation, ion excitation and mass analysis periods of time. During the ion injection time (0.001-1000 ms) the ions are gated electrostatically from an external electrospray source into QIT, where they are trapped by a quadrupole field. An isolation step (5-30 ms) is performed to select precursor ions. After the isolation, the energy is deposited into the ion during the excitation step accomplished with gases (5-30 ms). The last step of every scan function involves the mass analysis (10-400 ms). During the last step, ions are ejected sequentially out of the QIT chamber to the electron multiplier detector. One complete mass function in mass analysis is named a microscan.

The ESI coupled with the QIT MS is a powerful analytical tool. Electrospray ionization technique features set it apart from the other ionization techniques. The first and most important feature is the ability to produce a highly charged form of very large molecular weight compounds. The second advantage is the capability to ionize the sample directly from the liquid phase. This feature makes it possible to combine ESI with a wide range of existing separation techniques. The third feature is the extreme softness of the ionization process, which permits the study of three-dimensional molecular conformations. In more detail the physical mechanism behind the ESI will be discussed in the following sections.

1.2. Electrospray history background

The first allusion about the electrospray phenomena have been found in the book "De Magnete" of Gilbert. In this book, author described the following electrospray-related observation: "in the presence of a charged piece of amber, a drop of water deformed into a cone" [3]. In 1745, the German scientist Bose wrote about observations of liquids with an electrical potential applied to a glass capillary [4]. Later, in 1750 Jean-Antoine Nollet has

observed aerosol formation from the small hole in the electrified metal plate, placed near to the grounded metal bulk. Further investigations of this phenomena were done mostly in the physiological level in the consequence with the different view of the same reality. It was considered, that a person electrified by high voltage connection would not bleed normally if he was cut himself. Instead, the blood would spray from the wound. The next step was done by Lord Rayleigh in 1882 [5]. He considered, when the droplet with the radius R and charge Q_R is decreasing (during the evaporation process), it leads to an increase of the electrostatic repulsion of the charges at the droplet surface until droplets reach the stability limit.

$$Q_R = 8\pi(\epsilon_0 \gamma R^3)^{1/2} \qquad 1.3$$

The Rayleigh equation 1.3 gives the information when the electrostatic repulsion becomes equal to the surface tension of the water droplet and the droplet becomes unstable. The studies show that for each liquid droplet a maximum of carried charge Q_R exists. In the equation 1.3 γ is the liquid surface tension and ε_0 is the electric permittivity. The droplet becomes unstable, when Q_R and R satisfy equation 1.3. In the 20th century the phenomenon of an electrospray was described by Burton and Wiegand [6] and in more details by Zeleny [7]. Zeleny has shown the detailed behavior of liquid droplets by the influence of an electric field. The aim of experiments was to find an alternative to the metal-metal discharge process. The experimental setup consists of vertical glass tube (with a 0.92 mm inner diameter) connected to the liquid reservoir at the upper end. The liquid at the lower end was charged to several thousand volts using a static machine. The grounded plate was placed in the 2 cm distance from the end of the glass tube. The ethyl alcohol was used for these investigations. Due to analyte high surface tension, the potential where the instability of its surface is first obtained in air at atmospheric pressure, is nearly the same as the potential where an electric discharge begins. Also the first photo images of the instability were recorded. Taylor in 1965 [8] have shown theoretically, that horizontal interfaces between conducting and non-conducting fluids become unstable under the action of a sufficiently great electric field. He examined the opposite effects of the electrostatic force and surface tension of the liquid surface. It was concluded, that these are both in balance, when meniscus liquid becomes a shape of cone (now known as Taylor cone) with the straight sides, and the half of angle at the cone apex is 49.3°. This shape precedes to the development of a jet from the apex in the

static case. In the dynamic case, the Taylor cone observation depends on experimental conditions (flow rate, liquid conductivity).

For the analytical approach the electrospray ionization becomes popular after 1968, when Dole and co-workers [9] have produced a gas phase of high molecular weight polystyrene from benzine-acetone solution using the electrospray technique. This mechanism is based on ion generation using an external high electric field under atmospheric pressure for the formation of gas-phase ions and spray creation. The possibility to use the ESI for mass spectrometry was also discussed. In the late 1970s, Thomson and Iribarne have used a technique related to electrospray based on charge induction by an external electric field applied across the spray plume, without the direct connection between the capillary of the spray and the electric field [10], [11]. The big analytical interest for ionization methods from the scientific community was solved by works from Fenn [12]. He has brought electrospray technique as a valid and effective approach for the direct study of analytes present in the solution. In 1984 Yamashuta and Fenn [13] have reported about successfully interfacing of ESI to a quadrupole mass spectrometer. They have shown, that nonvolatile materials could be ionized without fragmentation using both positive and negative ionization. In 1987 Bruins and coworkers have introduced a pneumatically assisted electrospray [14], where a sheath gas was used to assist the formation of charged aerosols. In 1988, Fenn et al. have reported the observation of multiply charged gas-phase ions of polyethylene glycols formed by ESI-MS [15]. This was a landmark for ESI-MS. For this work John Fenn have got the Nobel Prize in 2002.

ESI technique has been widely used to analyze large molecules, such as peptides and proteins. The soft ionization mechanism and the possibility of multiple charging of ions allow to use more common and cheaper mass analyzers with limited mass ranges. ESI gives an effective and valid approach for the direct study of analytes present in the solution and consequently an easy coupling with the HPLC method.

1.3. Basic principles of the electrospray ionization process

The gas-phase ions formation process starts with the creation of charged droplets at the emitter tip by applying high potential to the solution. The sample is delivered to the emitter tip with the flow rate in the range of 0.3 – 20 μL/min. The charged drops of the analyte are

delivered to the emitter tip (emitter outlet), where the liquid meniscus is created. The penetration of an electric field into the solution leads to the polarization of the solvent near the meniscus. When the solution is sufficiently conducting, the positive and negative ions drift in the solution under the applied electric field. This movement process leads to an enrichment of the surface with the positively charged ions, while the negatively charged ions are pushed back to the capillary from the meniscus.

Different forces influence the meniscus form. The meniscus form can be destroyed by the downfield force. The surface tension of the liquid γ at the emitter tip opposes the Taylor cone formation (surface area is increasing due to the flow rate). When the applied electric field is sufficiently high to overcome the surface tension, the Taylor cone is formed. The required electric potential for the electrospray V_{ON} was established by Smith [16]:

$$V_{ON} = 2 \cdot 10^5 \sqrt{\gamma R_2} \ln(4d / R_2), \quad 1.4$$

where R_2 is the capillary (emitter) inner radius, d the distance from the emitter tip to the grounded counter electrode (or an orifice of the mass spectrometer), and γ is the surface tension (N/m). Methanol has the surface tension value of 0.0226 N/m and V_{ON} is 2.2 kV. For water the surface tension has value 0.073 N/m and V_{ON} is 4.0 kV.

The potential difference between the emitter tip and the counter electrode creates the high electric field. The maximum of this electric field value is concentrated at the emitter tip. The electric field can be estimated by the following equation [17]:

$$E_{ES} = \frac{2 V_{APP}}{R_2 \ln(\frac{4d}{R_2})}, \quad 1.5$$

where V_{APP} the applied potential. Since the emitter tip is very tiny and the distance from it to the counter electrode is several millimeters, the electric field will reach the values around 10^6 V/m [18]. The tip of the Taylor cone (Taylor cone apex) becomes unstable under the sufficiently high electric field, and the jet starts to spray from the liquid cone apex.

The second step in the mechanism of the electrospray is the shrinkage of the charged droplets in the jet due to the solvent evaporation and consequent droplet fragmentation. The initial evaporation of the solvent from larger droplets results in the decrease of the droplet size, while the number of ions and, correspondingly, the total charge stays the same. When

the droplet size decreases too much (according to the equation 1.3), the electric repulsion forces tear the droplet apart, what results in the appearance of even smaller charged droplets. These droplets are forming the spray plume. The process of evaporation and following droplet fragmentation continues until the droplets reach the minimum size. The schematic representation of the process is shown in figure 1.4.

The last step is the process of the gas phase ion production from the small highly charged droplets. Two mechanisms of the gas-phase formations are possible. The first mechanism called Charge Residue Model (CRM) was proposed by Dole in 1968 [9]. According to the CRM, the droplets are decreasing with the solvent evaporation process. As a result the electrostatic pressure overcomes the surface tension of the droplet. At this critical point, called the Rayleigh limit (equation 1.3), droplets break up and the process continues through the droplet evaporation and subdivision. In this model, the final droplets contain one or more unit charges, but only one analyte molecule. During the solvent evaporation, the charges are localized on the analyte giving rise to the most stable ions in the gas phase.

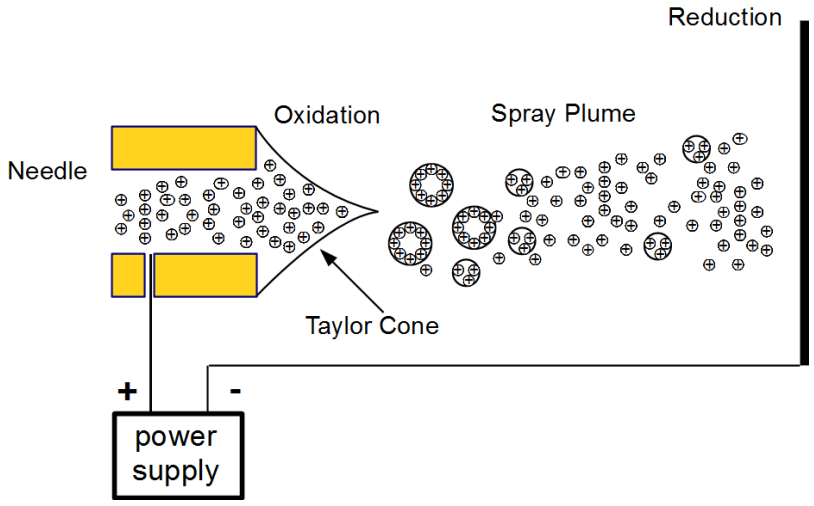

Figure 1.4 Ions formation process during the electrospray ionization.

The other mechanism called Ion Evaporation Model (IEM) was proposed by Iribarne and Thompson in 1976 [10]. In this alternative model an ion near the surface of a charged droplet and even of Taylor cone is pushed out by Columbic repulsion. The direct emission of ions from the small droplets is considered. Both of those mechanisms are involved to explain electrospray behavior in the experiments.

Anyway, the small positively charged ions arrive to the MS inlet (or to the opposite counter electrode). The nature of these ions depends on experimental conditions.

Wilm [19] has proposed to use the tiny electrospray capillaries instead of normal ones. When the capillaries inner diameter is decreasing, the amount of generated gas ions increases significantly. Hence, the capillary tip could be placed closer to the orifice of the MS and the amount of wasted analyte is diminished.

1.4. Electrospray as an electrolytic cell

The electrophoretic charge separation for droplet charging mechanism and charge balance consideration was investigated by Kebarle [20]. It was shown, that the electrospray is a special kind of an electrolytic cell. In this cell the one part of the redox reactions take place in the solution inside the capillary (the applied high potential is anode), and the other part of the reaction occurs in the gas phase at the counter electrode (cathode). The anode plays the role of an electron acceptor and the cathode plays role of an electron donor. Under the applied voltage, the electrochemical reactions take place at the surface of both electrodes. The reaction of oxidation occurs at the anode surface, and the reaction of reduction occurs at the cathode. The current in the electrospray cell is given by the following equation [21]:

$$i_{ES} = H \nu_f^{\nu} \sigma_n^{S} E_{ES}^{\epsilon} \quad , \qquad 1.6$$

where H is a constant containing dielectric permittivity and surface tension of the solvent, ν_f is the volumetric flow rate through the capillary, σ_n is specific conductivity of the solution, and E_{ES} the electric field imposed at the capillary tip.

The equation 1.6 shows the electrospray current as a function of the electric field. The electric field in it's turn is a function of the applied high voltage (eq. 1.5). From the electrolytic cell point of view, the electrospray current flows through the chain of elements, connected in series. This includes the redox reactions at the the source electrode (anode in the positive ionization mode), the charge transfer through the solution, the emission from the emitter tip, the transfer of ions in the air gap and the redox reactions at the counter electrode (charge neutralization at the cathode is taken place). The charge transfer through the solution is dependent on multiple factors, incl. the electrpohoretic mobility of the ion in the solution,

the capillary geometry and the total ion concentration. The charge transfer in the spray plume within the air gap is the drift of charged particles (droplets and ions) in the electric field.

An equivalent circuit for such an electrospray electrolytic cell consists of the electrical devices for each involved physical process, connected in series according to the electrospray current path [22]. The circuit includes the voltage source for applied voltage (U_{APP}), the voltage source for the electrochemical contact (U_{ES}), the solution resistance (R_S), the the voltage source for the charge separation process in the capillary, the charge transport from the emitter tip to the counter electrode via the air gap (U_{GAP}) and the charge neutralization process at the counter electrode (U_{CN}). All those elements are schematically presented at the figure 1.5.

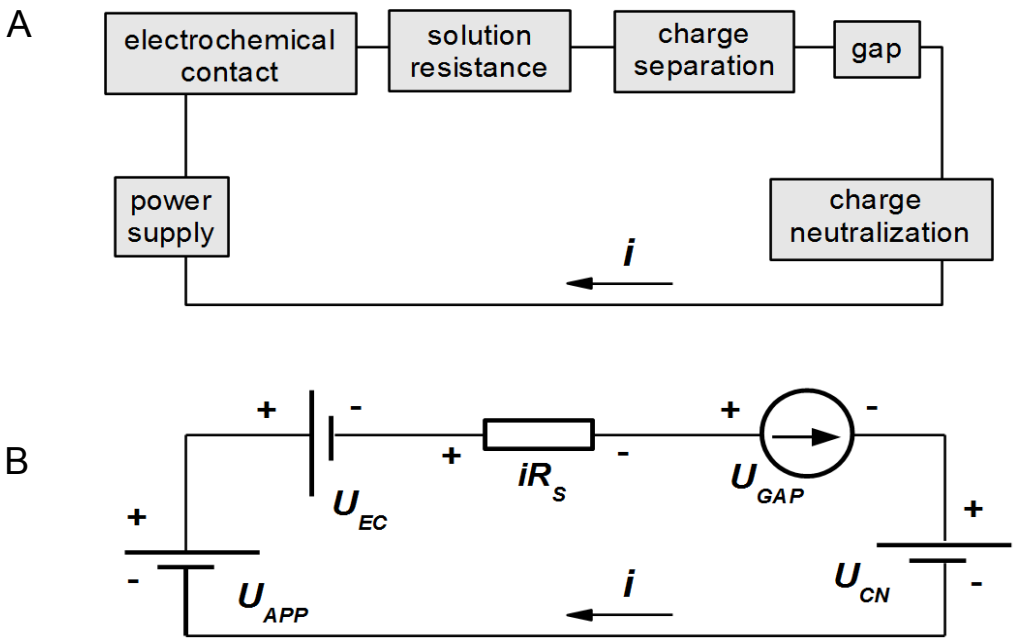

Figure 1.5 a) Schematic presentation of electrospray electrical cell elements; b) Equivalent circuit for normal electrospray process with direct contact of electrode to the electrolyte.

According to Kirchhoff second law [40], the sum of the electric potential differences around any closed circuit loop is zero:

$$\sum U = 0 \qquad 1.7$$

$$U_{APP} - U_{GAP} - U_{EC} - U_{CN} - iR_S = 0 \qquad 1.8$$

This equation shows, that not the entire amplitude of the applied voltage is involved in the electric field and tailor cone formation. A voltage drop is present at the

electrode-to-electrolyte interface due to the redox reaction, and a similar voltage drop can be observed due to charge neutralization process at the counter electrode.

The oxidation reactions however take place with a voltage drop of a few volts, which is significantly lower than the applied voltage (several kV). The reaction of neutralization also has smaller voltage value in comparison to the applied voltage. Thus, these components can be neglected in the equation.

A more significant voltage drop (iR_s) takes place due to electrolyte resistivity. In the works of Enke [41] this is clearly shown, that the resistance of the electrolyte plays a significant role in the charge transfer to the emitter tip, and affects significantly the electric field formation. When the emitter is made from non-conductive material, then the voltage drop at the resistance is involved in the equation as following:

$$U_{APP} \approx iR_S + U_{GAP} \qquad 1.9$$

when a metal needle is used instead of dielectric capillary, the current takes the path of lowest resistance, i.e. it flows through the metal needle almost up to the tip, and the oxidation reaction takes place there. In this case the high electrolyte resistance is short-circuited by low resistance of the metal needle, i.e. almost the entire applied voltage drops at the air gap. The equation 1.9 can be further simplified (equation 1.10).

$$U_{APP} \approx U_{GAP} \qquad 1.10$$

1.5. Problems and assumptions of the electrospray ionization

Simple insertion of a wire conductor into the capillary is usually sufficient for the electrospray process initiation [23], [24]. However, in this case the redox reactions in the capillary volume lead to a gas bubble formation and to the reduction of the electrospray efficiency. For elecrospray process initiation the group of Valaskovic [25] used a gold layers deposition (25 μm thikness) to the tiny emitter tips (with 1 – 5 μm diameter). The loss of an electric contact due to the gold layer degradation was observed after 60 min of operation time. Methods, required to the better adhesion of metal layers were proposed by several groups. Different methods were established to optimize the stability of the electrospray ionization process. Nilsson [26] have compared different metal pairs and have concluded, that sputtering a titanium-gold metal pair on the emitter tip (with a thickness of 20 nm and

150 nm correspondingly) significantly increases the life time of the emitter. These emitters have shown the highest stability in the MS tests. Kniger [27] has improved the gold layers adhesion to the emitter with the thin films of organofunctional silane. Using this method, the electrospray life time was increased approx. 100 times. However, the application of metal coatings very often leads to an electric discharge process [28]. To overcome this limitation the author proposed to use SiO_x coatings, sputtered in order to cover the gold layers. Nilsson [26] have reported about cover layers made of a mixture of poyimide and graphite. These layers have shown a good stability during the oxidation stress and more than seven days life for electrospray duration was achieved. The electrospray ionization life time of 200 hours has been reached by Zhu [29]. He proposed to use a graphite coating over the metal layer on the emitter. Simple manufacturing procedure was performed at room temperature. In the experiment the 4 cm tip length was cleaned in acetone, then the colloidal graphite was brushed on it. It was shown, that the life time can be extended more with one more coating procedure. For the capillary electrophoresis interface Whitt [30] prepared a porous capillary. The small window in the capillary wall was made by drilling and etching techniques. The electric contact was achieved by inserting the conducting wire and filling the needle with the background electrolyte. The performance of this interface was demonstrated with the peptide and protein mixtures.

The group of described methods to make the electric contact to the ESI emitters can be extended with the latest methods, where the electric field for the electrospray operation is generated without any direct contact of the electrode to the liquid. Contactless electrochemical techniques based on capacitive coupling have been developed either to monitor the adsorption of molecules on a substrate by measuring variations of interfacial capacitance or to measure the conductivity of an electrolyte solution within an insulating container. The sensitive non-contact technique for monitoring the adsorption of molecules on a chemically modified substrate was presented by Gamby [31]. The method of electrostatic spray ionization provided in [32] also uses no direct contact to the liquid. The samples were placed onto the non-conducting substrate. The capacitive coupling was used for the ionization procedure. The operation principle is based on the charging of a liquid surface with the geometry of the system that allows the focusing of the electric field to onset the formation of a Taylor cone at the surface of the liquid. Additionally, a nonconducting needle

could be used in cooperation with a cylindrical capacitor between a central electrode and the dielectric material [33].

An attractive method to omit the direct contact in the electrospray ionization was offered by M. Schilling [34]. This is a soft ionization technique without electric contact to the solution, which decreases the risk of undesired discharges, induced by electric currents. The schematic representation of the setup is shown in figure 1.6. A ceramic plate served as a non-conducting insulator between the metal electrode and the liquid. It was shown, that the typical charge distribution for myoglobin ionized by dielectric barrier electrospray ionization (DB-ESI) is comparable with the charge distribution obtained by normal electrospray. The signals were obtained under the optimized conditions (8 kV for DB-ES and 3.5 kV for the convectional electrospray). The total intensity current (TIC) dependency on ceramic plate thickness was investigated. For the 3 mm thick ceramic plate the signal intensity was 19 % and for the 2 mm thick ceramic plate 37.5 % of the TIC obtained with the convectional electrospray.

In such electrospray ionization based on the dielectric polarization, the external potential is applied to the thin metal layer electrode, which is separated from the electrolyte by a thin dielectric layer. The generation of the electric field by dielectric polarization is the key factor in the ionization procedure. This process is based on the displacement of the charges across the insulator by dipole orientation (alignment) in the applied electric field. When external electric field is absent, the dipoles of the polar insulator are chaotically oriented. When the electric field is applied, the dipoles inside the molecules change their orientation due to the interaction with the electric field. This dipole orientation change is associated with a displacement current in the insulator.

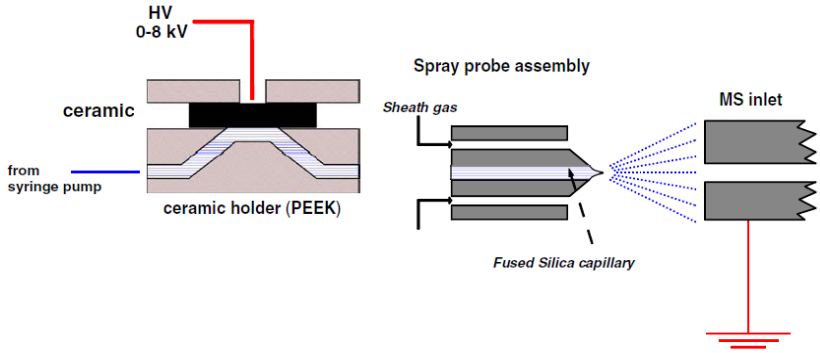

Figure 1.6 Schematic representation of the DB-ESI experiment arrangement. A ceramic plate is used as the dielectric barrier for the electrospray initiation [34]

In the later works [35], [36] the DB-ESI system was improved and metal covered fused silica emitters were used instead of the ceramic plate. The material of emitters plays the role of the dielectric barrier between applied potential and the liquid. The thin metal layer was sputtered on the emitter surface at the significant distance in order to avoid the direct contact with the analyte. A continuously running electrospray in a system without a direct electric contact can only be obtained when a sufficient displacement current is induced. In the case of a dielectric barrier with a DC potential, the emission of charged droplets produces a back coupling to the HV source which results again in a new displacement current. This effect can be better achieved by a continuous variation of the applied potential. A rectangular high-voltage (10 kV with 0.5 Hz frequency) was applied to the dielectric barrier of electrospray emitters (emitter geometry: 360 µm o.d., 20 µm i.d., 10 µm orifice). Positive as well as negative ions for the mass spectrometric detection regardless of the polarity of the applied voltage were detected. The TIC intensity in positive mode was $2.86 \cdot 10^6$ and $2.54 \cdot 10^4$ in the negative ion mode was achieved. It was shown, that the electrospray current intensity is significantly dependent on the emitter geometry. Emitters with thee different inner diameters (20 µm, 50 µm and 75 µm) were tested. The cut-off frequencies of 120 Hz, 750 Hz and 1.1 kHz for the 20 µm, 50 µm and 75 µm emitter were found, respectively. This frequencies equal to half-cycle times of $t_{120\ \mathrm{Hz}} \approx 4.16$ ms, $t_{75\ 0\mathrm{Hz}} \approx 0.67$ ms and $t_{1.1\ \mathrm{kHz}} \approx 0.45$ ms. When fewer than 0.5 nC charges per half cycle are generated, no spray can be established. This certain amount of charges have to be generated in order to overcome the surface tension of the solvent. If the amount of charges per half cycle becomes close to the amount of charges of the cut-off frequency, the spray gets unstable. When the amount of charges in single half

period is lower than the required charges to overcome the surface tension, no spray will be established. This observation leads to the conclusion that this minimum amount of charges is necessary to establish a spray.

To investigate the analytical potential of the DB-ESI technique and compare it with conventional ESI, lysine spectrum was measured as a model substance with the LTQ Ultra mass spectrometer utilizing only the ion trap of the instrument. Maximum injection time was adjusted to 1 ms. A DC voltage of 1.5 kV was applied for the conventional ESI process. For the DB-ESI experiments the emitter with 20-µm i.d. and 5.5 cm length was coated with a 2.5 cm copper layer and a square wave modulated voltage of 5.5 kV at 1 Hz was applied. The distance between the emitter tip and the MS inlet was set to 3 mm in both experiments. Solution of 10 µM/L lysine solution in 0.1 % formic acid was pumped with a flow rate of 0.3 µL/min towards the emitter tip. The obtained analyte spectra were identical, i.e. they have had the same isotopic pattern. An 80 % more intense signal could be measured with the DB-ESI in comparison with the conventional ESI.

1.6. Conclusions

Ionization sources are a large group of various techniques, which allow to deliver the ionized analyte to the MS for further analysis. The electrospray ionization is one of the soft ionization techniques. With electrospray technique, the analyte can be delivered to the MS inlet directly from the liquid phase. The physical mechanism of electrospray ionization is based on ion generation using an external high electric field under the atmospheric pressure. Operated under the direct contact of high voltage to the analyte, electrospray has several limitations. Direct contact of the high voltage to the liquid interface leads to an erosion process and gas bubble formation in the capillary. The metal coated emitter tips can be used to obtain a direct contact to the liquid. However, metal layer is also eroded during the electrospray procedure. This process leads to impairment of electrospray and decreases MS signal intensity. Electrospray based on the dielectric barrier technique is an alternative ionization source. Comparing to conventional ESI, no direct contact of the metal to the electrolyte is present in the method. A dielectric barrier is present between the electrode and the electrolyte, and the displacement current in the dielectric barrier is used as an intermediate charge transfer mechanism. DB-ESI technique prevents the emitters from

erosion process. For the DB-ESI approach, the metal covered fused-silica emitters with different inner diameters were used. Under 5.5 kV operation voltage it was shown, that signal intensity is 80 % higher in comparison with the conventional ESI tests. Further investigation of DB-ESI mechanism is required for better understanding the charge transfer mechanism in the capillary.

Chapter 2 Effects of Various Electrolyte and Capillary Properties in Dielectric Barrier Electrospray Ionization

2.1. Motivation

The absence of the direct electric contact in the DB-ESI source makes it attractive for analytical applications. However, the mechanisms behind the charge transfer in the system with a dielectric barrier electrospray (DB-ES) should be investigated in details. The ion behavior under the ionization driven by dielectric polarization should be investigated. The amount of ions emitted from the capillary outlet can be measured in terms of the electric current with electrode located close to the emitter outlet. The investigation of an electrospray current formation helps to find the optimal conditions for the DB-ESI operation in order to obtain the best possible MS signal properties.

2.2. Experimental setup general description

The overview of the capillary system, which was used in the different experiments is presented as a sketch in the figure 2.1. The setup components such as fused silica capillaries, emitter, syringe pump and counter electrode are connected together as presented in the figure. The capillary part in the middle position has a sputtered coupling electrode. The combination of the sputtered electrode and the dielectric material of the capillary form the driving mechanism of the DB-ESI. The electrode position is fixed far away from the emitter tip. This significant distance from the coupling electrode to the emitter allows to analyze the effects due to the ion movement through the capillary

volume. The counter electrode is used instead of MS inlet in order to detect a generated current signal. The DB-ESI system is operated by an applied square wave signal.

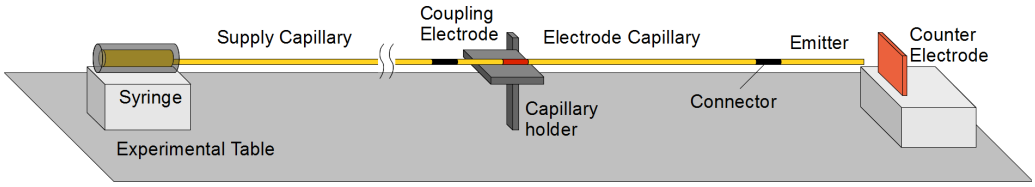

Figure 2.1 DB-ESI experimental setup overview: tree capillary parts are connected together the supply capillary, the electrode capillary with the sputtered coupling electrode, and the emitter tip. The liquid flow in the system is managed by syringe pump.

2.2.1. Setup components

The square wave signal was modulated with a function generator (HM 8130, HAMEG Instruments, Kaiserslautern, Germany). A high voltage amplifier (TREK, Model 610D-K-CE-EX, COR-ATROL, USA) was used to supply the HV edges to the coupling electrode. The signal response on the counter electrode was measured with an oscilloscope (Tektronix, TDS 3014D Digital Phosphor Oscilloscope 100 MHz 1.25 GS/s, Reutlingen, Germany).

The counter electrode was used for the electrospray output current detection. In the present research the square copper plate with side length of 2 cm was used. The counter electrode was placed in 3 mm in front of the emitter tip and grounded with a resistor of 1 MΩ. The potential at the counter electrode was measured with the oscilloscope probe with internal resistance of 1 MΩ to ground. The response current from the electrode to the ground was calculated from the measured potential at the counter electrode and the resulting total resistance of 500 kΩ according to the Ohm's law. The total transferred charge for every input high voltage edge can be calculated by integrating the response current.

The overview of the capillary system used in the experiment is presented in figure 2.1.

The glass syringe in the experiment has no inner electrical parts.

2.3. Charge transfer process in the capillary system

2.3.1. Experimental setup and chemicals

The close view of the capillary system is presented as a sketch in the figure 2.2 a. The syringe was connected to the fused silica capillary. The part of the capillary connected directly to the pump hereinafter is called “supply capillary”. It has 360 µm outer diameter (o.d.) and 75 µm inner diameter (i.d.) and 80 cm length. The supply capillary was connected with the next capillary part (i.d. 75 µm and 360 µm o.d.) by the silicon tubes (tube i.d. 270 µm). This capillary part is called “electrode capillary”, because it contains the sputtered coupling electrode. The sputtered electrode has two layers: titanium layer with thickness of 20 nm and copper layer on it with 200 nm thickness.

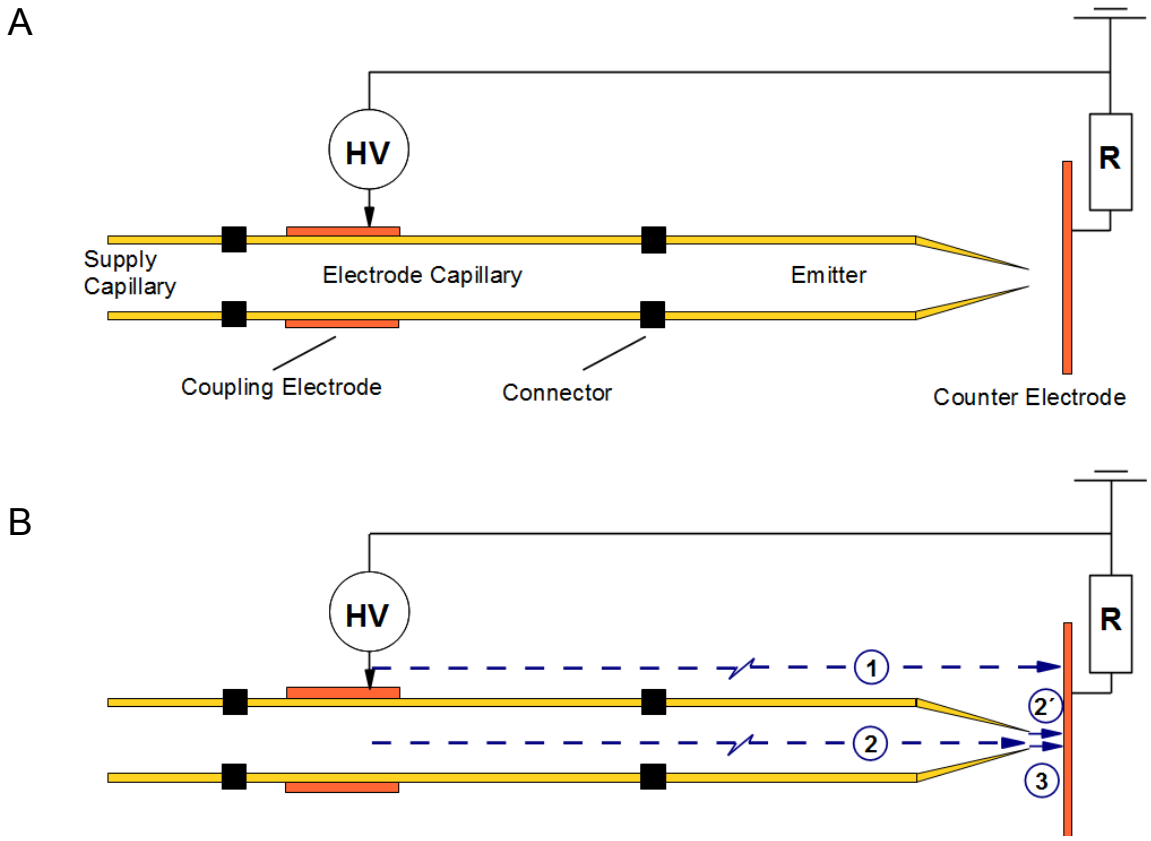

Figure 2.2 a) Schematic representation of the capillary setup: supply, electrode and emitter capillaries are connected together. Coupling electrode is placed on the electrode capillary; b) Different parts of the response signal formation in the capillary system 1 - electromagnetic coupling signal, 2 - ion current signal, 2' – EMT signal in the air gap, due to rising tip potential, produced by ion current, 3 - Electrospray current (physical transfer of charged ions in the gas phase).

The titanium layer was used to improve the adhesion properties of copper to the fused silica capillary. The coupling electrode was placed 2 cm away from the supply capillary and had a 4 cm length. The distance from the middle of the coupling electrode to the emitter tip was variable in different experiments. In the following work this distance will be referred to as "electrode capillary length". The electrospray emitter was connected to the electrode capillary with the teflon tube (tube i.d. 270 µm). Emitters in the current investigation have the length of 5.5 cm, o.d. 360 µm, i.d 75 µm. and i.d. 8 µm at the tip. The narrowing of the inner diameter starts approximately at the 1 cm in front of the end of the emitter. In more details this geometry peculiarity will be discussed later in chapter 3.

The emitter tip was placed 3 mm in front of a counter electrode. The counter electrode is the square copper plate with 2 cm side length. The counter electrode was grounded with a 1 MΩ resistance. The potential at the counter electrode was measured with an oscilloscope probe with inner resistance of 1 MΩ. The response current from the counter electrode to the ground was calculated from the measured potential using the resulting total resistance of 500 kΩ according to Ohm's law.

2.3.2. Physical mechanism of charge transfer

For the investigation of the charge transfer, the mixture 1:1 (v:v) of purified water and methanol with 1 % acetic acid was prepared. The mixture was placed into the ultrasonic base for 2 minutes in order to remove the gas bubbles. The mixture was pumped using the syringe into the capillary system.

The electrode capillary length was fixed at 10 cm in this case. The copper electrode was sputtered 2 cm away from the supply capillary connection. The distance from the middle of the coupling electrode to the emitter tip was 17.5 cm. The electrode had a 4 cm length.

The 5.5 kV high positive and negative voltage slopes were applied to the coupling electrode with the 7 Hz frequency. The measured response at the counter electrode is presented in figure 2.3. In both figures the applied voltage is indicated with a blue line. The current response is depicted by a red line. Figure 2.3 a demonstrates the view of the whole current response and figure 2.3 b demonstrates the same measurement, but with the changed (zoomed) current scale.

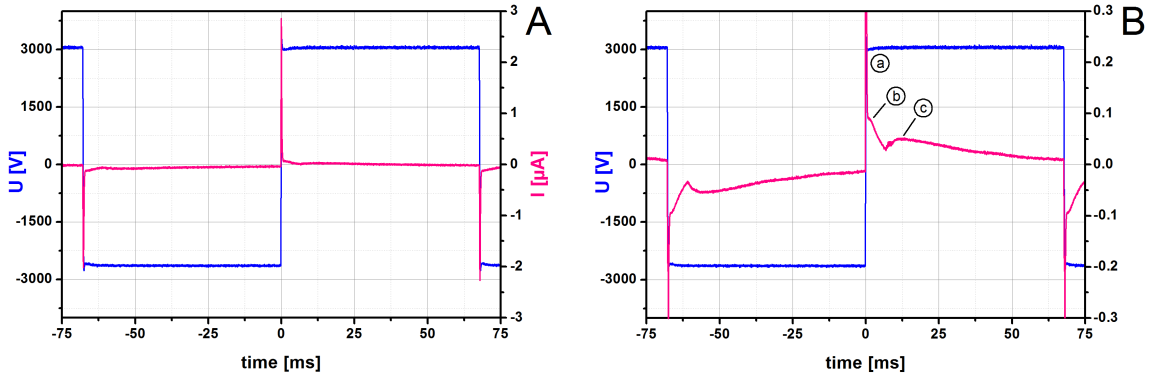

Figure 2.3 Current responses (red lines), when the square wave voltage (blue lines) are applied to the electrode capillary; U=5.5kV, *f*=7 Hz, flow rate 0.3 µL/min); a) The overview of the current response; b) Zoomed view of the current response under the same experiment conditions.

In the overall current response three separate peaks can be directly observed. They are designated with “a”; ”b”; ”c” letters in the figure 2.3 b. Three different current transfer mechanisms are marked in the capillary sketch with the dashed arrows (figure 2.2 b). The first mechanism is the electromagnetic transmission (EMT) from the coupling electrode to the counter electrode through the air marked with the number 1 in figure 2.2 b. The part of the current response corresponding to this mechanism is marked with the letter “a” on the picture 2.3 b. The second peak appears due to the charge transfer by ions inside the electrolyte to the emitter tip. This is referred to as “ion transfer current” and the corresponding output current component is marked with the number 2 in figure 2.2 b. When the electrospray starts, the ions are transferred to the counter electrode, what results in the appearance of the final third current component. The electrospray current peak is marked with the “c” in figure 2.3 b, and the electrospray signal formation is marked with number 3 in the sketch 2.2 b.

2.3.3. EMT signal

Electromagnetic transfer signal is the first mechanism which is involved in the additional charge transfer to the counter electrode. Electromagnetic transfer current from coupling electrode to the counter electrode comes through the air with the speed of light. It immediately charges the capacitance at the counter electrode and can be observed as a sharp peak directly after the applied input voltage edge. The intensity of EMT peak depends on the

distance between two electrodes (source and receiver) and the slope of the edge of the amplifier.

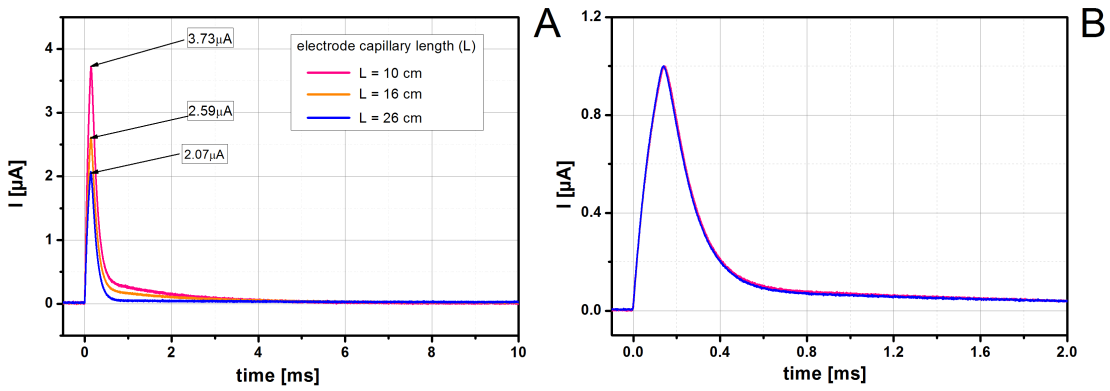

Figure 2.4 EMT signals for different length of the electrode capillary (10 cm, 16 cm and 26 cm) a) Absolute; b) Normalized.

In order to show the distance dependency of the EMT signal three different capillary lengths were used. The lengths of the emitter and the supply capillary were fixed (5.5 cm and 80 cm respectively), distance between the coupling electrode and the emitter was variable. In the experiment three different electrode capillary lengths were used: 10, 16 and 26 cm. The peak intensity for three different electrode capillary distances under the 5.5 kV high voltage and 7 Hz frequency for the standard solution is shown in figure 2.4 a. The height of the response at the positive applied edge for the electrode capillary with a length of 10 cm is 3.73 μA, for the 16 cm capillary length is 2.59 μA and for the 26 cm capillary length is 2.07 μA. The normalized current curves for three lengths are presented in figure 2.4 b. The EMT part of the current response is obviously the parasitic charge transfer.

2.3.4. Ion current signal

At the first moment, when the positive edge of the applied voltage is rising, the charges from the source are transferred to the capillary volume under the coupling electrode. The polarization of the dielectric material is the cause of this transfer.

Displacement current is very fast and obviously all transferred charges are concentrated under the coupling electrode. Internal potential under the capillary wall immediately increases during the rising edge. The increasing slope value depends on the slope value of the applied voltage edge.

The involved charge further starts to transfer along the capillary by means of ion current. The anions are attracted towards the inner capillary wall beneath the coupling electrode (figure 2.5 b), and the cations are instead pushed towards the emitter tip (figure 2.5 c). Physically, the ion current in the electrolyte is a much more complex process, but all together the positive charges are transferred to the emitter tip. This ion transfer in the capillary volume is called “ion transfer current”. During time while the positive ions are transferred to the emitter tip, the potential at the emitter tip starts to increase. The time course for the potential increase might be explained by the time the cations need to be transferred through the entire length of the capillary from the coupling electrode to the emitter tip (figure 2.5 b).

During the negative edge of the applied voltage, the same process goes vice versa (figure 2.5 c). The anions are moving to the emitter tip at the same time as the cations are attracted by inner capillary wall under the coupling electrode. The time requirement to transfer the anions and cations is obviously based on the capillary dimensions (diameter, length) and the electrolyte properties (conductivity). If the electric potential at the coupling electrode is removed and the electric field between coupling electrode and counter electrode decreases, the ion distribution will be set back by diffusion to the state depicted in figure 2.5 a, which results in the decrease of the ion concentration and the corresponding potential at the emitter tip.

In order to analyze the charge transfer in the capillary the appearance of the electrospray current (component “c”) should be prevented. For this reason, the emitter tip was clogged and the whole capillary system was filed in with the solution water-methanol (1:1) + 1 % acetic acid. Under the potential 5.5 kV and 7 Hz frequency for the electrode capillary length of 16 cm the current response was observed as presented in the figure 2.6 a with a blue line. Figure 2.6 a presents only the positive part of the current response. The red line depicts the current under the same conditions for open emitter (when the emitter is not clogged and electrospray exists).

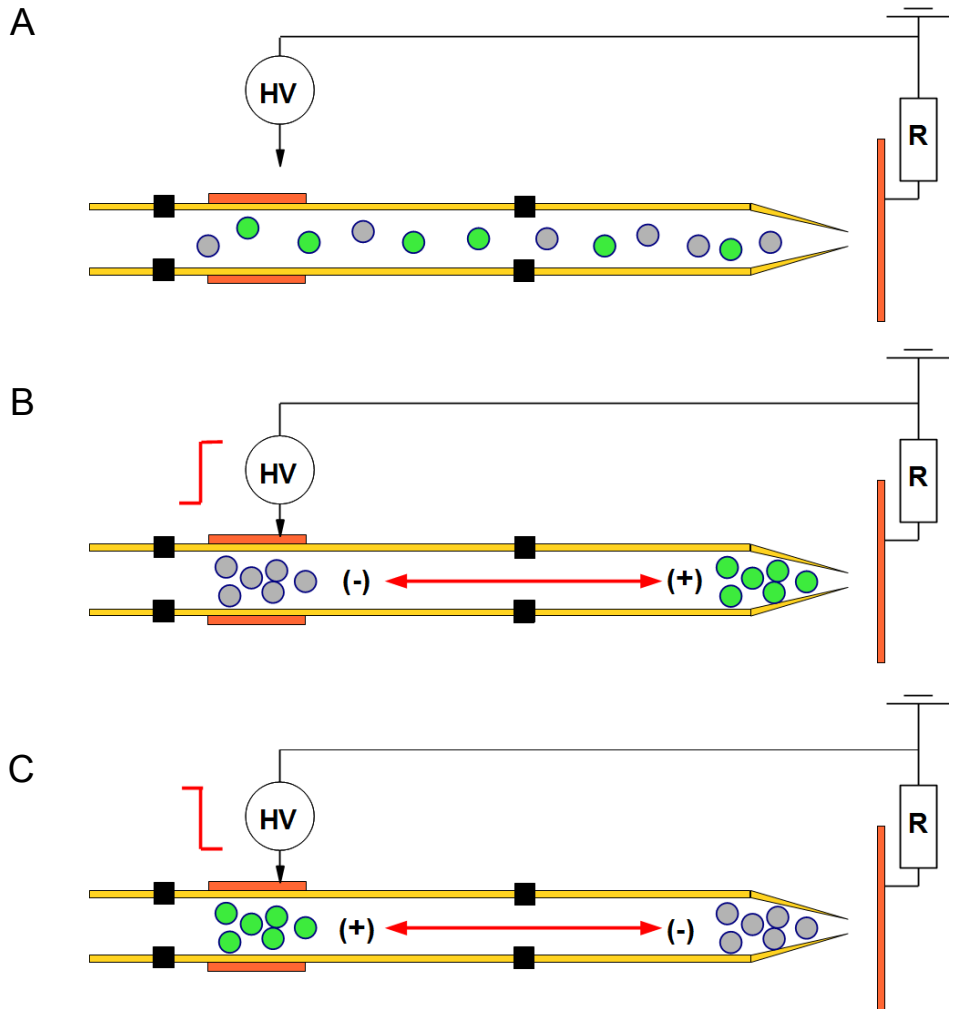

Figure 2.5 Simplified illustrations of the ion transfer process inside the capillary under the different operation conditions: a) HV does not applied to the electrode; b) Positive slope is applied to the electrode; Positive ions are pushed to the emitter tip, negative ions are attracted under the coupling electrode; c) The negative slope is applied to the electrode, negative ions are pushed to the emitter tip, positive ions are attracted under the coupling electrode.

As could be seen, in the case of a clogged emitter, the EMT and the ion current components of the total current response are still existing at the same time positions and have the same height. The second peak (ion current peak in figure 2.6 a) appearing after a time delay of 1.1 ms, is significantly smaller (0.3 µA) and smoother in comparison to EMT signal peak.

The potential at the emitter tip is rising because of the charge transfer with the ion current to the emitter tip. The rising tip potential leads to another much weaker EMT signal between the emitter tip and the counter electrode. This process is marked in figure 2.2 b with the number 2´. This is observed as the second peak in the total measured signal.

The observed time delay of 1.1 ms is the time necessary for the ions to reach the emitter tip and the counter-ions to reach the coupling electrode. This matches the hypothesis that the signal peak is caused by a charge transfer process inside the capillary system, which increases the electric potential at the emitter tip. Measured for positive and negative applied voltage edge the ion current signals have equal amplitude and appear with the same time delay for the same capillary and solution conditions, as shown in figure 2.6 b.

In the positive ion peak formation both cations and anions movement are essential. When the positive voltage edge is applied to the coupling electrode, the positive ions are pushed towards to the emitter tip. At the same time negative ions are moving to the area under the coupling electrode. The sum of both ion currents forms the total ion current peak. When the negative voltage edge is applied, positive ions move to the part of the capillary under the coupling electrode and negative ions are attracted to the emitter tip. With this process the negative ion current peak is formed. The absolute times necessary for each ion type to move from the counter electrode to the emitter tip can not be separated, instead the total exchanging time of the cations and anions is observed as the time delay in the ion current signal peak. The positive current formation is impossible without negative ions movement and vice versa.

In the figures 2.6 c, d the ion current responses for the different capillary lengths are presented for the both positive and negative responses. The variation of the capillary length shows strong influence on both second current peak formation and the electrospray current as well. In order to show the capillary length influence on the ion current formation in the system, the coupling electrode was placed in a fixed position in 3 mm to the emitter tip, and the distance from the coupling electrode to the emitter was set to 10 cm. Capillaries of larger lengths (10, 16 and 26 cm) were connected between the coupling electrode and the emitter in loop shapes in order to keep the same physical distance from the electrode to the emitter from one side, and to change the total ion current path from the other side.

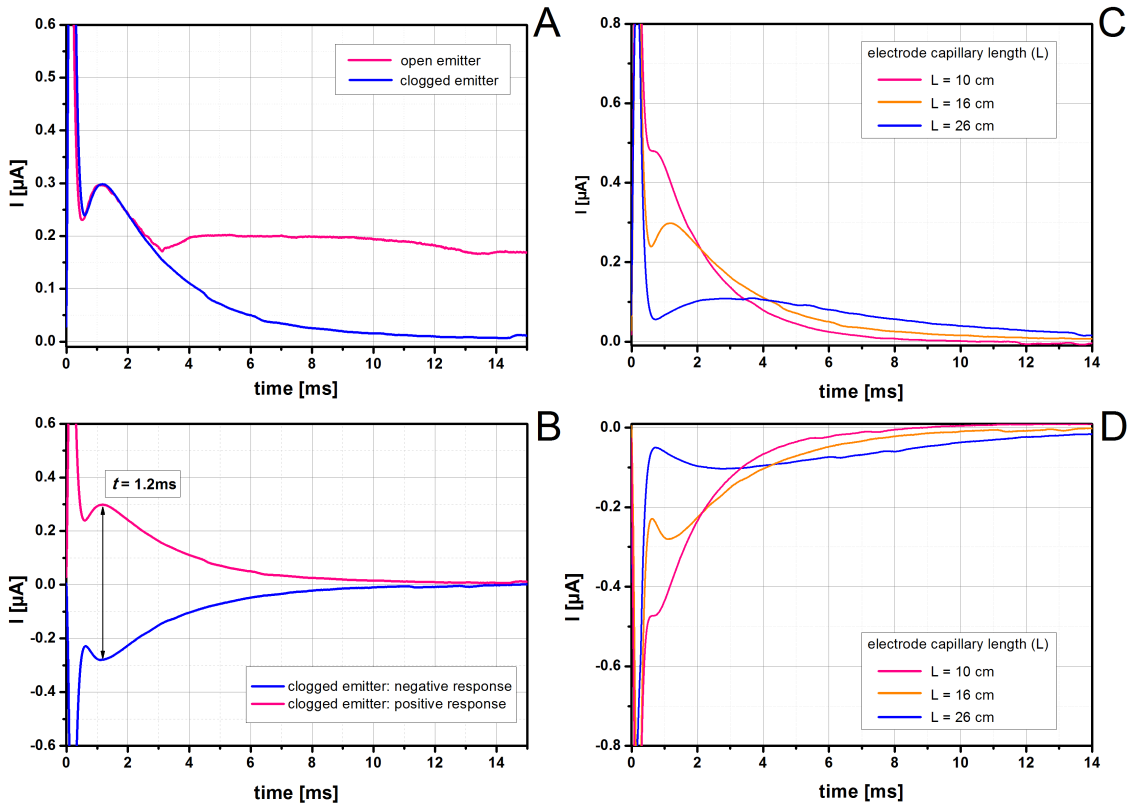

Figure 2.6 Measured current responses for the applied 5.5 kV voltage slopes at 7 Hz frequency; a) The positive part of the current response for open emitter (red line) and for clogged emitter (blue line), electrode capillary length is 16 cm; b) Positive and negative ion current responses for clogged emitter case, electrode capillary length is 16 cm; c) The positive ion current responses for the clogged emitter case for three different length of electrode capillary (L); d) The negative ion current responses for the clogged emitter case for three different length of electrode capillary (L).

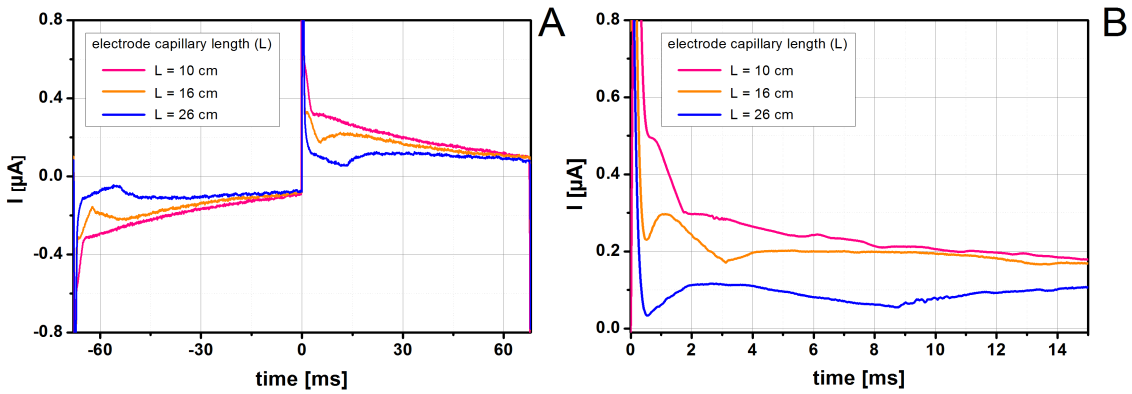

Figure 2.7 Current responses for the applied 5.5 kV voltage slopes with 7 Hz frequency for different electrode capillary lengths; flow rate: 0.3 µL/min; a) Overview of positive and negative responses; b) Zoomed view for positive responses.

With such capillary loops it is possible to show, that there is no influence of the EMT signal peaks on the ion current formation. Three different lengths of the electrode capillary (L= 10 cm, L= 16 cm and L= 26 cm) were used in the measurements. The resulting responses of 5.5 kV and 7 Hz for both positive and negative slopes edges of an applied voltage are presented in figure 2.6 c, d. The same EMT signal peak was observed in all cases, while the ion current peak appeared with a larger time delay and had significantly lower amplitudes with the increase of the capillary length.

The changing of the electrode capillary length under the same experimental conditions affects the total current response measured at the counter electrode. Figure 2.7 demonstrates the current responses for three different lengths of the electrode capillary (different distances between coupling and emitter tip) in the case of an open emitter. The same capillary configuration with fixed distance between coupling electrode and emitter tip was used here also. The effect can be seen in positive and negative current responses.

2.4. Parameter influence on charge transfer process

2.4.1. Applied voltage amplitude

For the investigation of the applied voltage amplitude influence on the different parts of the current response formation, the electrode capillary length was fixed at 16 cm and purified water and methanol (1:1) with 1 % acetic acid solution was used in the experiment. The voltages from 3.0 kV up to 5.5 kV with steps of 0.2 kV were applied at 7 Hz frequency, and the current response was measured. Figure 2.8 a shows the positive current curves for different amplitudes of the applied voltage pulses. It can be observed in figure 2.8 a, that the ion transfer current response increases linear-proportionally to the applied voltage (corresponding to the Ohm´s law). While the resistance of the capillary remains the same and no changes in the conductivity properties of the electrolyte were done, the ion current changes are proportionally to the applied voltage. Therefore, the ion current peak position at the time scale remains the same for the different applied voltage values (1.2 ms).

The electrospray current under 3.4 kV of applied voltage appears at approx. 14 ms and is not present in figure. The electrospray current is lower and appears later for lower voltage amplitudes. The shape of the response peak does not change. This can be explained by the

fact, that for the ignition of the electrospray a certain amount of ions and a certain potential value are necessary at the emitter tip.

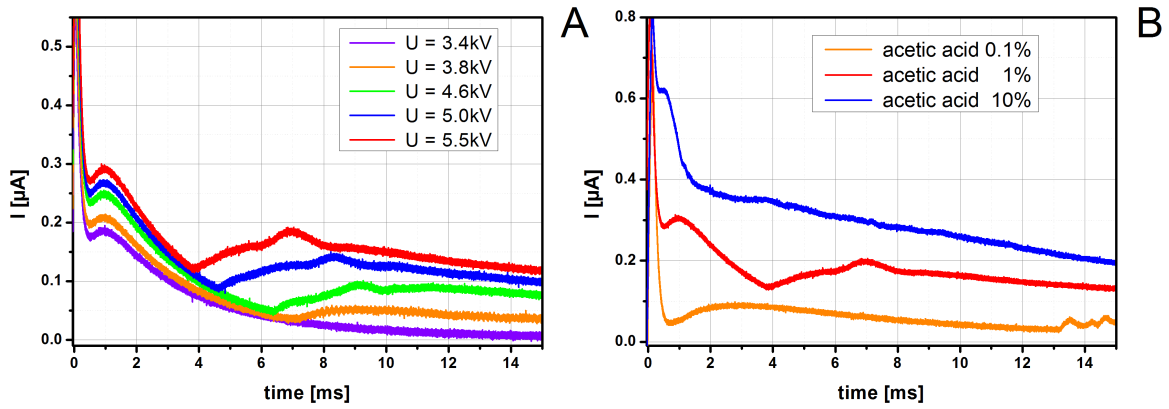

Figure 2.8 a) Positive response current for different amplitude values of applied voltage;
b) Positive response current for various concentrations of acetic acid (0.1 %, 1 % and 10 %) U= 5.5 kV, f = 10 Hz, flow rate: 0.3 µL/min.

A lower applied voltage means that the electric field between coupling electrode and counter electrode is lower, resulting in less ions being transferred towards the emitter tip. As a result, the necessary amount of charge is delivered with a larger time delay. A higher HV amplitude correspondingly results in a higher ion transfer current, thus the necessary amount of charges is delivered earlier.

2.4.2. Electrolyte concentration and ion properties

Since the ion current plays a significant role in the charge transfer to the emitter tip, the results must also depend on the electrolyte concentration.

Figure 2.8 b shows the current signals obtained for three different concentrations of acetic acid in the solution. In the experiment the electrode capillary length was fixed at 16 cm and responses were obtained under 5.5 kV applied voltage pulses at 10 Hz frequency. For the 1 % acetic acid concentration in the water-methanol solution, the ion current peak appears at 1.1 ms and has a height of 0.3 µA. For 10 % acetic acid, the ion current peak appears at the 0.52 ms with the height of 0.62 µA. When the concentration of acetic acid is 0.1 % in the solution, the ion current peak appears at 3.02 ms and has a height of 0.08 µA. With lower concentrations of the acetic acid in the mixture, the observed ion transfer current response decreases and appears later.

The same behavior could be observed for the electrospray peak. The lowest value is observed for 0.1 % acid concentration in the solution. For 10 % acid concentration in the solution the electrospray current signal increases significantly. The lower concentration means that fewer ions take part in the charge transfer process, and the overall conductivity of the electrolyte is lower. The ion current in the capillary is lower for the same electric field, the time necessary to transfer the charge to the emitter tip is higher, and both ion transfer current and electrospray responses appear later and weaker.

The electrolyte conductivity is the key factor in this process. Since the ion transfer current in the electrolyte is the movement of the ions, the value of the current and the current density depend on the ion concentration and movement velocities [36]:

$$I = j \cdot A \tag{2.1}$$

$$j = n_+ \cdot |q_+| \cdot \nu_+ + n_- \cdot |q_-| \cdot \nu_- \tag{2.2}$$

where I is the electric current, j the current density, A the area of the internal cross section of the capillary, q_+, q_- the unit charges of the charge carriers (ions), n_+, n_- the concentrations of the charge carriers, and v_+, v_- the velocities of the charges. In the equilibrium state, the electrolyte is neutral. This means the concentrations of the cations and anions are equal ($n_+ = n = n_-$) The velocity of the ion drift can be described by the ion mobility and the electric field E:

$$j = (\nu_+ + \nu_-) n \cdot q \text{ , where } n_+ = n_- = n \text{ and } q_+ = q_- = q \tag{2.3}$$

$$j = (\mu_+ + \mu_-) n \cdot q \cdot E \text{ , where } \nu_{(+/-)} = E \cdot \mu_{(+/-)} \tag{2.4}$$

$$j = \sigma \cdot E \text{ , where } \sigma = (\mu_+ + \mu_-) n \cdot q \tag{2.5}$$

where σ is the total electrolyte conductivity. According to equation 2.4, the ion movement depends on the electrophoretic mobilities of both positive and negative ions.

Three different electrolytes were prepared. Each solution includes water-methanol 1:1 mixture, but the acid compound was different in each case. In order to get different molecule sizes and different mobilities in the each solution, formic acid, acetic acid and propionic acid in concentrations 0.1 mol/L were used in this experiment. The mobility value and the molecular masses for acids are shown in the table 2.1. The positive voltage edge was applied to the coupling electrode. The coupling electrode was placed in 16 cm distance away from

the emitter. The current responses for the applied voltage of 5.5 kV and 10 Hz are shown in figure 2.9.

For the smallest and fastest molecules of formic acid (green line at the figure 2.9) the formation of the ion current signal occurs faster. The ion current peak was observed at the time 0.7 ms and has an intensity of 0.71 µA. With the red line in figure 2.9 the current response for the mixture with acetic acid is presented. The blue line depicts the response for the mixture with propionic acid. Since the mobility values of acetic acid and propionic acid are very close to each other (see table 2.1), the ion current peaks appear with almost identical time delay of 1.3 ms for acetic acid and 1.5 ms for propionic acid. When the molecule radius is bigger, the ion current peak appears later and has a weaker intensity. As expected, for the molecule with the biggest radius (propionic acid) the ion transfer current signal was observed at the latest time (1.5 ms), and the signal amplitude has the lowest value (0.18 µA).

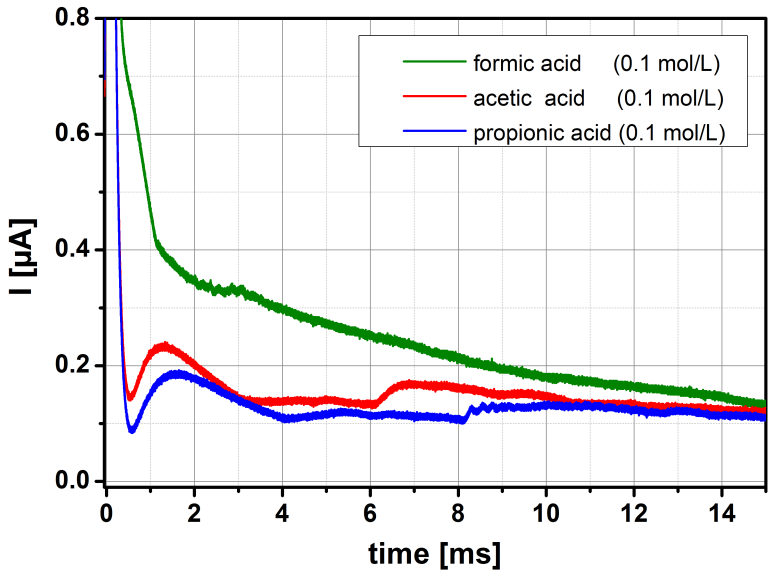

Figure 2.9 Current responses under positive applied edge for three different acids; further parameters: U=5.5 kV, f=10 Hz, flow 0.3 µL/min, acid concentration 0.1 mol/L.

Each of the presented acids has a different dissociation constant, i.e. for the same acid concentration of 0.1 mol/L in the water-methanol solution, a different amount of ions would be present depending on the acid type. The dissociation constant is the quantitative characteristic of the acid ability to dissociate to the cations and anions and can be presented with the equation [37]:

$$K_S = \frac{[H^+][A^-]}{[HA]} \tag{2.6}$$

where $[H^+]$ and $[A^-]$ is the concentration of completely dissociated anions and cations in the solution respectively and $[HA]$ is the concentration of the non-dissociated part of acid molecules. The concentration of the totally dissociated ions can be calculated. In practice the most common used value instead of dissociation constant is the logarithmic measure of the acid dissociation constant:

$$pK_S = -\log_{10} K_S \tag{2.7}$$

The amount of totally dissociated cations and anions in the solution is almost equal and the dissociation constant can be rewritten in the following way:

$$[H^+] \approx [A^-] \rightarrow K_S \approx \frac{[H^+][H^+]}{[HA]} \tag{2.8}$$

For formic acid the dissociation constant pK_S in aqueous solution has a value of 3.77 [37]. Acid dissociation constants are sometimes expressed by pK_S, which is defined as:

$$pK_{S.FA} = 3.77 \rightarrow K_{S.FA} = 1.70 \times 10^{-4} \tag{2.9}$$

$$K_{S.FA} = \frac{[H^+][H^+]}{[HA]} = 1.70 \times 10^{-4} \tag{2.10}$$

$$C_{H^+} = \sqrt{1.70 \times 10^{-4} \cdot 0.1} = 4.12 \cdot 10^{-3}\, mol/L \tag{2.11}$$

where C_{H+} is the concentration of ions, totally dissociated in the solution. In order to have in the volumes the equal number of dissociated ions, the acid concentrations should be recalculated in the following way:

$$[H^+][A^-] = K_S[HA] \tag{2.12}$$

$$[HA] \approx \frac{[H^+][H^+]}{K_S} \tag{2.13}$$

The formic acid concentration (0.1mol/L) and the concentration of the dissociated ions ($4.12 \cdot 10^{-3}$ mol/L) were taken as a base for the calculations. The acetic acid acid concentration can be calculated:

$$[HA]_{AA} = \frac{(4.12 \cdot 10^{-3})^2}{1.78 \cdot 10^{-5}} = 0.96\, mol/L \tag{2.14}$$

The calculation results for totally dissociated ions in the solution are presented in table 2.1.

Table 2.1– Main properties of acid substances

acid and abbreviation	Hydrochloric ("HCL")	Formic ("FA")	Acetic ("AA")	Pronionic ("PA")	Octansulfonic ("OsA)
chemical formula	HCL	HCO_2H	CH_3CO_2H	CH_3CH_2-COOH	$C_8H_{18}O_3S$
pK_S	-6	3.77	4.75	4.87	-1.41
K_S	10^{-6}	$1.70 \cdot 10^{-4}$	$1.78 \cdot 10^{-5}$	$1.66 \cdot 10^{-5}$	$3.89 \cdot 10^{-2}$
acid concentration (mol/L)	10^{-3}	0.1	0.96	1.26	$2.4 \cdot 10^{-2}$

The time delay between the applied voltage edge and the appearance of the electrospray signal depends on several factors. Among them the conductivity and geometrical properties of setup are playing a significant role. From the other side the mobility of the particles is very important. The mobility of ions in the medium can be described using the Einstein relation [36]:

$$D = \mu k_B T \tag{2.15}$$

where D is the diffusion coefficient, μ the mobility, k_B the Boltzmann's constant and T the absolute temperature. The hydrodynamic radius of the drift molecule (named also as Stokes radius) is the radius of a hard sphere that would diffuse in the solution at the same rate as the molecule. The behavior of this sphere includes the hydration and shape effects. Since the molecules are mostly not spherical, the Stokes radius is smaller, than the effective radius and more extended molecule will have a larger Stokes radius in comparison with the more compact one. In liquids, where considerable interactions are between solute and solvent molecule, Stokes radius is proportional to the frictional coefficient and inverse proportional to the viscosity η. The frictional coefficient can be determined by the size and the shape of the molecule under consideration and the diffusion constant can be given by equation:

$$D = \frac{k_B T}{6 \pi \nu R_H} \tag{2.16}$$

The diffusion constant can be defined in terms of mobility, according to the Fick´s law (eq. 2.17).The viscosity value of the water–methanol medium at the temperature 25 °C and

atmospheric pressure has the value $1.32 \cdot 10^{-3}$ Pa·s [39]. The calculated values of Stokes radius and the values of molar mass and mobility data for different acids are presented in the table 2.2.

$$R_H = \frac{k_B T}{6 \pi \nu D} = \frac{1}{6 \pi \nu \mu} \qquad 2.17$$

Figure 2.10 a,b depicts the current responses measured for three electrolytes with acid concentrations adjusted in such a way that the amount of dissociated ions was the same according to the known values of the dissociation constants (see table 2.1). The calculated concentrations of acids in the solution have values of 0.1 mol/L for formic acid, 0.96 mol/L for acetic acid and 1.26 mol/L for propionic acid. The length of the electrode capillary was fixed at 16 cm, the flow rate had a value 0.3 µl/min. The signals were measured with an applied voltage of 5.5 kV, at the 10 Hz frequency.

Table 2.2 – Main properties of acid substances

acid	Hydrochloric	Formic	Acetic	Pronionic	Octansulfonic
Mobility, µ	79.1	56.6	42.4	36.9	26.2
Molar mass, g·mol^{-1}	36.46	46.03	60.05	74.08	234.3
Stokes radius, nm	6	11.2	8.4	12.9	18
electrospray starting time, ms	2	2.21	2.54	2.94	3.39

The measured curves for positive current responses are presented in figure 2.10 a. They are similar to the responses depicted in figure 2.9, i.e. for the larger ion radius the ion current peak was observed later and the measurement response was weaker. Finally, the measurement was also performed for the negative applied voltage edge (figure 2.10 b). According to equations 2.2 - 2.5, both positive and negative ions take part in charge transfer inside the capillary. The total ion transfer current is always a sum of both cation and anion transfer currents. That means, that the ion transfer current should be the same for positive and negative transitions. The measured response for the negative applied edge is shown in figure 2.10 b. The setup parameters and the electrolyte properties are the same as for the curves in figure 2.10 a. It was observed that for positive and negative applied voltage edges,

the first two signal peaks (the EMT peak, and the ion transfer current peak) have had the same height and position with an opposite polarity. The third current peak, i.e. the electrospray current, was different for positive and negative applied voltage edges. In the electrospray process either positive or negative ions are sprayed, and therefore the electrospray charge transfer is defined by the properties of only one type of ions, either positive or negative. The starting time of the electrospray current signal after the applied voltage edge has been applied depends on two factors, namely the conductivity of the solution and geometry of the setup. The conductivity of the solution in its turn depends on the mobility and the concentration of ions.

The total ion current is always a sum of both cation and anion transfer currents. It means, that the ion transfer current should be the same for positive and negative transitions.

Figure 2.11 shows the dependence of the electrospray starting time on the calculated hydrodynamic radius of the molecule (see table 2.2). The concentrations of the five employed acids were adjusted in such a way that the same amount of dissociated anions was present. The measured time delay is higher for larger hydrodynamic radius values, and correspondingly for smaller values of the electrophoretic mobility, because of the longer time necessary for the ions to travel through the capillary towards the emitter tip.

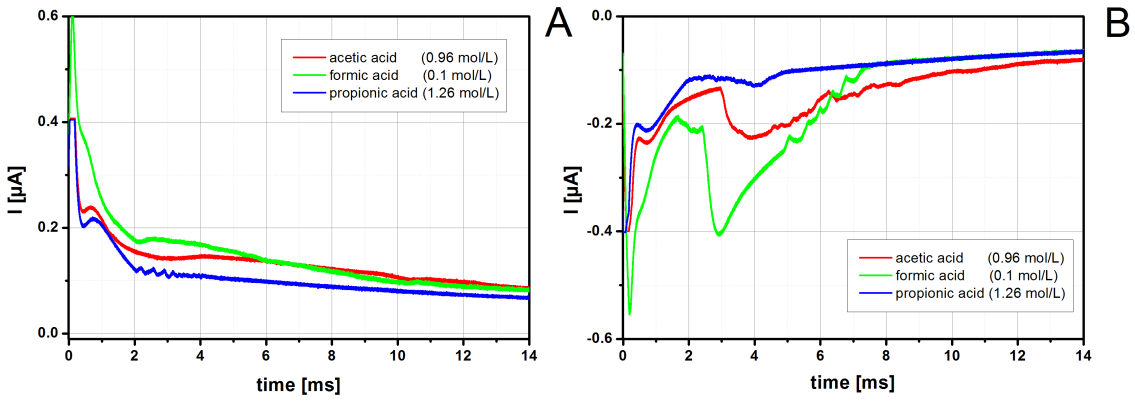

Figure 2.10 Current signals for different acids with the same ion concentration (considering acid concentration and dissociation constant); a) Positive current response; b) Negative current response. Experiment parameters: U=5.5 kV; f = 10 Hz; flow rate: 0.3 µL/min; electrode capillary length 16 cm; concentration of free anions 0.1 mol/L.

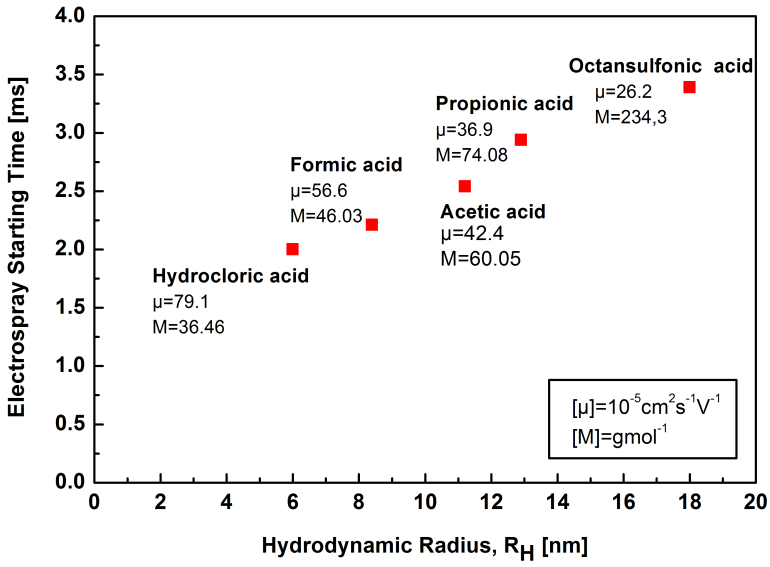

Figure 2.11 Dependency of the electrospray starting time on the hydrodynamic radius. Experiment parameters: U=5.5 kV; f = 10 Hz; flow rate: 0.3 µL/min; electrode capillary length 16 cm; concentration of free anions 0.1 mol/L.

2.5. Conclusions

The charge transfer process in the DB-ES capillary system was investigated empirically. The electric current was measured at counter electrode located close to the emitter tip as the response on the applied voltage edges. The measured signal was analyzed for various setup and experiment configurations.

The measured current response comprises several components, namely, the current initiated by electromagnetic transmission (EMT), the ion transfer current inside the capillary, which is responsible for the forming of the potential at the emitter tip, and the electrospray current itself. The capillary system with a clogged emitter was used to exclude the electrospray current from the total output current and to analyze the current components separately.

The capillary properties, e.g. the distance from coupling electrode to the emitter tip, and have shown significant influence on the formation of the ion current, and correspondingly on the total output signal.

That the electrolyte concentration and the ion properties (size and mobility) have also shown significant influence on the ion current formation and hence on the electrospray starting time and intensity.

Moreover, it was shown that both ion types, i.e. both anions and cations, are involved in the charge transfer through the capillary and the formation of the potential at the emitter tip, and therefore in the positive electrospray formation.

The empirical investigations allow the analysis of the externally-measurable quantities only. The internal processes within the setup, e. g. the charge transfer and the electrospray formation, can be analyzed at deeper level by development of electric models and simulation of the current components separately.

Chapter 3 DB-ESI Electric Model

3.1. Introduction

The electric circuit is often drawn in order to better understand difficult processes in current-voltage relations in a real systems. The circuit consists of individual components such as resistors, capacitors, diodes, transistors, inductors and others, which are connected in different ways. The system may include active and passive elements. Active elements supply the energy or control the energy flow. Passive elements do not create the power and do not depend on other elements. An analogue electronic circuits are those in which current or voltage may vary continuously with time to correspond to the information being represented.

Such equivalent circuit model always presumes a significant simplification of a real object or a physical process. The electric properties of complex objects distributed in space are often reduced to equivalent discrete circuit elements with concentrated properties. The term “equivalent” here means that despite the significant assumptions and simplifications, the discrete circuit element performs an almost equivalent function as the original object. Such simplification usually allows to understand the processes in detail at simpler level of abstraction, and afterwards to use this new knowledge to understand the process with it's original complexity in the original setup.

The equicalent circuit model of DB-ESI system is developed here to learn more about the charge transfer process in the system and the electrospray current regulation. The possibility to analyze the whole system under different conditions and extract different current components from the whole signal response in DB-ESI system makes the modeling process quite attractive and useful.

3.2. Principles and assumptions in the model

The modeling process was performed in two steps. The first part of the modeling includes the detailed consideration of each element involved in the physical setup, the definition of the equivalent circuit element, and the calculation of corresponding parameters. The first developed model includes the detailed explanation of the potential behavior in the system, when electrospray is absent. Electrically, this is equivalent to the experimental setup when the closed emitter is operated under high potentials, or the potential is not high enough to establish the spray mode (those processes were described in more detail in the Chapter 2). This model is named “Closed Emitter Model”.

In the second part of modeling procedure, the “Closed Emitter Model” will be extended with an additional active element for the charge transfer due to the electrospray itself. The simulations for both circuits are performed under the same operating conditions. Second model is called “DB-ES Final Model”. The influence of the electrospray current on the charge transfer dynamic in the system and the potential behavior is described in detail.

3.3. Basic elements calculation

The sketch of the DB-ESI experimental setup is presented in figure 3.1.

The setup was split into several separate components with the individual parameters. For each component the detailed description and parameter calculations were performed. The relationships between all elements of the setup were presented.

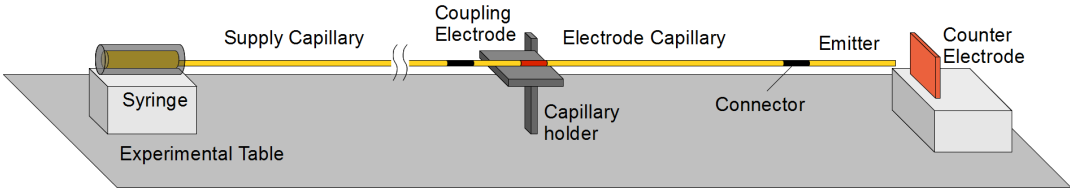

Figure 3.1 DB-ESI experimental setup overview: three capillary parts, namely the supply capillary, the electrode capillary with the sputtered coupling electrode, and the emitter, are connected together. The liquid flow in the system is managed by syringe pump.

The experimental setup consists of several elements, connected in series to each other. These are the syringe, the supply capillary, the electrode capillary with the coupling electrode on it,

the emitter and the counter electrode. The parameters of each of those components should be included in the model.

First of all the capillaries in the system (excluding the 4 cm length capillary part under the coupling electrode), syringe capillary and emitter capillary were grouped. All the capillaries in the experimental setup were characterized with electrolyte resistance and self capacitance properties. The capillary part under the coupling electrode (4 cm of the capillary covered with an electrode) was characterized as a cylindrical capacitor. The third component of the circuit was the emitter tip and counter electrode pair. In absence of the electrospray ("Closed Emitter Model"), i.e. when the active element of the electrospray is absent a weak capacitive interaction across the air gap was considered. When the electrospray was established (in the case of the "DB-ES Final Model"), the model for the electrospray current was included.

3.3.1. Capillary unit length

The capillary system together with the syringe and emitter (except the 4 cm length of the capillary part directly under the coupling electrode) can be characterized with two electrical properties, the electrolyte resistance and the self-capacitance. For modeling purposes, the capillary was divided in small segments (units with the length of 0.5 cm each) and the properties for each segment were calculated. One unit length has the properties of one electrolyte resistor and one electrolyte self-capacitor. The schematic representation of the capillary unit element is shown in the figure 3.2 below.

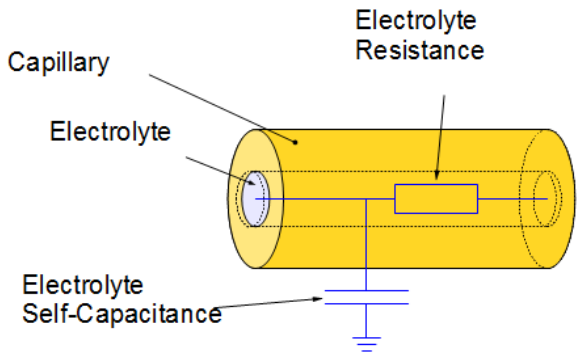

Figure 3.2 Capillary unit length and corresponding part of the equivalent circuit: resistor and capacitor, which describe the electrolyte properties.

The capacitor in this circuit presents the self-capacitance of the capillary unit length. The self-capacitance is a property of an isolated conductor, which defines the amount of electric

charge that must be added to the conductor to increase its potential by a unit value. The self-capacitance does not belong to the capillary but to the conducting substance (electrolyte within the capillary). The electrolyte as a conducting substance has a form of a long thin wire in open space. The value of the self-capacitance can be estimated using the equation for a conducting rod of a finite length in open space [40]. This is described by equation 3.1:

$$C_{unit} = 2\pi\epsilon_0 \frac{l}{\ln(\frac{l}{R_2})} l + \frac{l - \ln(2)}{\ln(\frac{l}{R_2})} + \frac{l - \ln^2(2) - \frac{\pi^2}{12}}{\ln^2 \frac{l}{R_2}} \qquad 3.1$$

The resistor characteristic R_{unit} includes the properties of the liquid inside the capillary and can be calculated using the following equation:

$$R_{unit} = \frac{\rho l}{A} = \frac{l}{\pi \sigma a^2}, \qquad 3.2$$

where l is the segment length, ρ the resistivity of the solution, A cross-section area of the capillary inner diameter, a the inner capillary diameter and σ the electrolyte conductivity. The cross-section of the liquid rod has a round form and could be calculated using equation 3.3:

$$A = \pi r^2, \qquad 3.3$$

where r is the inner radius of the capillary. The measured value for the solution conductivity σ is 116 μS/cm = 0.012 S/m. The solution resistivity is inversely proportional to the solution conductivity and equal $\rho = 1/\sigma = 86.2\ \Omega\cdot m$. The total calculated resistance value for a capillary unit with the length of 0.5 cm is $9.76\cdot10^6\ \Omega$.

The capillary parts were modeled as a chain of unit elements. Each unit element consists of a self-capacitance and resistance of this capillary unit. Such chain can be simplified to a single circuit element called RC-line. When the charge is transferred along the capillary from the coupling electrode to the emitter tip, the self-capacitance of the electrolyte is being charged. The charge flows further to the next unit only when the self-capacitance of the current segment is at least a little bit charged. This results in a time delay in signal propagation along the capillary.

The emitter tip has more complex geometrical parameters. Because the diameter of the emitter tip at the outlet has a value of 8 µm, and at the inlet the diameter is 75 µm, the last unit length could not be calculated using the common formula for resistance (equation 3.2).

The photo of the real emitter geometry is presented in figure 3.3. The emitter length was measured from the tip and has a value of 55 mm. The inner diameters were measured at the different emitter points. At the emitter tip the inner diameter has measured value of 8 µm. At the distance 0.5 mm from the tip, inner diameter has a value of 14 µm and at a distance of 10 mm inner diameter has a value of 75 µm. The emitter was split into the set of ideal truncated cones, and the partial resistance of each of them was calculated with integration. The calculated resistance of the first emitter part (with the length of 0.5 mm) has a value of $4.737 \cdot 10^8\,\Omega$. The second part of the emitter (length from 0.5 mm to 10 mm) has a calculated resistance value of $9.6 \cdot 10^8\,\Omega$. The third part of the emitter (length from 10 mm to 55 mm) has a resistance value of $8.48 \cdot 10^8\,\Omega$. The sum of those resistances and hence the total emitter resistance is $2.282 \cdot 10^9\,\Omega$.

It can be observed, that the resistance of the emitter has a value much higher in comparison with the normal capillary unit length resistance ($9.76 \cdot 10^6\,\Omega$). The resistance value for the emitter tip was included as a last element in the RC-element chain.

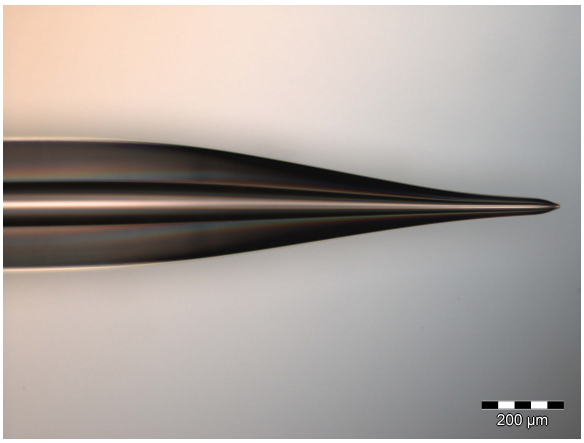

Figure 3.3 Photo of the fused silica emitter with parameters: 360 µm outer diameter, 75 µm inner diameter, 8 µm diameter at the tip.

The syringe parameters also were included in the calculations. The 500 mL volume syringe has 6 cm length. The capacitance of the syringe was calculated using the equation for the capacitance of rod in the open space 3.1 (0.43 pF).

3.3.2. Displacement current in injection electrode

The second model component is the capillary with the coupling electrode. The sputtered coupling electrode together with the silica capillary and electrolyte inside forms a cylindrical capacitor as shown in figure 3.4.

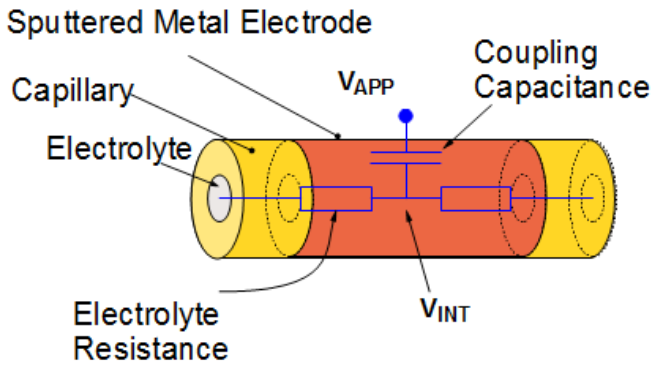

Figure 3.4 Schematic illustration of the capillary part with the sputtered coupling electrode and corresponding equivalent electrical elements.

An expression for capacitance C_m of the cylindrical capacitor, which consists of two conductors, when $R_1<R_2<<L_m$, is following:

$$C_m = \frac{Q}{V} = 2\pi\epsilon_0\epsilon_r \frac{L_m}{\ln(R_2/R_1)} \qquad 3.4$$

where L_m is the capacitor length (4 cm), R_1 the outer radius of the capillary (180 µm), R_2 the inner radius of the capillary (37.5 µm), ε_r the relative permittivity of the capillary material (3.82), ε_0 the dielectric permittivity of vacuum. The calculated value of the capacitance is 4.306 pF. The inner resistance of the electrolyte under the coupling electrode must also be considered. The value can be calculated using an equation from the resistor calculation for the unit length of the capillary (equation 3.2). Since the length of the injection electrode is 4 cm, the resistance was calculated for two pieces 2 cm each.

During the charging pulse, the top plate will be charged immediately with the corresponding sign. The inner capillary wall will be charged with the same sign.

3.3.3. Emitter geometry and counter electrode

The third part of the circuit consists of the emitter tip and counter electrode relationships description. In a physical setup, the counter electrode is grounded with the load resistance

R_{load}. The counter electrode also has a significant capacitance C_{load} to ground (see figure 3.5). In the case of a clogged emitter, the gap between emitter tip and counter electrode can be estimated with a gap capacitance. In the final open-emitter case, the non-linear element for electrospray current must be included.

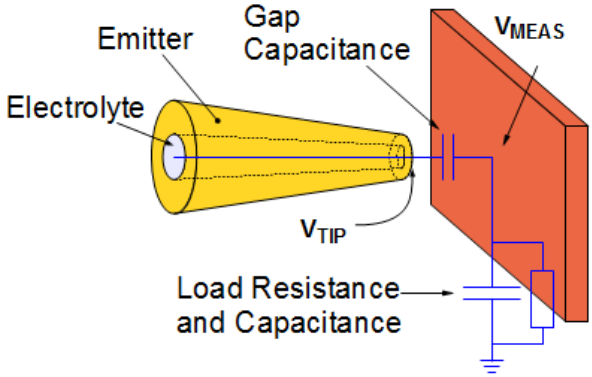

Figure 3.5 Schematic representation: emitter tip with the counter electrode.

In the current part of the work the electrospray element is not included in the model, because the ion movement in the capillary system should first be investigated without the electrospray formation process. In more detail the behavior including electrospray will be consider in paragraph 3.6.

3.4. Closed emitter model

All described elements were assembled in an equivalent circuit. The equivalent circuit of the real setup is presented in figure 3.6. The supply capillary consists of multiple discrete units (R_{unit}, C_{unit}), the number is determined by the physical length of the capillary. Emitter capillary consists of the same RC unit elements and an additional unit for the the emitter tip resistance (R_{TIP}). The supply capillary and the electrode capillary both creates two separate RC lines, which are connected together by the coupling electrode element. The coupling electrode includes two resistors and a cylindrical capacitor (R_{CPL}, C_{CPL}). The electromagnetic interaction between the initial edge of the the applied high voltage and the counter electrode, separated by a significant distance, is represented by a capacitance C_{EM_CPL}. The capacitance value is very small (a value of 0.075 pF was found in empirical way) and can be calculated in advance only using complex 3D field simulations. Being just a parasitic coupling, it is not critical for further electrospray analysis. The value has been empirically adapted in such a

way that the simulation of the electromagnetic signal peak height has been fitted to the measurements.

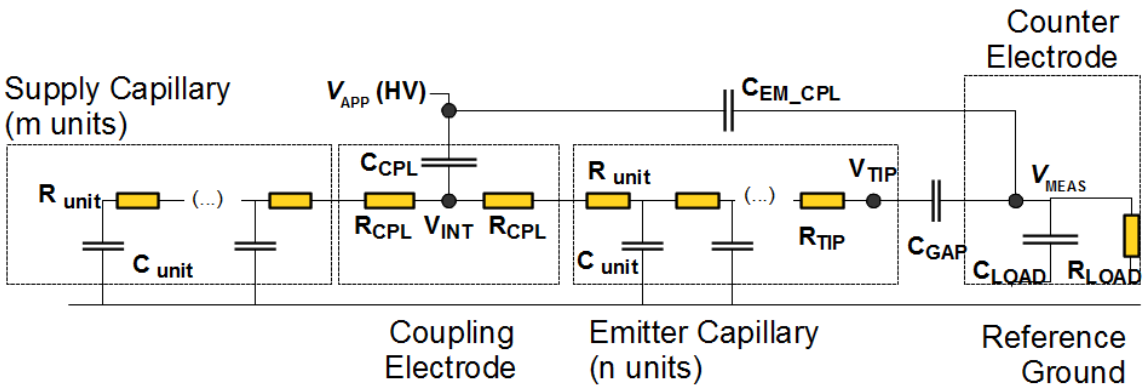

Figure 3.6 Equivalent circuit model for the experimental setup including all components except for the electrospray itself ("Closed Emitter Model")

Using this equivalent, circuit the potentials behavior in the different nodes of the setup was obtained. The most important characteristic for the electrospray formation process – formation of the voltage at the emitter tip will be described in the following paragraph.

3.4.1. Ion current in the capillary system

A square-wave V_{APP} have been applied to the coupling electrode. The applied voltage contains two phases. The first phase is the positive HV edge with a voltage slope of 20 V/µs (detemined by the HV generator capabilities). During the rising time, the capacitance C_{CPL} will be charged. The electrical charges are transferred by displacement current through the dielectric barrier of the fused silica capillary wall to the inner wall of the capillary. The opposite charges are accumulated at the outer and the inner wall of the capillary. The total amount of the charge transferred through the dielectric barrier can be estimated by the following equation:

$$dQ = dV_{APP} C_{CPL} \qquad 3.5$$

The value of this capacitance determines the total amount of charges, which is transferred to the inner wall of the capillary and forms the potential V_{INT} (see figure 3.7a). After the rising time, the applied voltage is constant (till time t_2), and the maximum amount of charges at the inner wall of the capillary beneath the coupling electrode is reached. The charges in the electrolyte affected by V_{INT} start to distribute in the capillary. The speed of this charge

transfer is limited by the resistance and self-capacitance of the electrolyte (R_{unit} and C_{unit}). In the electric model, the charges flow is gradually charging the segment self-capacitances.

From the physical point of view, the charge is transferred by the ion current in the electrolyte. When the charges reach the emitter tip, the potential V_{TIP} starts to rise. The final value of the potential at the emitter tip V_{TIP} depends on the applied voltage amplitude as well as on the ratio of the coupling electrode capacitance C_{CPL} and the total capillary self capacitance.

3.4.2. Charge and potential formation at the emitter tip

Figure 3.7 a shows a sketch of the applied voltage V_{APP}, the potential at the inner wall of the electrode capillary beneath the coupling electrode V_{INT} and the potential at the emitter tip V_{TIP}. With the positive HV edge at the time t_0, the polarization of the dielectric wall starts and positive charges will be accumulate at the inner wall of the capillary, forming the potential V_{INT}. The potentials at all other capillary points including the emitter tip still remain zero. In the time after t_0, when V_{APP} is constant, the anions are attracted towards the coupling electrode to the inner capillary wall, and the cations are pushed towards the emitter tip as well as to the opposite direction (to the syringe pump). As the anions reach the inner wall beneath the coupling electrode, they start to neutralize the positive charges in the inner wall of the capillary leading to the decrease of V_{INT}. At the same time V_{TIP} starts to rise (time period from t_0 to t_1). Both potentials tend to reach the same level, i.e. to “equipotentialize” the electrolyte). At the time t_2 a negative voltage edge with the same amplitude is applied. The negative charges will accumulate at the inner wall of the capillary and V_{INT} changes to a negative value. Subsequently the cations are attracted towards the inner capillary wall beneath the coupling electrode, and the anions are pushed towards the emitter tip as well as to the electrolyte source. As the cations reach the inner wall beneath the coupling electrode they start to neutralize the negative charges in the inner wall of the capillary leading to the decrease of V_{INT} and the decrease of V_{TIP}. Both potentials will again reach the same value. Since the amount of positive and negative charges accumulated by polarization at the inner wall of the capillary is equal, the total charge in the system is zero before the next period starts.

When the positive HV edge is applied, a small charge transfer occurs by electromagnetic transmission between the cables of the HV source and the counter electrode. The counter electrode capacitance C_{LOAD} is charged. The potential at the counter electrode discharges immediately through the grounding resistance R_{LOAD}. This process causes the first high and short peak (in the range of µs) of the measured current response, which is obviously a parasitic effect. The position of this peak is schematically presented in figure 3.7 b with the red line.

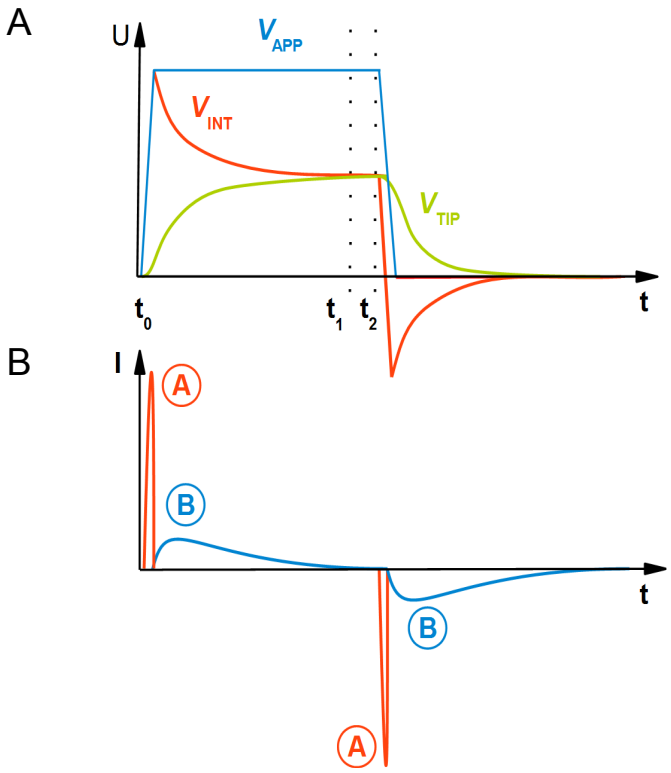

Figure 3.7 a) Applied HV signal form (red line) and initiated responses in the system: potential under the coupling electrode V_{INT} (green line) and potential at the emitter tip V_{TIP} (blue line); b) Current signals in the system as an responses for potential changes in the system (a – EMT signal response, b – ion current signal response).

The charge transfer through the capillary leads to a rising potential V_{TIP}. This rising potential produces the second much slower and weaker EMT via the air gap capacitor C_{GAP}. The current depends on the voltage rising edge at V_{TIP}, i.e. dV_{TIP}/dt, thus this current reaches a maximum in the beginning, and decreases exponentially over time. The charges are transferred to the counter electrode across the air gap by the EMT, resulting in the ion transfer current. When the EMT via the air gap decreases, the counter electrode is discharged through R_{LOAD}.

3.4.3. Model and experiment results comparison

In order to simulate the current response, the potential at the inner wall of the electrode capillary beneath the coupling electrode V_{INT} and the potential at the emitter tip V_{TIP} have to be determined depending on the applied voltage V_{APP} by simulation. Figure 3.8 depicts V_{APP} as well as the simulations of V_{INT} and V_{TIP} for three different electrode capillary lengths. Three length were involved in the simulation. The distance from the middle of the coupling electrode to the emitter tip was 17.5 cm, 23.5 cm and 33.5 cm. The supply capillary length was set to 80 cm. This corresponds to the physical measurement setups used in previous chapter.

The V_{INT} potential increases simultaneously with the applied HV edge (5.5 kV) leading to the separation of the charges according to figure 2.5 b. The potential V_{TIP} also increases. With the shortest emitter capillary (17.5 cm length), the tip potential V_{TIP} increases fastest (red dashed line at the figure 3.8 a. For longer capillaries, the charge transfer process occurs slower. Also, for all three lengths, a small time delay can be observed between the moment, when the HV edge is applied and the moment when V_{TIP} starts to increase (in the beginning of the time scale). This time is necessary for the first charges to reach the emitter tip. In the case of the longer emitter, the emitter tip potential reaches almost the same values as for the shortest emitter but slowly and hence later.

The rising potential at the emitter tip causes the EMT via the air gap, resulting in the ion transfer current signals which are shown in figure 3.8 b. Here, the simulated currents are presented for the three distances from the coupling electrode to the emitter tip (17.5 cm, 23.5 cm and 33.5 cm). This simulation shows a good correlation with the measured current signals at the load resistance R_{LOAD}.

For longer emitter capillaries, the transient processes in the system are slower, the voltage rising slope at the emitter tip is smaller, and the response current peak lower and appears later. This corresponds to the empirical observations made in the previous chapter.

Altogether, the charge transfer in the system from the coupling electrode to the emitter tip and then to the counter electrode has been modeled correctly.

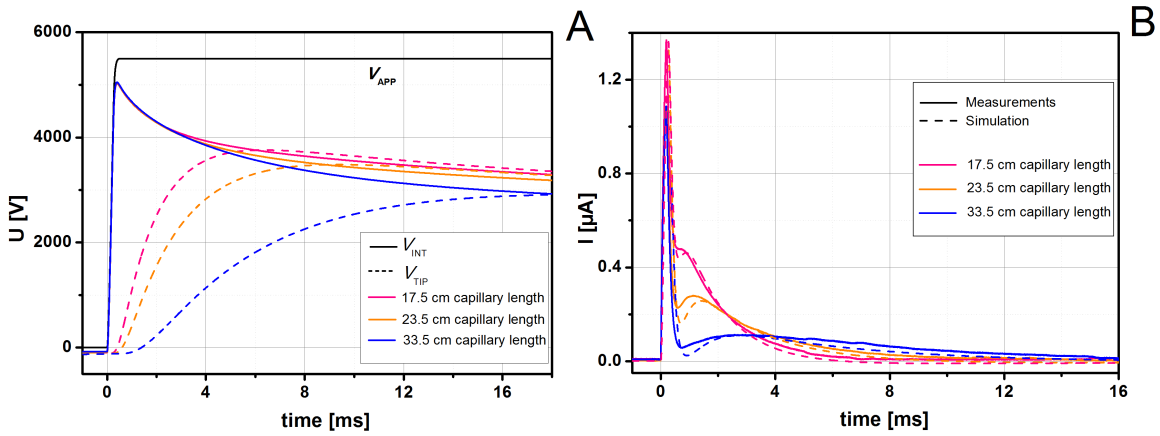

Figure 3.8 a) Simulated node potentials and b) Simulated currents. Clogged emitter case for various distances between coupling electrode and emitter tip: V_{APP}, applied voltage to the electrode; V_{INT}, potential at the inner wall of the electrode capillary beneath the coupling electrode; V_{TIP} potential of the electrolyte at the emitter tip; applied voltage 5.5 kV; f = 10 Hz; flow rate 0.3 µL/min; 1 % acetic acid.

The developed "Closed Emitter Model" is valid primarily for the clogged emitter case. However, the same behavior would be observed in an open-emitter case when the applied voltage is too low to ignite the electrospray. In this case the developed model can also be used for potential and current simulation.

3.4.4. Supply capillary influence on potential formation

During the phase after external voltage slope, where the applied voltage is constant (see figure 3.7 a, the charge in the capillary distributes in both directions from coupling electrode, i.e. to the emitter tip and to the supply capillary as well. The charge flows from higher to lower potential, tending to reach equipotential distribution along the capillary. In a simplified case when the supply capillary has a length same or similar to the emitter capillary, the charge will distribute somehow evenly. The charge distribution will stop, since there is no further way for the charge flow.

In the experimental system, the supply capillary length is significantly higher (80 cm), than the length of an emitter capillary (the maximum length was 33.5 cm). In this case the injected charge is also first evenly distributed into both directions. The charges reach the emitter tip and forms the potential V_{TIP}, and, hence the ion current peak can be detected. However, the charges pushed toward in the supply capillary direction do not meet any capillary end, and continue traveling forward. The supply capillary is long enough, and

sufficient time is available. The charge would equipotentially spread along the entire capillary length. This would mean, that the charges at the emitter tip will also travel back in the direction of the source, and the emitter tip potential would slowly decrease comparing to previously-discussed case. This however does not happen in practical setups, since the pulses are applied with sufficient frequency. Due to the same reason the influence of the components at far supply capillary end can be neglected – the charges are incapable to spread that far in a short time between the applied voltage pulse edges.

3.5. ESI – DC voltage-current characteristic

In the electrospray equivalent system the potential at the emitter tip, or more exactly, the voltage across the air gap, manages the electrospray current formation. Electrospray can be initiated, i.e. the electrospray current appears, when the potential at the emitter tip reaches the threshold value. Under the applied voltage pulses the potential at the emitter tip has rather complex time dependence, and the electrospray current will be produced in time depending on this tip potential.

Electrospray current could be introduced in such system using an active circuit element, the arbitrary voltage-dependent current source. The device is connected between the emitter tip node and the counter electrode and delivers an electric current which is dependent on the voltage between the nodes. This current-voltage dependency is initially not known, and has to be determined within this step.

3.5.1. Measurement of electrospray voltage-current characteristic

The current-voltage dependency for the electrospray was measured using the direct contact of the applied voltage to the solution inside the emitter tip with an approach similar to that proposed by Jackson and Enke [41].

An electrospray setup with direct contact electrode was assembled. An additional T-connector was inserted between emitter and supply capillary. A 50 μm metal wire was inserted as an external electrode and fixed to the third inlet of the connector (figure 3.9 a). The emitter was filled with the solution (water-methanol (1:1) + 1 % acetic acid) and a direct contact of wire to the solution was obtained. A standard load resistance of 500 kΩ was attached to the counter electrode. The load voltage was measured with an oscilloscope probe,

and the load current is calculated according to Ohm´s law. In such a system the high voltage was applied directly to the electrolyte, and the output ES current level can be measured for each applied voltage value.

The physical effects like the electrochemical contact at the electrode-to-electrolyte interface, the voltage drop at the solution resistance, the voltage drop at the air gap, and the charge neutralization process at the counter electrode are considered. An equivalent circuit for such setup is shown in figure 1.5. The electrospray current I_{ES} is measured as a function of the applied voltage V_{APP}. Using the equivalent circuit equations, the dependence of I_{ES} on the gap voltage V_{GAP} is calculated:

$$I_{ES} = f(U_{GAP}) \tag{3.6}$$

The voltages of electrochemical contact and charge neutralization are relatively small (several volts) compared to the applied voltage (several kV). Thus these effects may be neglected without any effect on the accuracy. Various couplings were described in the previous chapter have only an effect during the transient processes, i.e. immediately after some pulse has been applied to the system. DC mode measurement assumes that the current value is captured with significant time delay after the input voltage is applied, so that all capacitors are charged to their final state and the transient process is over. Hence the effects of these couplings are reasonably neglected for this measurement. The final equivalent circuit for this measurement is shown in figure 3.9 c.

In the described setup a square wave signal of 5 Hz with amplitudes from 1.0 kV to 2.2 kV with 0.2 kV step (zero offset) were applied to the input electrode. The current response was measured at the load connected to the counter electrode. One measurement with an applied voltage of 1.6 kV is shown in figure 3.10.

A high, but short current peak at the HV edges is the parasitic EMT signal, as described for the system with a closed emitter. A small fluctuations on the current signal in the first several milliseconds correspond to the current stabilization process, i.e. transient processes in the circuit involving capacitive recharge. After this transient process is finished, the current level stabilizes, and does not change anymore. This corresponds to system DC state under the applied voltage level. The averaged DC values can be captured for positive and negative currents.

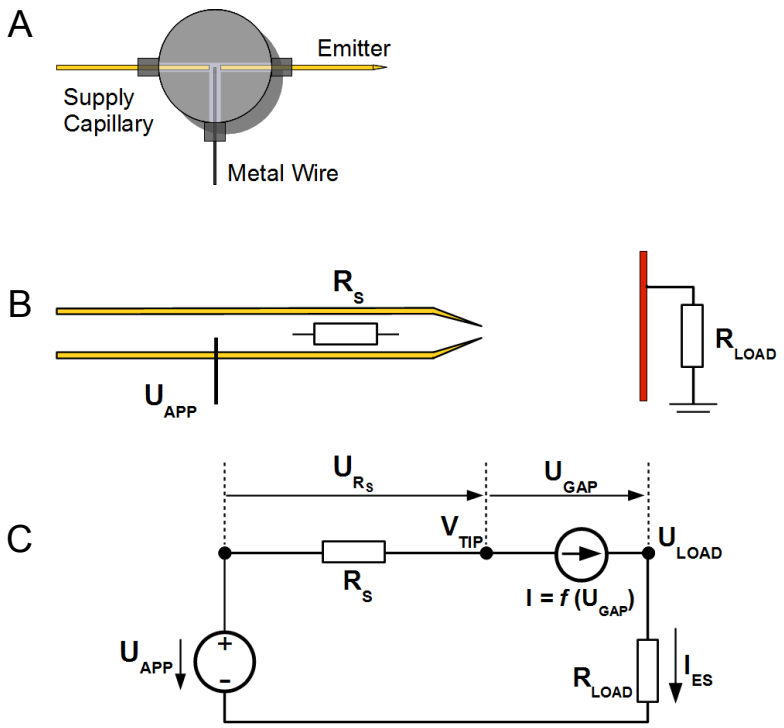

Figure 3.9 a) Overview of the T-connector for current-voltage characteristic measurements using the direct contact to the electrolyte solution; b) Sketch of measurement setup; c) Equivalent circuit with an active element for electrospray.

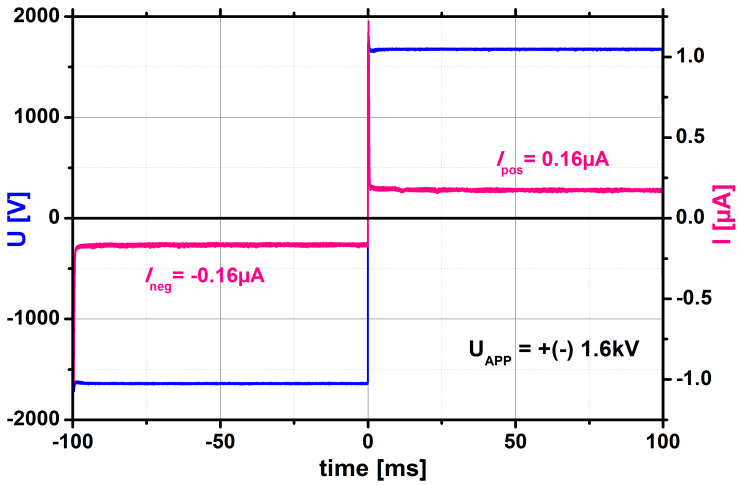

Figure 3.10 Single measurement of the current response (red line) for applied DC voltage with an amplitude of +1.6 kV and -1.6 kV (blue line).

3.5.2. Consideration of voltage drop at electrolyte resistance

In the case of non-conducting needles a significant voltage drop at electrolyte resistance was predicted, and must also be considered in the calculation.

During the measurement, a high voltage V_{APP} is applied, and the response voltage U_{LOAD} is measured. Since the circuit is a closed loop, the same current flows though all elements, and the electrospray current is equal to the load current and can be calculated as:

$$I_{ES} = I_{LOAD} = \frac{U_{LOAD}}{R_{LOAD}} \tag{3.7}$$

The total applied voltage V_{APP} drops on the three series elements in the current flow:

$$U_{APP} = U_{Rs} + U_{GAP} + U_{LOAD} \tag{3.8}$$

where U_{RS} , U_{GAP} and U_{LOAD} are the voltage drops on the electrolyte resistivity, on the air gap with electrospray, and on the resistive load, respectively. The potential at the emitter tip, V_{TIP} can be written with equation:

$$V_{TIP} = U_{GAP} + U_{LOAD} \tag{3.9}$$

The measured currents have peak values of several hundred nanoamperes, so the expected load voltages do not exceed units of volts. Under this assumption, the load voltage can also be neglected comparing to the capillary and air gap voltage drops. The gap voltage is then almost equal to the potential at the emitter tip, and the equations may be simplified to the form:

$$V_{TIP} \approx U_{GAP} \tag{3.10}$$

$$U_{APP} = U_{Rs} + U_{GAP} \tag{3.11}$$

The voltage drop on the electrolyte is directly proportional to the current:

$$U_{Rs} = I_{ES} R_s \tag{3.12}$$

The unknown gap voltage can be calculated as

$$U_{GAP} = U_{APP} - I_{ES} R_S \tag{3.13}$$

where the value of the electrolyte resistance R_S for the totally involved emitter length can be calculated using method, explained in the paragraph 3.3.1. For the current setup R_S had a value of $2.28 \cdot 10^9\,\Omega$.

The dependence of electrospray DC current on the applied DC voltage V_{APP} is measured. Assuming the equation 3.13, for each applied DC voltage V_{APP} the corresponding gap voltage U_{GAP} is calculated, and the dependence of electrospray current on the gap voltage is obtained. The resulting curves are shown in the figure 3.11 in next section.

3.6. Final DB – ESI model

In order to get a comprehensive model for the processes involved in the electrospray formation, the "Closed Emitter Model" has to be extended by the electrospray current itself. The voltage-current characteristic was obtained by the measurement with a common electrospray setup where the voltage electrode is directly contacted with the electrolyte (see section 3.5.1) and is further implemented as an arbitrary voltage-dependent current source containing the piece-wise linear approximation of the measured dependence.

3.6.1. Current source implementation in the circuit model

In terms of an electric circuit, the dependency of the electrospray current on the air gap voltage U_{GAP} must be obtained by measurement and subsequently substituted into a circuit element. The electrospray current I_{ES} was measured as a function of the applied DC voltage $U_{APP\,DC}$. The result is given in figure 3.11 with the black dots. Using a procedure described in section 3.5.2, the voltage drop at the internal electrolyte resistance was considered, and the I_{ES} current dependence on the gap voltage U_{GAP} was obtained. The curve is shown at the figure 3.11 with the red dots.

The voltage-current characteristic U_{GAP} vs I_{ES} was approximated with a few-points tabular model with the linear interpolation between the points. Positive and negative current directions are handled separately, i.e. the same piece-wise linear approximation principle is used, but the points are defined independently.

The simple form of this tabular approximation allows good understanding of the model behavior. Below some threshold voltage level, the current is considered to be zero. This corresponds to the case where the gap voltage is insufficient for the electrospray to be started. Above the threshold voltage, the electrospray current appears and increases strongly within a smaller voltage range.

This piece-wise linear dependency shown in figure 3.11 with the red line was implemented into the voltage-controlled current source $I = f(U)$. Controlled current source was implemented in the existing circuit, described in the "Closed Emitter Model" (figure 3.6). In the resulting circuit the electrospray current is considered, and the electrospray formation can be simulated. The resulting circuit with the implemented controlled electrospray current is presented at the figure 3.12.

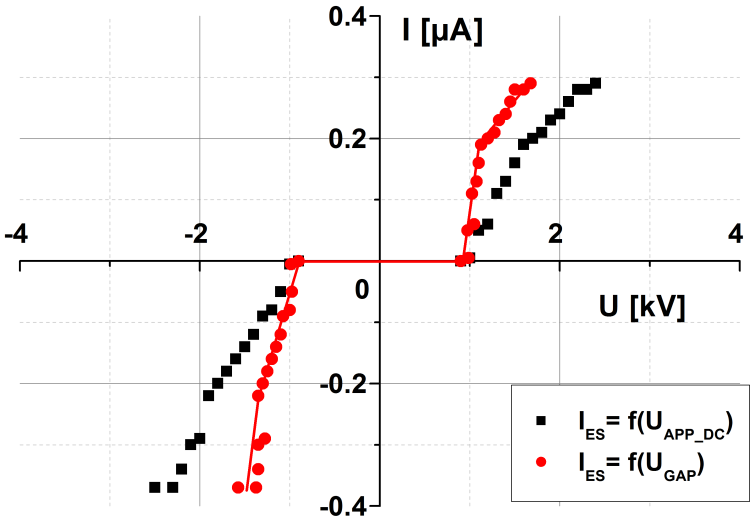

Figure 3.11 Black dots: measured electrospray current as a function of the applied DC voltage; Red dots: measured electrospray current as a function of calculated gap voltage.

The simulation of potentials and currents in the setup under the applied voltage pulse was performed for three fixed distances from coupling electrode to the emitter tip. The distances were the same, as in the case of "Closed Emitter Model" and have values of 17.5 cm, 23.5 cm and 33.5 cm. A simulation of the potential formation was performed for two cases: foe the first pulse applied to the system and after approx. 1000 pulses of applied voltage.

The formation of the potentials at the emitter tip as well as at the capillary under the coupling electrode is shown in figure 3.13 a. Straight lines are used for the potentials under the coupling electrode V_{INT}, dashed lines are used for the potential at the emitter tip V_{TIP}. The resulting emitter tip potential that appears in the open system is different from the same potential in the closed emitter model.

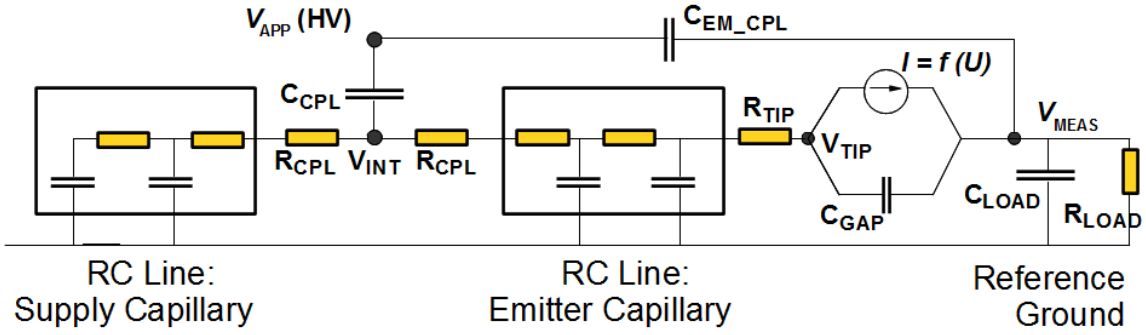

Figure 3.12 Final equivalent circuit for the DB-ES system. Supply capillary and electrode capillary are presented as a RC line objects, the electrospray controlled current source is included.

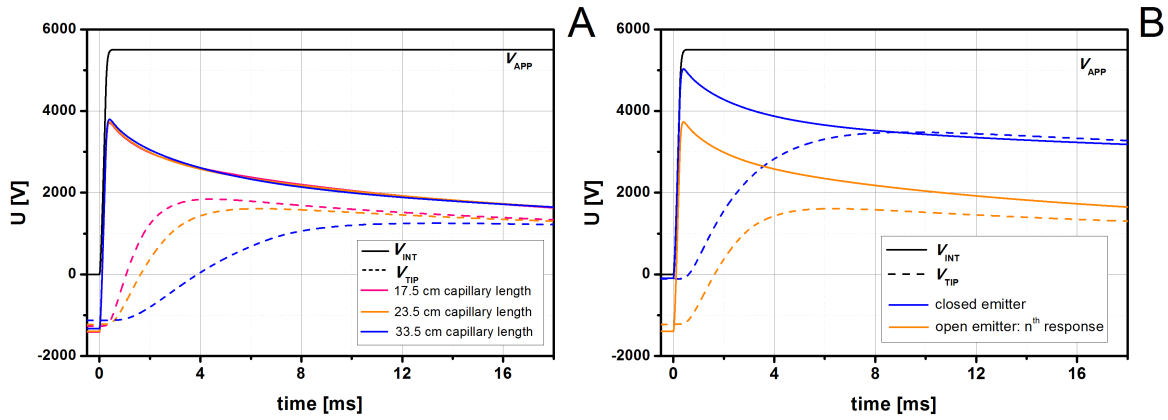

Figure 3.13 a) Simulated potentials at the inner wall of the electrode capillary beneath the coupling electrode V_{INT} (straight lines) and potential of the electrolyte at the emitter tip V_{TIP} (dashed lines) for open emitter for nth responses number for three different distances from coupling to emitter tip; b) Simulated potentials at the inner wall of the electrode capillary beneath the coupling electrode V_{INT} and potential of the electrolyte at the emitter tip V_{TIP} for closed emitter (blue lines) and for open emitter (red lines) for nth responses for fixed from coupling to emitter tip distance 23.5 cm. V_{APP} value in all cases was 5.5 kV

The potential formation with and without electrospray current is shown explicitly for one fixed distance from coupling to the emitter tip (23.5 cm) in the figure 3.13 b. The difference is best observed after some time of system operation, e.g. after 1000 applied voltage pulses are applied (nth pulse). Blue lines show the potentials under the coupling electrode V_{INT} (straight line) and at the emitter tip V_{TIP} (dashed line) for the closed emitter case. Red line shows both potentials in the case, when the system is open and the controlled current source is used to initiate the electrospray current. An obvious shift of the initial signal levels at the moment of the applied voltage edge can be observed.

3.6.2. Potential formation in the system with the electrospray

Figure 3.13 b shows the significant difference in the potential formation process, when the system is closed and when electrospray is initiated. An obvious shift of the initial signal levels at the moment of the applied voltage edge can be observed.

The potential formation at two nodes (under coupling electrode and at the emitter tip) in the case without the electrospray current is shown in figure 3.14 a. At the time t_0 the applied voltage V_{APP} initiates the charge movement in the closed capillary system. During the rising edge of the applied voltage the potential under the coupling electrode immediately rises. With a short time delay the emitter potential also starts increasing. In the time, when the applied voltage is constant, the potential at the tip tends to reach the equilibrium with the potential under the coupling electrode. If the applied pulse is long enough, the equipotential state will be reached, and the system will remain stable until the negative edge of the applied voltage appears at t_1.

In the closed emitter case all charge transfer processes in the electrolyte occur due to the polarization inside the capillary wall and thereby due to displacement current. When the applied voltage returns back to its initial value (after one cycle of positive and negative edge), the total amount of charges in the electrolyte will be the same as before the applied pulse. The total charge of the electrolyte does not change from one cycle to another, and the results obtained for the first and the rest consecutively applied pulses are the same.

Figure 3.14 b shows the potential behavior at the same nodes, when electrospray current is present in the system. The potential formation in the system with the open emitter are shown in the figure 3.14 b together with the closed emitter case. When the positive voltage edge is applied, it leads to an immediately increased potential under the coupling electrode and in the time after t_0 the potential at the tip starts to increase in the same way as was described for the closed emitter system. When the potential at the emitter tip rises over the threshold necessary for electrospray ionization (V_{ES+}), the electrospray current appears in the system. In figure 3.14 b the electrospray threshold voltage is shown with the straight line V_{ES+}.

The electrospray current carries the charge from the tip to counter electrode. Due to this discharge current the tip potential starts to decrease comparing to the closed emitter case. The positive electrospray current would continue until V_{TIP} decreases asymptotic with V_{INT} to the respective electrospray threshold value V_{ES+}. At this moment, when the tip potential is

insufficient to produce electrospray anymore, the system comes to a stable state, and no more currents are present in the system until then the negative voltage edge is applied.

During the negative edge, the V_{INT} potential is decreased by the displacement current in the coupling electrode. The injected negative charge spreads throughout the capillary to the tip. When the potential value at the emitter goes below the V_{ES-} value, the negative electrospray is initiated. In the same way, as described for the positive spray, the negative electrospray current will discharge the tip towards zero potential, until both V_{TIP} and V_{INT} reach asymptotically the respective electrospray threshold value V_{ES-} from below. The potential remains at this level until the new voltage edge is applied.

As could be seen from the figure 3.14 b, the potential levels in the closed and open systems after one positive and one negative cycle are different. In the closed system (dashed lines) the electrolyte potential returns to zero after the entire cycle. In the open system case the potential stays at the value V_{ES-}. This is caused by the presence of the electrospray current. In the closed emitter case the charge is transferred to and from the electrolyte with displacement currents only. These currents perform the temporary reversible charge transfer only, i.e. after the applied voltage returns to zero and the corresponding transients are over, the total amount of charge transferred to the electrolyte also returns to zero. In the open emitter case due to the electrospray current the charge is irreversibly transferred from the system. Therefore, the total charge in the electrolyte after the applied voltage returns to the original value will be different from its initial value by the amount of charge transferred by the electrospray current.

After the negative electrospray current has stopped in the end of the cycle, some amount of negative charge remains at the tip. This is the charge necessary to keep the tip potential at V_{ES-} level. When the next positive edge is applied, these negative charges have first to be compensated. Electrically, both potentials start from V_{ES-} level which remains in the system since the time t_2 instead of original zero level. This is the reason why the first and n^{th} responses in the open-emitter case emitter has to be distinguished.

As a proof for this discussed theory, the potential simulation in case of the first electrospray response and the n^{th} response were performed. Simulated potentials at the inner wall of the electrode capillary beneath the coupling electrode V_{INT} and the potential of the electrolyte at the emitter tip V_{TIP} for an open emitter for 1^{st} and for n^{th} responses are shown in figure 3.15 a.

The system parameters remain the same as in the simulation in the previous paragraph: the distance from the coupling electrode to the emitter is fixed at 23.5 cm, the applied voltage is 5.5 kV. The first positive electrospray current component will be faster initiated (from t_0 to the intersection of V_{TIP} with V_{ES+}) than the negative one (from t_1 to the intersection of V_{TIP} with V_{ES-}) or the second positive electrospray current component (from t_2 to the intersection of V_{TIP} with V_{ES+}). It could be observed in the simulation results for the consequent edges that V_{TIP} starts with a negative value and reaches the electrospray threshold later as in the 1st response.

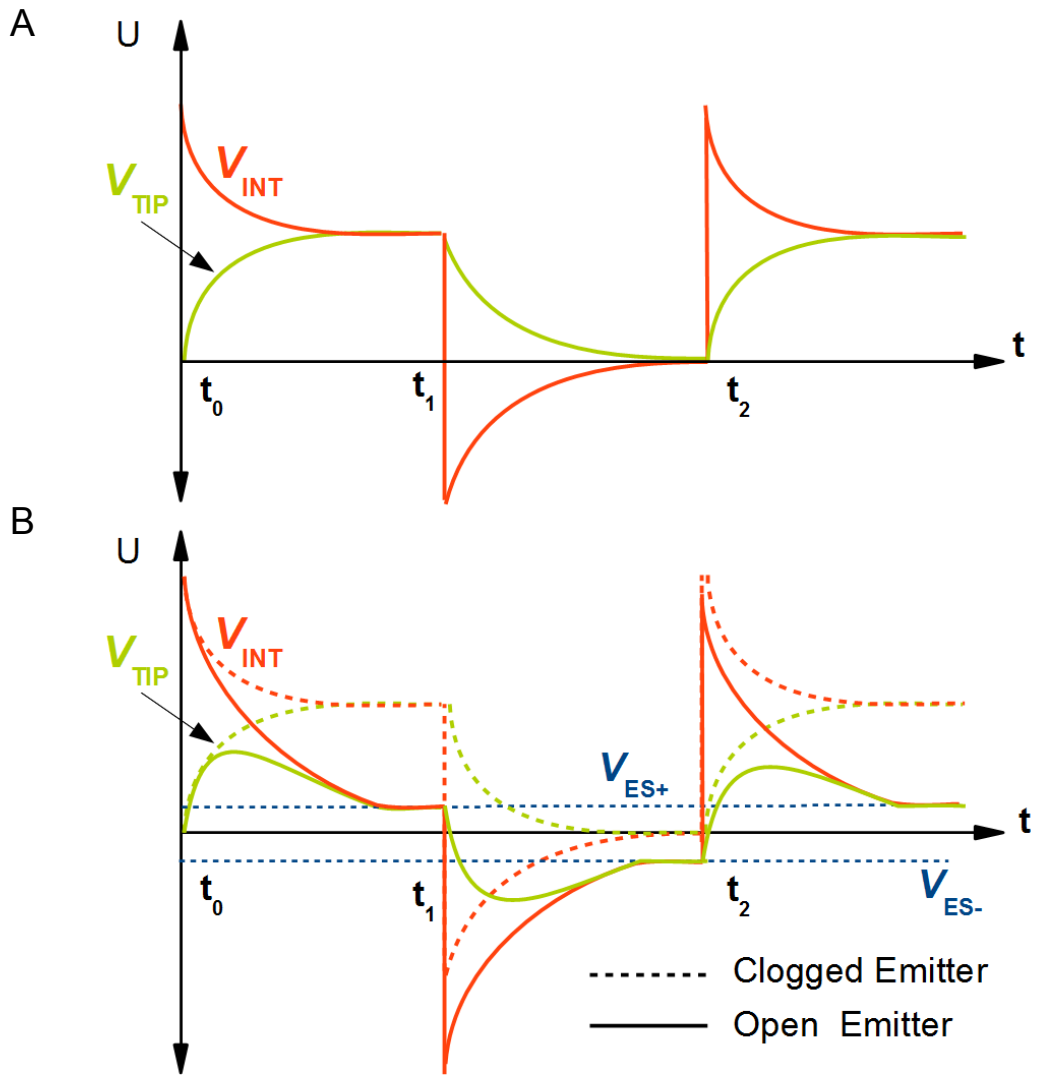

Figure 3.14 a) Potential formation process under the coupling electrode (V_{INT}) and at the emitter tip (V_{TIP}) in the closed capillary system, when electrospray is not initiated; b) Potential formation process under the coupling electrode (V_{INT}) and at the emitter tip (V_{TIP}) in the closed capillary system, when electrospray is not initiated (dashed lines) and potential formation process under the coupling electrode (V_{INT}) and at the emitter tip (V_{TIP}) in the open capillary system, when electrospray is initiated (straight lines).

Figure 3.15 b shows the simulated at the same conditions potentials at the wall under the coupling electrode and potential at the emitter tip for the first response (green lines) and the same potentials for the closed emitter case after n^{th} applied voltage edge. The potential at the tip starts to rise with the same derivative. When the potential value at the emitter tip reaches the threshold value, the electrospray current appears and potential at the tip starts to decrease. After electrospray starts, the derivative of potential curve at the emitter tip for the open emitter is lower in comparison with the closed emitter system. The stable electrospray formation in the open system is a cause of the negative derivative of the second part of the potential at the emitter tip curve.

A small time delay can be observed between the moment, when the HV edge is applied and the moment when V_{TIP} starts to increase (in the beginning of the time scale). This time is necessary for the first charges to reach the emitter tip. In the case of the longer emitter capillary, the emitter tip potential reaches almost the same values as for the shortest emitter but slowly and hence later.

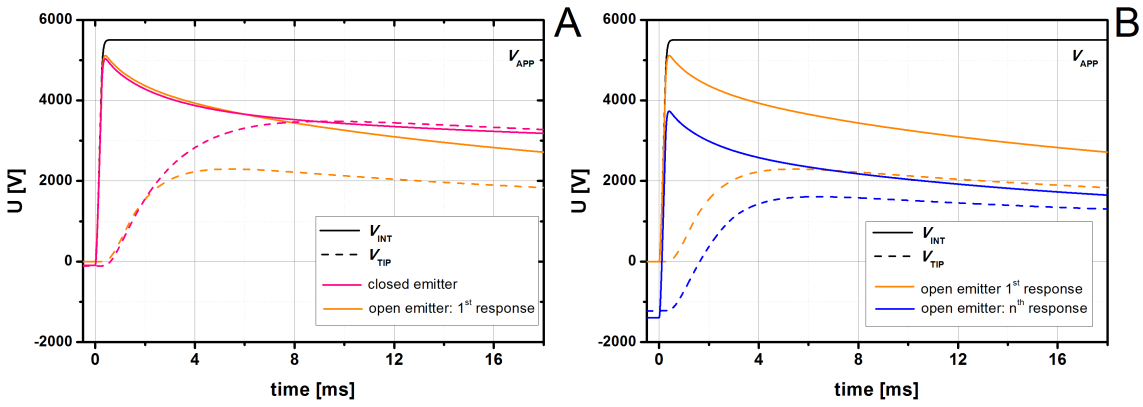

Figure 3.15 a) Simulated potentials at the inner wall of the electrode capillary beneath the coupling electrode V_{INT} and potential of the electrolyte at the emitter tip V_{TIP} for closed emitter for n^{th} (blue lines) and for 1^{st} (green lines) responses. Distance from coupling to emitter tip is fixed at 23.5 cm. b) Simulated potentials at the inner wall of the electrode capillary beneath the coupling electrode V_{INT} and potential of the electrolyte at the emitter tip V_{TIP} for open emitter for n^{th} (red lines) and for 1^{st} (green lines) responses . Distance from coupling to emitter tip is fixed at 23.5 cm;

3.6.3. Model and experiment results comparison

With the developed model the individual current components in the system with initiated electrospray can be simulated.

The distance between coupling and emitter tip was fixed at 23.5 cm. The supply capillary length was fixed at 80 cm. Positive and negative edges with an amplitude of 5.5 kV at 10 Hz frequency were applied. The comparison of the simulated current components for open and closed emitter models are shown in figure 3.16 a.

The EMT signal remains the same in both cases, since it physically doesn't depend on the emitter state.

In the open emitter case, the electrospray current (presented with the black line) appears when the gap voltage and thereby V_{INT} exceeds the necessary threshold.

The ion current peak has a different shape in closed and open cases. The ion current peak corresponding to the system with the closed emitter is presented in red color. The ion current peak formed in the open emitter system is shown using green color. In the system where the electrospray current is present, the ion current starts to decrease faster, than in the closed system. Faster decreasing starts at the moment, when V_{TIP} have reached the V_{ES+} value (see figure 3.14 b) and the electrospray current appears. This electrospray current additionally discharges the tip, reducing the signal transfer to coupling electrode.

Figure 3.16 b shows the difference in formation of electrospray current components after the first n^{th} positive applied voltage pulses. The response for the first pulse is shown with the straight lines, the response for the following positive pulses is shown with the dashed line. The electrospray current formed with the first pulse is larger in comparison with the n^{th} applied pulse. This behavior is the direct consequence of the internal charge accumulation in the electrolyte, described in figure 3.15 a. The presence of the negative charge at the emitter tip before the n^{th} applied pulse edge is the cause of the later and weaker electrospray current response.

Under the same operation conditions, at the figure 3.16 c the simulated for total current at the counter electrode for closed and open emitter systems are presented in comparison with the measurement results. Dashed lines show the simulated data, straight lines show the measured response. The formation of all three current components at the counter electrode is handled by the model with high accuracy. Moreover, almost the same response can be observed in both open- and closed emitter cases up to the moment when the third current

component, the electrospray current, appears. The same behaviour is observed in both simulation and measurement.

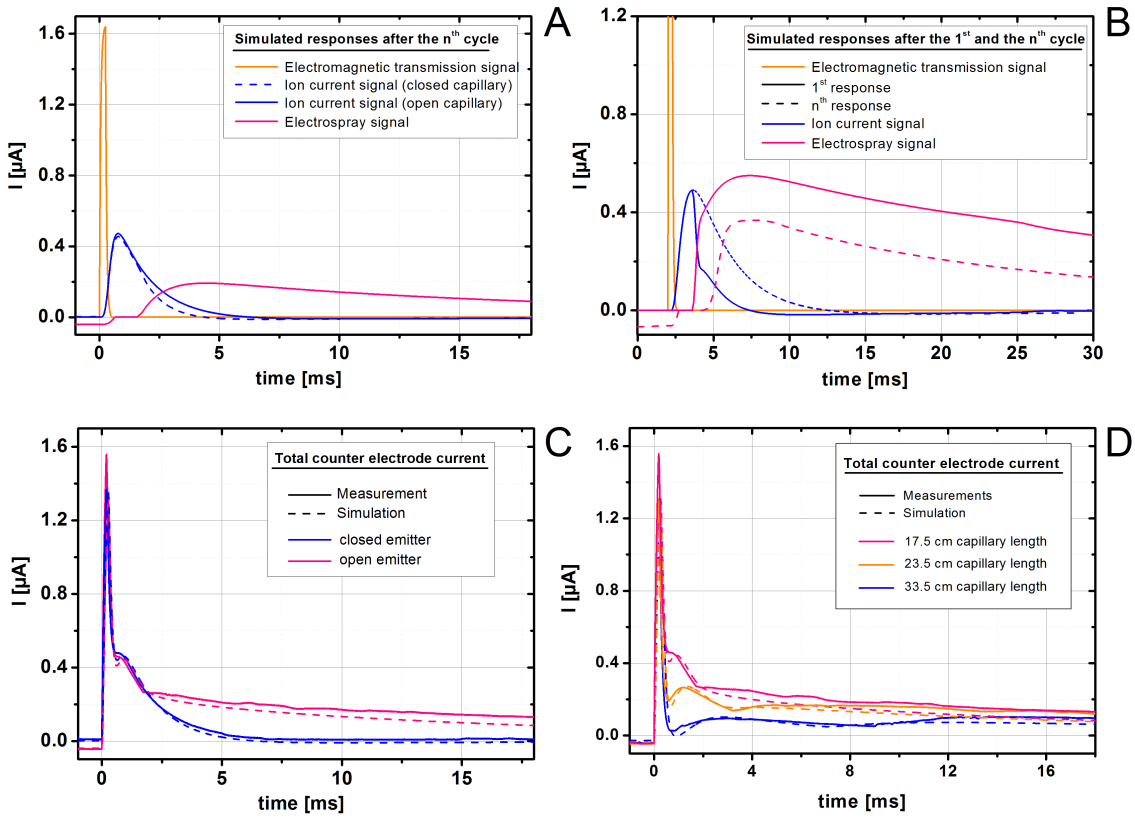

Figure 3.16 a) Simulations of the individual components of the current response the closed and the open emitter. n^{th} applied voltage edge, distance between emitter tip and coupling electrode is 23.5 cm; b) Simulation of the individual current components for the open emitter under the first applied pulse (straight lines) and n^{th} applied pulse (dashed lines), distance between emitter tip and coupling electrode is 23.5 cm; c) Total counter electrode current for the open and closed emitters, simulation vs measurements; d) Total counter electrode current for open emitter setups with different distances from coupling electrode to emitter tip; other parameters: 5,5 kV applied voltage, 10 Hz frequency.

The same total counter electrode current curves for the open emitter case are presented at the figure 3.16 d for three different distances from the coupling electrode to the emitter tip. The distance from the middle of coupling electrode to the emitter tip was 17.5 cm, 23.5 cm and 33.5 cm. As before, the dashed lines show simulated curves and straight lines show the measured current responses. This simulation shows good correlation with the measured signals.

The accuracy of the presented electric model is confirmed by a comparison between simulated and measured current signals for different capillary lengths with open emitter. The

electrospray current response for consequently applied pulses in simulation also appears later, and is significantly weaker, than for the first pulse.

Since mainly the n^{th} response is essential for a stable electrospray, in most of the presented simulation results (except the figure 3.16 b), the responses on the n^{th} applied pulse were shown and discussed.

3.7. DB-ESI-MS: the signal intensity control

3.7.1. Model-based optimizations of the DB-ESI setup

The knowledge obtained using the developed DB-ESI setup electric model allows to optimize the parameters of the DB-ESI setup to obtain the stable and high electrospray signal levels.

The first and obvious optimization is the location of the coupling electrode. The simulations have shown that the time delay necessary for the ions to travel to the tip increases significantly with the capillary length, and may not be neglected. In the following experiments with the MS the coupling electrode is always be located at the emitter with shortest possible distance to the tip.

The second much less obvious optimization concerns the usage of single instead of sequential applied pulses. The simulation has shown, that due to uncompensated charge transfer by the one-polarity electrospray current, the uncompensated charge of opposite polarity may accumulate in the capillary at the end of the pulse. The sequentially-applied pulses must first neutralize these charges, and therefore a later and weaker electrospray signal may be observed.

The measurement verification of the effect was performed. The setup of the default configuration was assembled. The emitter (360 o.d., 50 i.d. and 5.5 cm length) was connected with the supply capillary. The coupling electrode (2 cm length) was sputtered on the emitter. The middle of the sputtered electrode was at 2.5 cm distance from the emitter tip. The HV pulses were applied as sequences of two pulses with large time delay between these sequences, and the total counter electrode current was measured. The results are presented in the figure 3.17.

Since in current configuration the coupling electrode was located almost at the emitter, the first two parasitic peaks can not be separated. However, the ES current during the first pulse is obviously higher than during the second pulse. The time between the first and the second pulse is too short for the negative electrospray to compensate the charge in the electrolyte. Therefore the second pulse is applied with unfavorable initial conditions with high initial negative charge in the capillary. The large time delay between the sequences is sufficient for the negative spray to discharge the electrolyte, thus the "first" pulse of the next sequence again shown higher electrospray signal value.

The observed effect confirms empirically the necessity of using the single applied pulses with sufficient time delays between them in final configuration with MS.

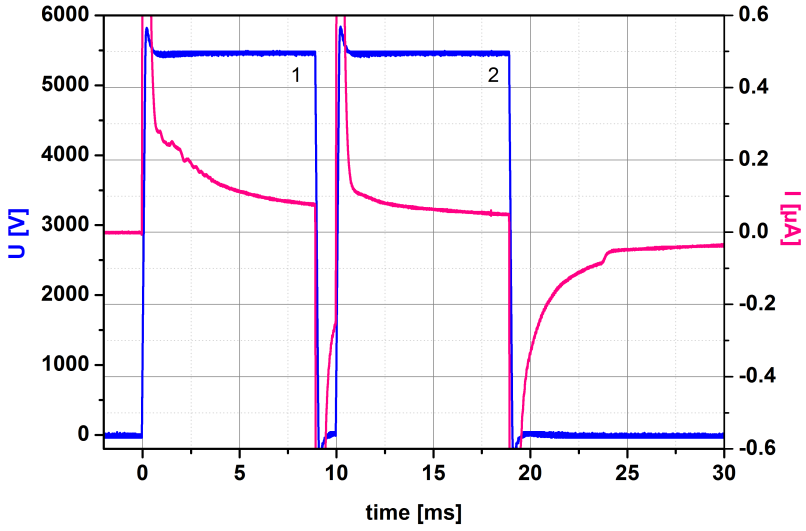

Figure 3.17 Measured first and second current responses for the DB-ESI in the triggered mode. Trigger time 18 ms, voltage 5.5 kV, f=100 Hz, Δt_{pos}=8 ms.

3.7.2. Positive and negative ions generation for MS analysis

With the DB-ESI source the positive and the negative ions generation is possible. The function generator determines the working frequency of DB-ESI source and hence, the pulses duration. During the positive half period of applied voltage Δt_{pos} positive ions and during the negative half period Δt_{neg} negative ions are sprayed.

The MS instrument provides the analysis only in one selected mode, where only the one polarity ions can be detected. The analytical time in MS consists of the ion injection time

and the time of mass analysis. During the injection time the ion trap opens for a discrete time to collect the analytes. The duration of the injection time is controlled with the instrument software. The injection time is followed by the time in which the received data is evaluated. This time is variable and dependents on the utilized mass/charge range and on the duration of the injection time.

In the DB-ESI-MS collaboration, the time of the ion production and the time of the ion analysis are independent. In Δt_{pos} charges are generated, which can be detected by the mass spectrometer in the positive mode. Since both systems, the DB-ESI and the MS, run independently, the initial points of Δt_{pos} in DB-ESI and the injection time of the ion trap are random. During the positive scan mode in MS, Δt_{neg} ions can be produced by DB-ES, however, they can not be detected. This means, that in different working cycles of MS the different amount of positive ions Δt_{pos} is detected, that hence leads to the total intensity current (TIC) signal decreasing. To withdraw the impact of Δt_{neg} it needs to be shifted towards the data evaluation time. This could be achieved by triggering the MS synchronously with the DB-ES. Technically, this could not be realized due to a limited control of the MS functionality. On the other hand, the DB electrospray can easily be synchronized ("triggered") to the MS ion injection time window.

3.7.3. Experimental investigation of triggering effectiveness

The measurements of the electrospray signal levels were performed with the MS in continuous and triggered DB ES using a sample analyte for experiment purposes.

The syringe was filled with the water-methanol solution (1:1) + 1 % acetic acid with reserpine concentration of 10^{-6} mol/L. The flow rate was fixed at 0.3 µL/min. The capillaries with the inner diameter of 50 µm were used. The coupling electrode with 2.5 cm length was placed on the emitter in the middle (emitter parameters: i.d. 50 µm, o.d. 360 µm, 8 µm at the tip). The square voltage pulses with 5.5 kV amplitude and 100 Hz frequency were applied with different duty cycles: 50 % and 80 %. Under this conditions, the times Δt_{pos} were 5 ms and 8 ms correspondingly and the Δt_{neg} was 5 ms and 2 ms correspondingly.

MS injection times were variable: 5 ms, 8 ms and 10 ms in the different experiments as shown in figure 3.18 (ion trap). The subsequent time for data evaluation was approximately 50 ms. The skimmer in front of the octopole leading to the ion trap was switched, when the

ion trap was opened. Here a 3 ms long signal could be taken by an opto-coupler and used as starting signal for the trigger initiating the DB-ES. (Skimmer 3 ms signal at the figure 3.18). The trigger pulse width here was adjusted to 1 ms. The rising edge of the signal was used to trigger the high voltage pulse applied to the DB-ES. For a single trigger only one period of the high voltage pulse was applied to generate the electrospray. The time of the positive electrospray depends on the HV pulse width, which is technically defined by total pulse period of 10 ms and the duty cycle of 50% and 80%. The negative edge is applied in any case, and due to the fact that no second positive edge follows, the negative spray is present for sufficient time during the MS data evaluation, so that the system is discharged to a possible maximum.

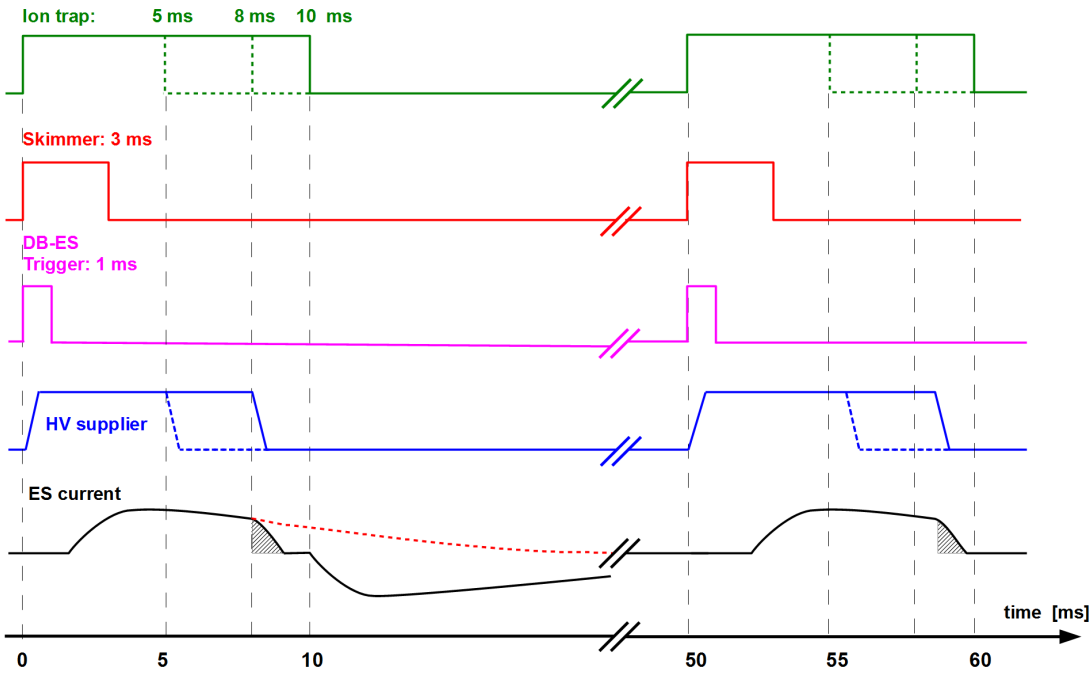

Figure 3.18 Schematic diagrams corresponding to one generated positive electrospray: MS ion trap open times (5, 8 and 10 ms for different experiments), skimmer 3 ms signal starts the trigger signal with the 1 ms duration. Triggered HV supplier signal with 50 % and 80 % duty cycles; generated electrospray current signal, which is detected by the MS.

The time necessary to transport the ions to the emitter tip can be found by simulations using the developed DB-ES model. The value is close to the 1.3 ms for the current setup configuration. This can also be proved by measurements shown in figure 3.19.

The total ion current was measured with continuous (non-triggered) DB ES with injection times of 0.5, 1.2, 1.3 and 1.5 ms. The same measurement was repeated for the triggered DB

ES. In triggered measurements with the injection time below 1.2 ms no signal was detected at all, whereas with an injection time of 1.3 ms a very weak signal and with 1.5 ms a stable signal level could be measured. This occurs due to the time necessary for the ion transport to the tip. In case of a too short injection time window, the triggered DB-ES is incapable of delivering the ions and starting the ES within the short time. If the injection time is sufficient, a signal of much better signal-to-noise ratio is delivered.

Figure 3.19 b presents the absolute intensity dependence on the MS injection time. The DB-ES HV voltage pulses of 5.5 kV amplitude, 100 Hz frequency and 80 % duty cycle were applied with the same triggering mechanism as described before. The MS injection time was increased from 0.1 to 30 ms with the some step. The first MS responses have been detected at the 1.25 ms injection time ($5.12 \cdot 10^2$). However, only starting with 1.3 ms of the injection time the stable non-interrupted spray could be observed.

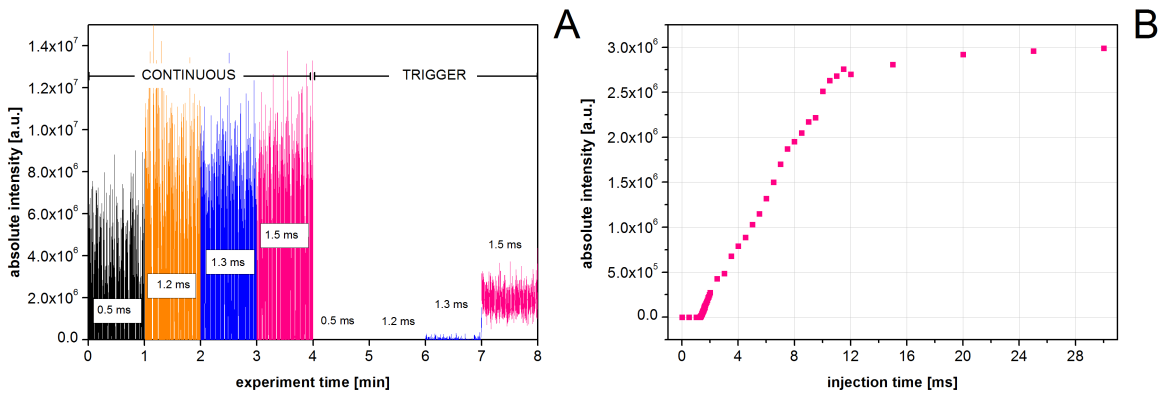

Figure 3.19 a) Measured TIC signal for different MS injection times (0.5 ms, 1 ms, 1.3 and 1.5 ms) for continuous and triggered mode; b) Absolute signal intensity dependence on MS injection time when trigger is used.

In order to investigate the impact of the properties of the continuous and the triggered DB electrospray the electrospray performance was monitored by the mass spectrometer. In the figure 3.20 a and 3.20 b the TIC and in figure 3.20 c and 3.20 d the spectra of the continuous and the triggered DB electrospray are shown.

A clear coherency between the shape of the TIC and the injection time was observed. When the injection time is set to 5 ms and the half period Δt_{pos} is 5 ms, the TIC of the continuous measurement varies between zero and the maximum of $6 \cdot 10^6$. The averaged value is $3 \cdot 10^6$. With an enhancement in injection time to 8 ms the TIC alters in between a minimum of

about 3 · 10^6 and a maximum of 6·10^6. Comparing the minimum of both experiments a clear shift from zero towards a higher minimum level wis obvious while the maximum remains at the same level. The averaged value increases compared to the case when the injection time is 5 ms.

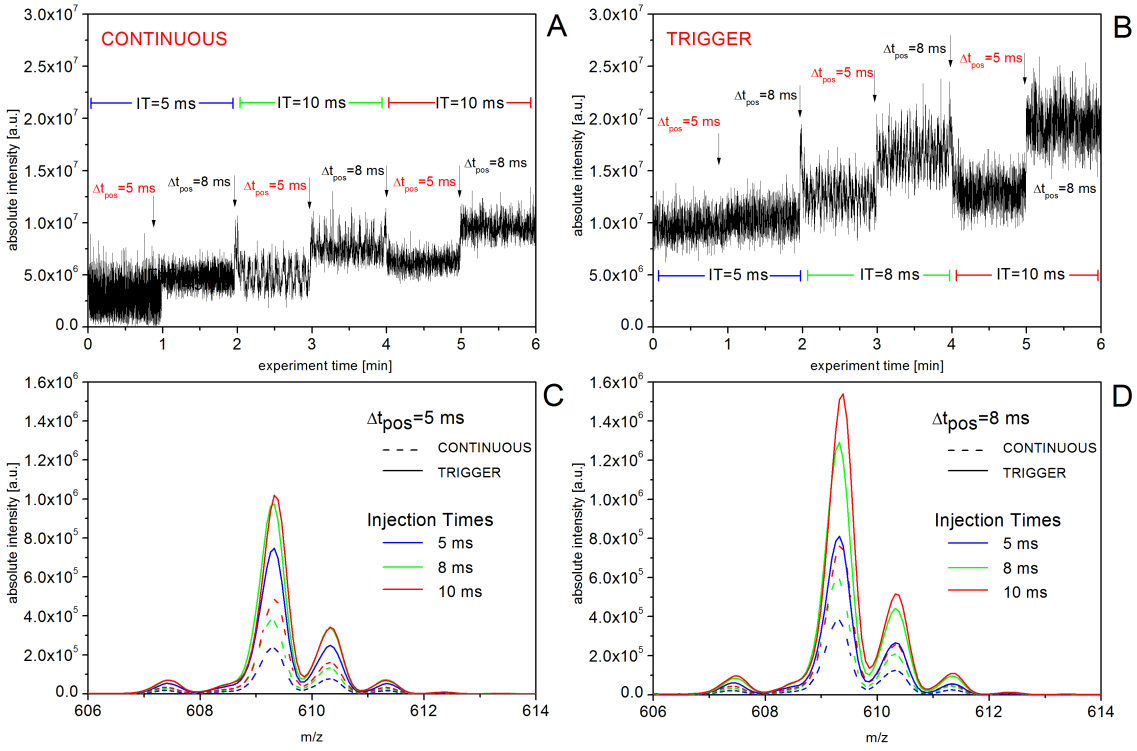

Figure 3.20 a) Measured TIC signal for the DB-ESI in the continuous mode when different MS injection times and different time durations of the positive applied pulses are involved; b) Measured TIC signal for the DB-ESI in the triggered mode, different injection times of MS and different time durations of the positive applied pulses are involved; c) Reserpine spectrum for the 5 ms HV positive pulse duration, when the applied pulses are triggered and in the continuous mode for different MS injection times; d) Reserpine spectrum for the 8 ms HV positive pulse duration, when the HV pulses are triggered and in the continuous mode for different MS injection times.

The TIC amplitude further decreases and the averaged value increases when the injection time is set to 8 ms. Again, the maximum remains at the same level. Finally, the TIC development is affirmed when the injection time is set to 10 ms which is equal to the period of the applied DB-ES pulse frequency. The TIC maximum is once more in the range of 6·10^6, the amplitude is the lowest and the averaged value reaches its maximum. The same behavior can be observed, when the half period Δt_{pos} is 8 ms and the injection time is adjusted to 5, 8 and 10 ms.

Figure 3.20 c and 3.20 d reflect the observation of the TIC performance. The absolute intensities increase with higher injection time of the ion trap. This observation can be explained by the relation of the positive half period in Δt_{pos} of the DB electrospray and the injection time of the ion trap. In the case when the half period Δt_{pos} is 5 ms the DB electrospray delivers the detectable ions for 5 ms and the non-detectable ions of other polarity for the rest 5 ms. The injection time differs during the experiments with 5 ms, 8 ms and 10 ms. Both systems are independent and so are the initial points of the positive half period and the injection time.

These experiments deliver further details for the understanding of the properties of the DB-ESI in combination with MS. When the injection time is set to 5 ms three different opening events of the ion trap are optional.

The first event describes when Δt_{pos} of the DB-ESI and the injection time start simultaneously. In this case the ion trap collects the maximum of ions. The second event is exactly the opposite of the previously explained. When Δt_{pos} ends at the same time when the ion trap opens only the non-detectable ions are generated by the DB-ESI during the injection time. Although the ion trap is open, it cannot collect and detect any ions. The third event represents the possibility when the injection time begins somewhere in Δt_{pos} or Δt_{neg}. In this case the ion trap can collect some amount of charges. That amount is above zero but less than the maximal possible amount described in the first event. These three events in combination cause the detected TIC which alters between zero and a maximum absolute intensity shown in figure 3.20 a.

In general, the measured TICs and mass spectra received by applying the triggered DB-ES depict a higher absolute intensity than by the DB-ES measured in the continuous mode. During DB-ES measured in the continuous mode the maximum intensity is gained when the injection time of the ion trap is set to 10 ms. Under the given experimental condition only one positive half period is considered during the experiments and therefore, all generated and detectable ions are captured by MS.

All the TICs measured with a triggered electrospray which are shown in figure 3.20 b as well as the triggered signals shown in figure 3.20 d are higher than in the case of an electrospray measured in a continuous mode. All generated charges are detected when the injection time is for example twice as high as the Δt_{pos}.

As shown in figure 3.18 the positive electrospray is started with a delay of 1.3 ms due to the fact that the ions have to be transferred from the coupling electrode to the tip of the emitter in order to build up the necessary electric field to initiate the electrospray. With the negative edge the positive spray stops, and a negative spray will be initiated. During the time necessary for the data evaluation the negative spray has sufficient time to discharge the system. For the next trigger pulse the positive electrospray will be initiated like for the first pulse because no residual negative charges have to be neutralized. This effect is comparable with the case where the duty cycle in the case of the continuous mode had been increased in order to avoid the negative electrospray.

3.8. Conclusions

The equivalent electric circuit model for the DB-ESI setup was developed. All components of the experimental capillary setup were presented with corresponding active and passive circuit elements. The modeling procedure was performed with two large steps.

Initially the “Closed Emitter Model” was developed, where all charge transfer processes in the setup were considered, except for the electrospray itself. The main focus was made on the explanation of the charge transfer from the coupling electrode to the emitter tip and on the potential formation in the different nodes of the system, i.e. under the coupling electrode and at the emitter tip.

In the second step the “DB-ESI Final Model” was developed, where the electrospray current was also considered. The dependence of the electrospray current on the air gap voltage was obtained by DC measurements and following data analysis. The initial model was extended with an active current source, containing the measured voltage-current dependence of the electrospray. The influence of the electrospray itself on the potential formation in the capillary system in comparison with the initial closed model was discussed. Using the developed “DB-ESI Final Model”, the simulation of the individual current components (EMT, ion current signal and electrospray signal) could be performed and the current components could be analyzed separately. The model has shown very good correlation with the measurement results presented in the previous chapter.

Several significant effects within the setup were observed in simulation.

The time delay necessary for the injected charge to be transferred, i.e. for the ions to travel to the emitter tip, resulted to be quite significant (units of ms) for large capillary lengths and thus comparable with the entire applied pulse widths. The time delay was directly dependent on the electrolyte properties, mainly the resistivity. In any case, the coupling electrode is recommended to be located as close to the emitter as possible.

The simulation has shown, that the electrospray of one polarity causes the accumulation of the charge of opposite polarity in the electrolyte after the applied pulse is over. When this charge is not sufficiently compensated by the electrospray of the opposite polarity, the intensity of the original electrospray decreases with each next applied pulse. Therefore, the continuous sequences of the applied n^{th} pulses results in lower electrospray signal levels, than a single "first" pulse applied after a sufficient time delay. This effect was confirmed by simulation and measurements and successfully implemented in the triggered DB-ES configuration.

With the TIC MS measurements the electrospray starting time have been detected. This value was very close to the value obtained by the theoretical investigations using the developed circuit model. It was shown, that triggering the pulses applied to DB-ES system synchronous with the MS injection time provides significantly higher efficiency in the MS measurements, than a simple continuous sequence of applied pulses. Using the advanced triggering procedures of the DB-ESI capillary system by mass spectrometer and different injection times in the mass spectrometer preferences, the effective usage of the DB-ESI source have been demonstrated. Using the triggering procedure it was possible to always use the "first" electrospray current response, which has the highest value in comparison with the following pulses.

With the same MS measurements the electrospray starting time for the fixed geometrical conditions of the DB-ESI capillary system setup have been measured as an additional proof to the effects discovered with the equivalent circuit model.

The knowledge on the physical processes in the DB ES setups, the charge transfer within the capillary system, the tip potential and electrospray formation, allow to efficiently optimize the DB-ES for the MS applications and increase the efficiency of the following MS analysis.

Chapter 4 Electrospray μ-Chip Development

4.1. Introduction

Miniaturized devices offer smaller dimensions of the channels and as a consequence fast analytical results, smaller dead volumes, lower power consumption and lower consumption of the chemicals. Micro total analytical systems (μTAS) offer to include various operation steps, such as separation techniques, and to deliver the analytes to the consumer in one device in order to reduce the dimensions. Capillary electrophoresis, as a high resolution separation tool, in combination with the miniaturized electrospray ionization source at the exit of a micro channel, provides the possibility to perform sequential analysis of proteins on femtomol levels using the mass spectrometer. Soft lithography technique together with PDMS silicone material is a good combination for the creation of separation channels on tens-of-nanometers scale. Integration of DB-ESI technology in the available manufacturing process of μ-Chip offers significant advantages, since long lasting non-contact electrospray ionization technique and existing separation technologies can be manufactured as powerful combination in a single device.

4.2. Available approaches for electrospray μ-Chips manufacturing

A common electrospray μ-Chip contains a capillary system and a direct contact electrode for ionization of the electrolyte in the capillary. The capillary system contains an inlet for the connection of an external capillary from the pump system, and an outlet where the ionized electrolyte is being sprayed from.

4.2.1. Capillary outlet as electrospray emitter

One of the most important features of µ-Chips with the electrospray ionization source is the design of the electrospray outlet at the end of the internal µ-Chip capillary. This outlet should provide stable and efficient spraying of the ionized sample solution.

The electrolyte meniscus at the capillary outlet is deformed when an electric field is applied. This deformation under the high electric field leads to the cone form, which is called Taylor cone. The cone arises due to the separation of electric charges within the electrolyte to form a thin polarized layer of counter ions near the meniscus interface. The formation of a stable Taylor cone is the main condition for observing good electrospray.

The surface conditions of the µ-Chip device is one of the most important parameter in the cone formation process. The coning and spraying is possible, when the electric field intensity at the exposed liquid surface is sufficiently high above the critical value. When this voltage is increased up to the level, where the surface tension can not maintain the liquid inside the droplet anymore, the liquid ejection appears through a thin jet at the cone apex. At the cone apex the electric field has the highest value.

Different approaches and substrate materials have been proposed to fabricate microfluidic devices for electrospray ionization. Most of them are focused on the nozzle formation. The presence of a nozzle at the capillary outlet leads to a specific electric field profile with the highest field at the emitter, which leads to more stable electrospray at lower applied voltages. The formation of a large droplet at the outlet surrounding surface is also avoided. The electrospray from a flat-surface outlet is also possible, however specific surface properties have to be considered.

4.2.2. Nozzle-type emitter formation techniques

Microfabricated electrospray emitters made from silicon nitride were proposed by Desay [42]. Parylene was used as a structure material for electrospray nozzles construction by Licklider e.t al. [43]. The bromide trifouride was used for the channel creation. The rectangular microchannels of 2.5 mm length and an orifice of 5 × 10 µm at the emitter tip were manufactured using the MEMS technology.

Polycarbonate microfluidic device fabrication using a deep reactive ion etching was used for the emitter tip formation by Schultz [44]. The nozzle with the dimensions of 10 µm inner

diameter and 20 µm outer diameter were demonstrated. For the larger signal intensity after 5 minutes the RSD value of 5 % was reached.

Polyimide material was used for microchips fabrication by Gorby [45]. Plasma etching technique were used for manufacturing procedure. The 75 µm thick polyimide was coated with a 5 µm copper from both sides. The pieces were patterned with the photoresist and exposed. The manufactured channel had 1 cm length, 120 µm width and 45 µm height. The emitter outlet was formed by cutting. The thickness of the microchip at the emitter tip was 20 µm in order to get a sharper shape of the structure. Muck [46] have reported about a well developed electrospray plume from the PMMA microchip. The sheathless electrospray from bare PMMA µ-Chip was fabricated successfully by atmospheric molding. For the production process no vacuum was used, only the drilling, hand polishing and dicing procedures were involved in the fabrication process.

Microemitters development using the PDMS material was done by Kim in different ways [47]. With the trimming method the channels of 4 cm length and 100 µm width were produced. The emitters at the end have a concave shape, produced by PDMS casting using film fixed at the emitter end. The emitter tips were designed with an angle of 30° and 60°. Using the soft lithography technique and two-layer photoresist method, the PDMS emitters were implemented as tips along the PDMS device. The RSD of the measured TIC signal was almost the same for each production method and has a value around 3.2 %. Electrospray devices using the SU-8 masters and PDMS material were also presented by Huiko [48]. Replicated polymer structure has 2 – 3 cm channel length with a width of 25 µm to 10 µm and height of 10 µm. Those microchips had very short life times. A stable work of these electrospray microchip was limited to 5 minutes because of the channel clogging process. The tips for the nanoelectrospray ionization microchips were fabricated using the PDMS for sample introduction by Kameoka [49]. The PDMS also could be used to create the nozzles [50], [51] and the open tips to produce electrospray [52].

Aebersold et al. [53] connected a fused-silica capillary to the outlet of a prefabricated PDMS channel; the other end of the capillary was connected to the ESI-MS. The interfaces between the PDMS and the silica capillary can be formed with minimal dead volumes by taking advantage of the molding properties of PDMS. The PDMS was cast directly on a fused-silica capillary. After curing the PDMS, the removal of the part of the embedded capillary

generated a PDMS microchannel that formed a smooth interface with the remaining embedded capillary [54]. The PDMS casting techniques were used to fabricate microchannels also by Chiou [55].

4.2.3. Flat-surface emitter formation techniques

The microfabrication processes of the systems described above is very time-consuming and laborious, and require relatively sophisticated facilities.

The alternative solution compared to the nozzle-type emitters is the flat-surface emitter outlet. Such outlets are easy to manufacture and allow very high compactness. Ramsey and Ramsey have built an glass chip with the ESI source for mass detection with open outlet at the end of the channel [56]. The flat emission surface was polished. Stable electrospray was obtained under 3 kV operation voltage. The spray solution is attached to the chip surface and tends to form a big droplet and soak the surrounding surface. To avoid the surface soaking, it was made hydrophobic by coating. The group of Karger [57] developed the same device with the multichannel ESI outlet. The design avoids the complexity associated with the nozzles-type emitter formation. The surface was processed with hydrophobic reagent and the device has worked at 4.2 kV. The author suggests to use the plastic materials instead of glass to solve wetting problems. Zhang et al. [58] mentioned that a tip is not necessary in this type of designs, suggesting that the field strength appeared to be high to form a Taylor cone. The authors have also recognized after several experiments with the glass surface, that avoiding wetting (or droplet formation over the flat edge) is necessary to produce a working device. Tang et al. [59] focused on the wetting problem and constructed the multiple-nozzle chip from carbonate substrates. They also mentioned to use CH_4 plasma treatment to increase the hydrophobicity. However, liquid spreading over the surface adjacent to the channels openings is unavoidable to some degree. The value of the radius of the capillary in the case of the flat surface is equivalent to the size of meniscus formed at the channel outlet.

In order for the liquid flowing from the channel outlet not to spread onto the emitter surface it is necessary to increase the contact angle of the outlet emitter surface and the liquid. For solving the spreading problem the hydrophobic materials are used. In the case, when hydrophobic material is used for the emitter outlet formation, electric force will decrease when the size of the meniscus is increasing. Hence the required value of the applied voltage

will decrease. An explanation, given by Byun [60] shows, that at hydrophobic surfaces with the contact angle around 110° the Taylor cone is not stable enough. A flat nozzle, composed of a super-hydrophobic surface with a static contact angle greater than 150° is most advantageous as the high-contact angle of the liquid meniscus at the nozzle's opening diminishes potentially hazardous spreading of the liquid and ensures long term stability and repeatability of the electrospray process.

4.2.4. Improvement of PDMS hydrophobic properties

The PDMS material was chosen for µ-Chip manufacturing in the current work. Hydrophobic PDMS surface makes this material very attractive for the formation of the flat surface emitter. The surface of PDMS itself is hydrophobic. However, the contact angle of the pure PDMS is rather small for the stable Taylor cone formation, and as was shown before [60], the hydrophobic properties of the material should be improved.

In the current work the hydrophobic surface of PDMS was improved in two ways, using the casting onto the nano-structured patterns on the metal surface and using the physical modification of PDMS surface. For the second case the influence of high temperature on the cured PDMS surface was investigated.

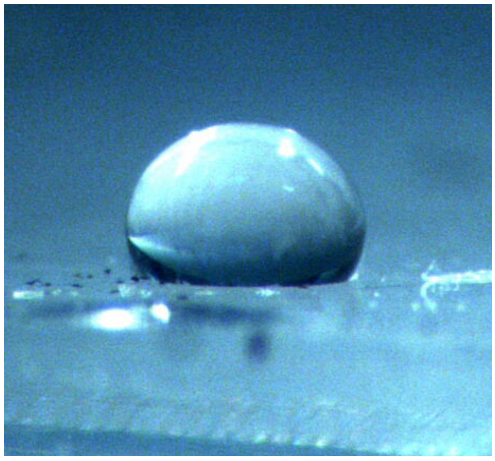

Figure 4.1 The pPhoto of deposited 1 mL water drop on the pure PDMS surface; Measured contact angle 95±1º.

The contact angle for pure PDMS was measured with a simple approach. The Sylgard 184 PDMS was mixed in proportion of 1:10 and degassed within 30 min. The liquid PDMS was cured on a flat wafer surface during 2 hours at 70 ºC in the oven. The 1 mL water drop was deposited on the cooled surface, the contact angle was measured with the microscope and the

mirror system using the corresponding software. The photo of the deposited water drop on the pure PDMS surface is presented in figure 4.1. The measured contact angle has a value of 95±1º.

4.2.4.1. PDMS surface with specific roughness pattern

To increase the contact angle, a specific roughness pattern was created on the PDMS surface using a casting method. The Ni plates were used as a mold for PDMS casting. The 2×2 mm pattern structures were created on these plates. The surface of these areas were modified to obtain high surface roughness using the laser.

The different sizes of grid were investigated. The dimensions were made with $\Delta x = \Delta y = 40$ μm to $\Delta x = \Delta y = 100$ μm steps. A sample structured surface for PDMS casting with the 40 μm step is shown at the figure 4.2 a. The liquid PDMS (mixed as was mentioned in 4.2.4) was hardened on this metal surface and the contact angle of 1 mL deposited water drop was measured as before. A photo of the deposited water droplet on the modified PDMS surface is presented at the figure 4.2 b. The measured contact angle has a value between 148±2° for $\Delta x = \Delta y = 100$ μm grid and 156±2° for the $\Delta x = \Delta y = 40$ μm grid.

For the characterization of the surface roughness the model of Cassie can be used [61]. Cassie proposed an equation for contact angle describing the heterogeneous surface composed of two different materials. When a unit area of the solid surface fraction in the contact with the water f_1 and f_2 is the air fraction in contact with the water, the contact angle on the surface can be expressed by the following equation:

$$\cos\theta_r = f_1 \cos\theta_s - f_2 \qquad 4.1$$

where θ_r is the contact angle of the water drop on a rough surface, θ_s is the contact angle of a water droplet an a smooth surface. The equation assumes, that the water droplet does not completely wet the rough surface. The air in the PDMS cavities creates the air pockets. The water droplet interacts with this air pockets and PDMS surface. The increasing of air pockets amount leads to the contact angle increasing.

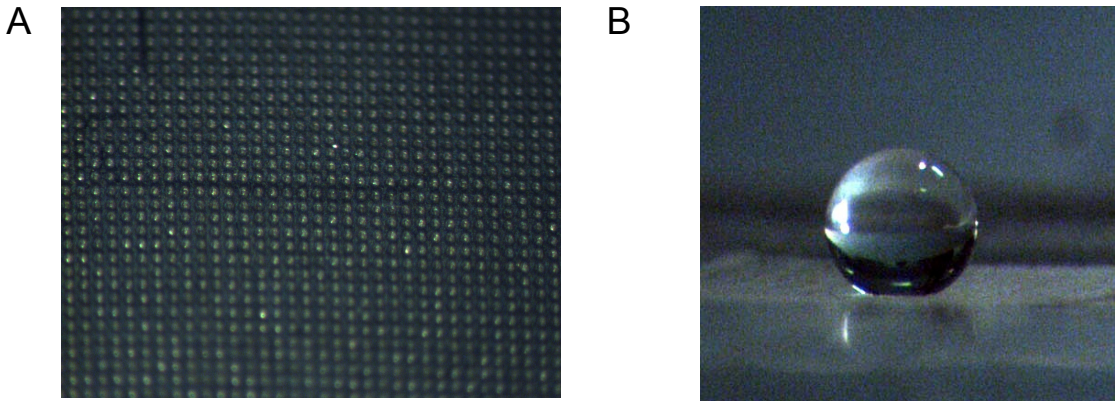

Figure 4.2 a) Photo of the structured metal surface for PDMS casting (Δx=Δy=100 μm); b) Photo of 1mL water drop deposited on the cured PDMS surface, measured contact angle 148±2°.

The proposed method has shown significant improvement of PDMS surface hydrophobic properties. However, the casting implied that only liquid PDMS can be used. A method to change the contact angle of a cured PDMS surface would be more useful.

4.2.4.2. High-temperature processing of PDMS surfaces

It was proposed by Hunter [62], that the temperature factor can be involved in the PDMS surface contact angle modification. The high contact angle in combination with the high thermal stability of films from dimethylsiloxane polymer was obtained.

To verify the influence of the temperature on the cured PDMS surface, the following experiment was performed. The cured PDMS surface was created as described before (see 4.2.4). The PDMS was mixed in proportion of 1:10, degassed during 30 min and then cured at 70 °C during 2 hours in the oven. The temperature of the surface was increased using the butane flame jet. The distance between flame tip and PDMS surface was varied from 0.5 to 5 cm. During different times periods (from 5 to 60 s), the PDMS surfaces were burned with the butane flame jet. The surface temperature was controlled with the Fe-thermocouple. Thermocouple was inserted in the PDMS body from the back side in such a way, that the tip of the device was in contact with the surface being processed. The contact angle was measured at the cooled PDMS surface. For each combination of surface temperature and impact time the contact angle was measured. The measurement results are presented in figure 4.3 a. The microscope photo of a PDMS sample burned surface and deposited 1 mL water drop on it are presented in figure 4.3 b, c.

It can be observed, that at the temperatures below 250 °C the PDMS surface becomes hydrophylic: the contact angle lower than 5° was observed. Terminal oxidation of the methyl

groups leads to increasing of the surface energy and hence to decreasing of the PDMS contact angle. Further increasing of the contact angle can be explained by cavities creation on the surface. These cavities affect the contact angle in the same way as it was described before (4.2.4.1). Those cavities play a role of non-structured surface roughness and the Cassie model [60] can be involved in the contact angle increasing explanation. The mechanical stability of the burned PDMS surface was proved by repeated measurements at significant time after surface modification.

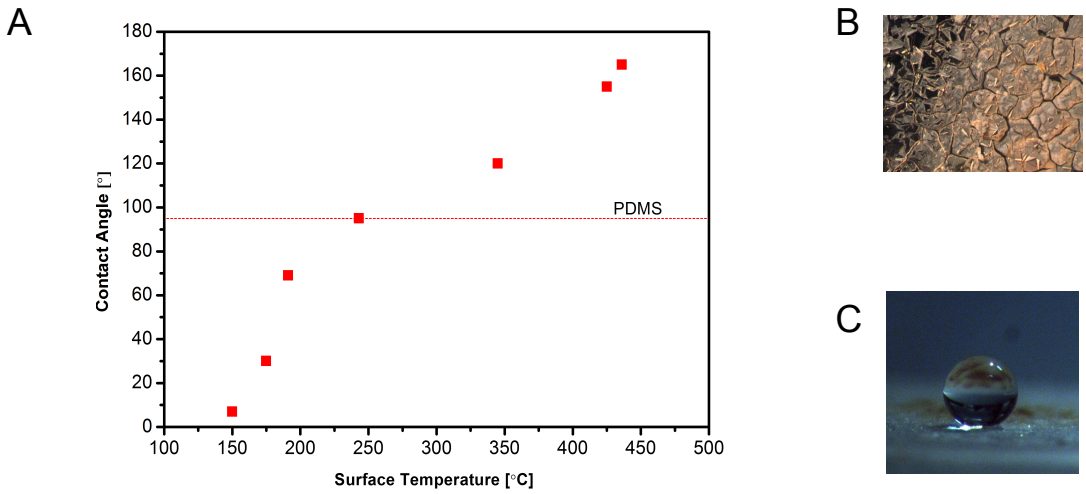

Figure 4.3 Dependence of the measured contact angle for 1 mL deposited water drop on the PDMS surface on the PDMS surface temperature. Dashed line shows the contact angle of the non-modified PDMS surface.

The contact angle measurements were repeated after one month after the surface modification. High contact angle of the sample surface was still observed by those measurements.

4.3. DB-ESI µ-Chip development

4.3.1. µ-Chip structure

The µ-Chip with the ESI source consists of a PDMS body containing a capillary channel with an inlet, an outlet and a built-in the coupling electrode. The capillary channel starts with the inlet, where the external input fused silica capillary is attached, and ends with an emitter tip, i.e. an outlet of a specific shape.

The µ-Chip proposed in the current work consists of the separate top and bottom structures. The top structure contains the capillary with the inlet and the outlet. The bottom structure is simply the glass base with deposited coupling electrode. In the final assembly process the structures are bonded together forming the entire µ-Chip body. A schematic view of a ready µ-Chip is shown in figure 4.4.

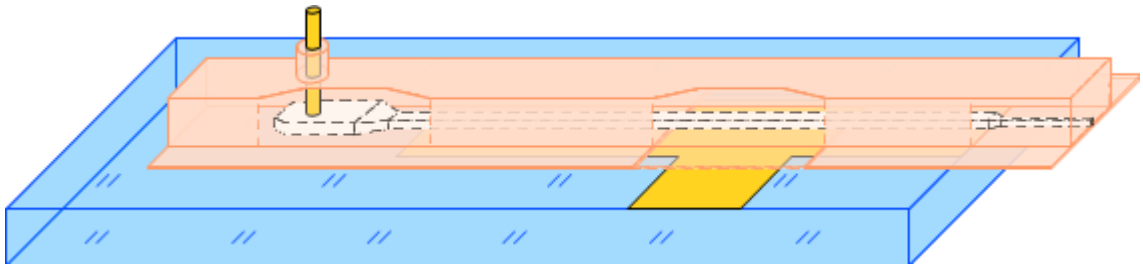

Figure 4.4 Overview of the DB-ESI µ-Chip. Bottom part includes the glass with the sputtered metal layer (coupling electrode). The top part includes the PDMS bulk with the capillary channel. The thin PDMS layer is placed as a dielectric layer between the metal layer and the channel. For the pump connection, the fused silica capillary is inserted.

The channels with either rectangle or round cross-sections can be manufactured. The channel manufacturing technology will be discussed in more details later.

In case of DB-ESI µ-Chip, the electrode must be separated from the channel by thin insulating layer (dielectric barrier). In the proposed structure a thin PDMS film located between the capillary and the coupling electrode was used for this purpose. This thin film can either be deposited on the surface of the µ-Chip base, or included as bottom layer in the top PDMS structure.

4.3.2. Glass base with coupling electrode

The bottom structure is realized as following. A thin glass substrate was used as a hard base for the µ-Chip. The gold electrode of 200 nm thickness was sputtered on the upper surface of the substrate.

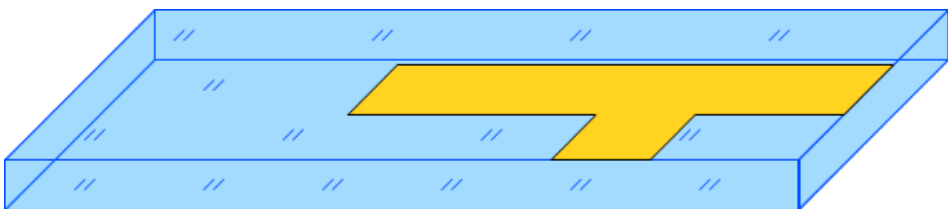

Figure 4.5 The glass base layer of the DB-ESI µ-Chip with the sputtered gold electrode (200 nm thikness).

If a dielectric barrier is included in the µ-Chip base, thin PDMS film of aprox. 50 µm thickness has to be deposited on the base surface. In current work the dielectric barrier was included in the top structure with capillary system, thus a simplified base shown in figure 4.5 was used. The same glass base was used for both types of structures discussed in this work.

4.3.3. PDMS casting for the structure formation

Polydimethylsiloxane (PDMS) is the polymer from the class of polysiloxanes. The silicon-based organic polymer is characterized through a good processing possibilities of a high form fidelity with a minimal shrinkage and is particularly suitable for a casting process. Methyl-side groups (-CH3) are attached to the silicon atoms, which are four-coordinate. PDMS is a heat-curable silicon supplied as two-linked part kit consisting of pre-polymer (base) and cross-linker (curing agent) components. Platinum catalyzer starts the reaction of hydrosilylation. HIghly reactive vinyl groups at the end of the polymer molecule bind with the hydrogen from curing agent one chain. The polymerization reaction does not produce any by-products and leads to the polymer hardening. The reaction does not need temperature activation and can run at the room temperature. However, the heating can be used for the reaction acceleration.

In the current work the Sylgard 184 PDMS was used for manufacturing of different parts of the µ-Chip (top structure with the channel, thin dielectric barrier film). The thin PDMS dielectric films were produced using the spin-coating procedure. The PDMS is highly transparent, has a sufficient dielectric constant, is chemically inert, and non-toxic. This hydrophobic material could be used in a wide temperature range from – 50 °C to 200 °C. The PDMS is a low cost and therefore an ideal material for rapid and simple fabrication using soft lithography technique.

4.3.4. Simple top structure with the mechanically formed channel

The first PDMS structures for DB-ESI were manufactured with a simple procedure similar to one proposed by [63]. The structure was manufactured using a PDMS casting. The process doesn't require any specific tools or devices.

A thin metal wire with 16 cm length and 50 µm diameter was used for the channel formation. Fused-silica capillaries (i.d. 50 µm, o.d. 360 µm, 5 cm length) were used for the formation of the µ-Chip inlet for connection to the pump. Thin wires were manually inserted

through the fused silica capillary as shown at the schematic representation 4.6 a. The wire was fixed with the magnets at the metal substrate and stretched above the surface. The wire in this case is separated from the surface with a thin air gap, determined by the capillary wall thickness.

With a glass mold the required nozzle shape with 30º angle was formed (4.6 b). The internal area surrounded by glass mold was filled with liquid PDMS (Sylgard 184, mixed 10:1) and cured for 2 hours in the oven at 70 ºC (figure 4.6 c). After the curing procedure the wire was extracted from the PDMS bulk and from the fused silica capillary (figure 4.6 c). As the result, the channel with the round cross-section of 50 μm internal diameter and a ready hermetic connector to the external capillary system was formed (figure 4.6 d).

The capillary in this structure is already separated from outside by a thin PDMS wall with a thickness determined by initial distance of the wire to the underlying surface (~150 μm). On necessity, an additional thin PDMS film can be manufactured and attached to the bottom surface as discussed in following chapter 4.3.5.3. and 4.3.5.4.

The further assembly procedure is discussed in chapters 4.3.6. The plasma activation procedure of the bottom structure is performed, and the PDMS structure is assembled together with the glass base.

The μ-Chips with the DB-ESI source manufactured with such a method have several significant advantages. The smallest possible dead volumes are achieved this way. The sharp micro-nozzle shape formation results in a very small surface area around the channel orifice, hence the Taylor cone can be easily established.

An obvious disadvantage of such procedure is the impossibility to assemble multiple-emitter μ-Chips. For advanced purposes of e.g. combination of DB-ESI emitter in a single μ-Chip with the separation technique, a complex channel structure with multiple electrodes will be necessary. Thus another process was considered in the project.

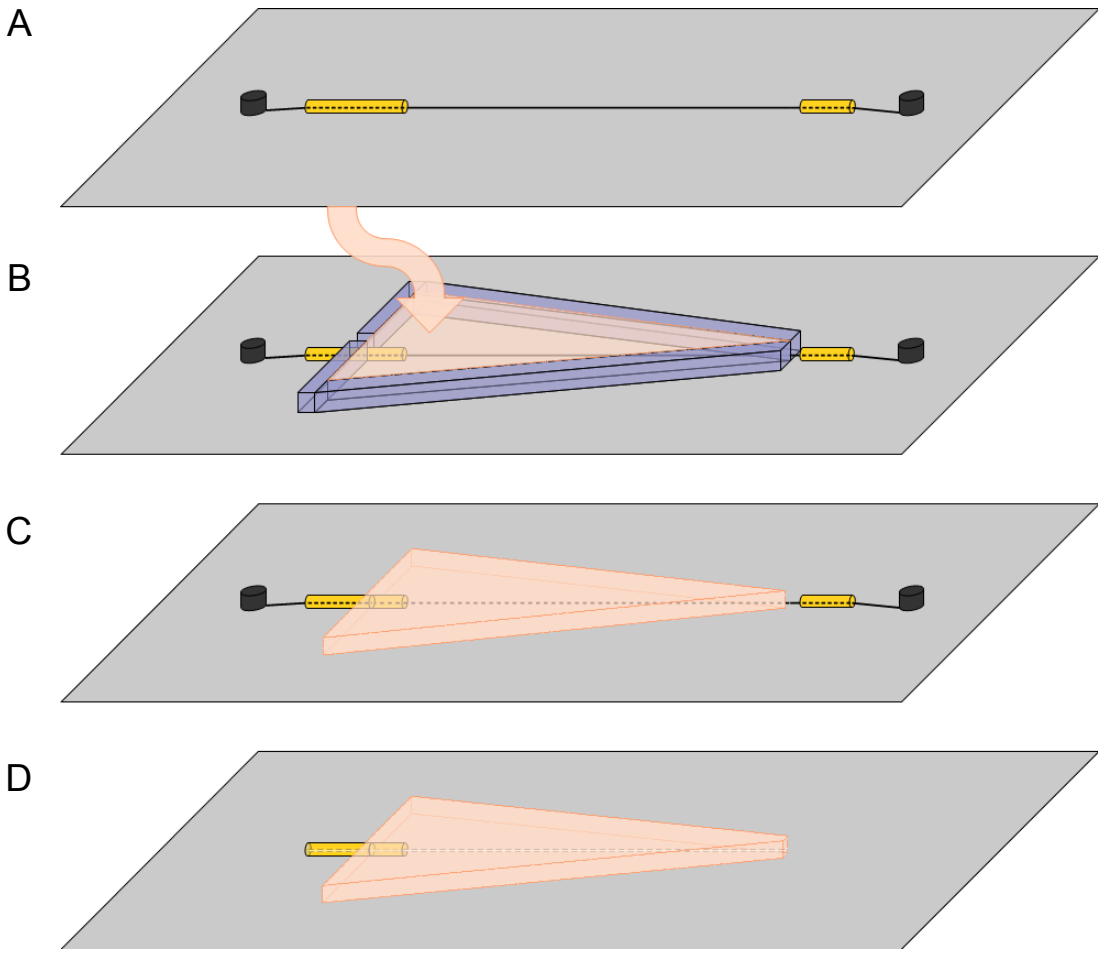

Figure 4.6 a) Metal wire (50 µm diameter) is inserted through the fused silica capillary (i.d. 50 µm, o.d. 360 µm) and fixed with the magnets; b) The glass mold is used for the µ-Chip triangle shape creation. Inner area is filled with the liquid PDMS; c) The glass mold is removed after PDMS curing; d) Metal wire is removed from the cured PDMS bulk. The top structure of the µ-Chip with the sharp channel outlet (30º) and thin PDMS dielectric layer is created.

4.3.5. Advanced top structure with wafer-casting channel formation

A common approach for the capillary system formation using PDMS is the casting and following hardening of PDMS on the wafer with specific micro-pattern. The wafer pattern forms grooves in the PDMS surface. At the second step this surface is covered with a thin PDMS film as with a lid, and the capillaries are formed.

Classical photolithography process has been mastered as a tool for the micro structures creation on the master wafer surface. The radiation sensitive layers were deposited on the wafer surface. The layers were exposed to the UV light using a special mask with the

designed channel shapes. The exposed image was developed and the mask image becomes visible on the substrate as a relief. The thickness of the structure depends on the photoresist type and it's deposition properties. The liquid polymer was deposited on the created channel structure and after curing was easy removed from it. The negative structure on the master wafer creates the positive structure (channel) in the polymer surface.

4.3.5.1. The master wafer mask design

The mask design for the master wafer was created with AutoCAD 2004. The design was elaborated for a six inch master wafer (orientation 0-0-1) and divided in two parts. The first part contains the 10 µm layer of the structure and contain the channels of 10 µm width and 0.5 cm length. The second part comprises the main channel structure with 50 µm width and 5 cm length. A combination of the special figures at the mask edges allows to achieve complete alignment of the two layers of design in one structure.

The film mask with a resolution of 10 µm was printed by "JD Photo-Tools", UK. The mask is very sensitive to water; therefore a glass copy has been created. The glass wafers with a positive lacquer layer and a chromium layer were used for mask copy procedure. „Nano-film glass mask" of Soda Lite glass type has a photoresist AZ 1518 with 5300 Å thickness and a chrome layer of 100 nm thickness. The light exposure of 3 s was performed. The film mask and the glass substrate were in direct contact during the exposure process. For the exposure process a light intensity of 20 mW/cm^2 with the wavelength of 366 nm was used. In order to smooth out the roughness of the original mask, the exposure time was increased up to 5 s. The positive photoresist development process was performed in the solution of AR300-26 diluted in the proportion of 1:4 with water. Then the glass mask was dried and the chrome layer was etched. Washed in acetone and then with the isopropanol, the toughly dried mask was ready for further use.

4.3.5.2. Master wafer manufacturing

The negative epoxy resist SU-8 is the most widely used material in the photolithography procedure. The oligomers in the SU-8 have high density of epoxy-groups that can form tightly cross-linked structures during curing. The properties of the epoxy allow to create vertical walls with the high aspect ratio. The SU-8 resists are designed to produce low defect coatings over a the very broad range of film thickness. The negative resists have different

viscosity and are used for creation of the layers of different thickness. The viscosity parameters and solid content data for different SU-8 resists are presented in table 4.1.

Table 4.1. - Specification data for the SU-8 family negative resists

Negative resist	SU-8 2	SU-8 10	SU-8 50
Solid content	40 %	59 %	69 %
Viscosity at 25 °C	44 cst	1070 cst	12500 cst

To avoid typical “comet-shaped” inhomogeneities in the film thickness, the bonding layer without any structure was created. A thin SU-8 2 layer on the wafer surface improves the adhesion of the next deposited SU-8 layer. For the narrow capillary outlet formation at the end of the channel, the SU-8 10 negative photoresist was deposited onto the wafer. For the channel “body” creation (including the inlet area) the SU-8 50 negative resist was deposited.

For each layer the standard procedure was used. The cycle includes substrate cleaning, spin coating, soft baking procedure for the solvent evaporation, edge bead removal with acetone (EBR), exposure with the UV light, post exposure baking procedure (PEB), development of the structures, rinsing and drying procedures. The manufactured structures at the wafer surface are insufficiently hard after standard soft baking procedures, and may be damaged by the physical forces being applied during later PDMS molding procedures. The additional hard baking step is necessary to prevent structure damages during the later steps.

In order to reach the maximum stability in the process, the wafer substrate should be completely dry during the photoresist deposition. For this purpose the wafer was placed on the hot plate for 5 minutes at a temperature of 200 °C.

The appropriate SU-8 resist and spin coating conditions were required to archive the designed film thickness. For each layer 6 mL of SU-8 negative resist was used. The amount of substance was taken from the calculation as 1 mL pro one wafer inch. Centripetal acceleration causes the resist to spread to, and eventually off, the edge of the substrate leaving a thin film on the wafer surface. The final film thickness and other properties will depend on the nature of the resist (viscosity, drying rate, percent solids, surface tension, etc.) and the parameters chosen for the spin process. In table 4.2 the appropriate spin coatings parameters for each used negative resist are presented.

Table 4.2 - Spin coating parameters for creation of layers with different thickness

Sub-steps during layer creation procedure	layer 1 SU-8 2	layer 2 SU-8 10	layer 3 SU-8 50
Step 1	15 s at 500 rpm	15 s at 500 rpm	15 s at 500 rpm
Step 2	40 s at 2000 rpm	40 s at 3000 rpm	40 s at 2000 rpm
Step 3	10 s at 0 rpm	10 s at 0 rpm	10 s at 0 rpm

After the resist was deposited on the substrate, the soft backing process is required to evaporate the solvent and densify the resist film. For the soft baking procedure, both the hot plate and convectional oven were used. For the best results, the procedure was divided in several steps with different temperatures. Lower temperatures allow the solvent to evaporate out of the film in a more controlled mode, which results in a better coating fidelity, reduced edge bred and better adhesion of the resist to substrate.

Table 4.3 - Soft baking parameters for the creation of the layers with different thickness

Layer number and thickness	Step 1	Step 2	Step 3
layer 1 2 μm (hot plate)	1 min at the 65 °C	1 min at the 95 °C	-
layer 2 10 μm (oven)	10 min at the 65 °C (15 min ramp)	60 min at the 95 °C (15 min ramp)	30 min at the 30 °C (180 min ramp)
layer 3 50 μm (oven)	10 min at the 65 °C (15 min ramp)	60 min at the 95 °C (15 min ramp)	30 min at the 30 °C (180 min ramp)

Table 4.4 - Exposure parameters

Layer number and thickness	layer 1 2 μm	layer 2 10 μm	layer 3 50 μm
Exposure time, s	60	10	25

The SU-8 resist is optimized for the near UV exposure. The necessary exposure dose depends on the layer thickness. The exposure of the first layer was performed without mask

for the whole wafer area. The exposure procedure of the second and third layers required two different masks to manufacture separately the very thin capillary at the outlet and the base capillary through the entire μ-Chip body. The structures matching was done using the alignment marks placed in the corners on the glass mask design.

The PEB must be performed to selectively cross-link the exposed areas of the structure. The optimal cross-link density can be realized by careful adjustment of the exposure and PEB conditions. To minimize the mechanical stress and avoid resist cracking, a slow ramp and two step contact hot plate were used. The PEB parameters for each layer are shown in the table 4.5 below.

Table 4.5 - Post exposure backing process for different layers thickness

Layer number and thickness	Step 1	Step 2
Layer 1 2 μm (hot plate)	1 min at the 65 °C	1 min at the 95 °C
Layer 2 10 μm (oven), wafer in the metal holder	30 min at the 90 °C	Slowly cooling down in the hot metal holder
Layer 3 50 μm (oven), wafer in the metal holder	30 min at the 90 °C	Slowly cooling down in the hot metal holder

The developing process was performed, when all the layers were deposited and the last post backing process was finished. The developing time used for the thick several-layer structure was around 10 min in the fresh developer solution. The developing process was controlled with a microscope. In order to explicitly remove the unnecessary resist from the corners of the channels (10 μm structures on the second layer), the spin-coater and syringe with the developer were used. After the developing procedure, the wafer was rinsed with the isopropanol and carefully dried with the air stream. Because of the necessity of the later PDMS peel-off procedure, where significant force might be applied to the structure, the hard bake procedure was inavoidable as the last step in the master wafer creation procedure. The ready master wafer was heated in the oven for 2 hours at 160 °C.

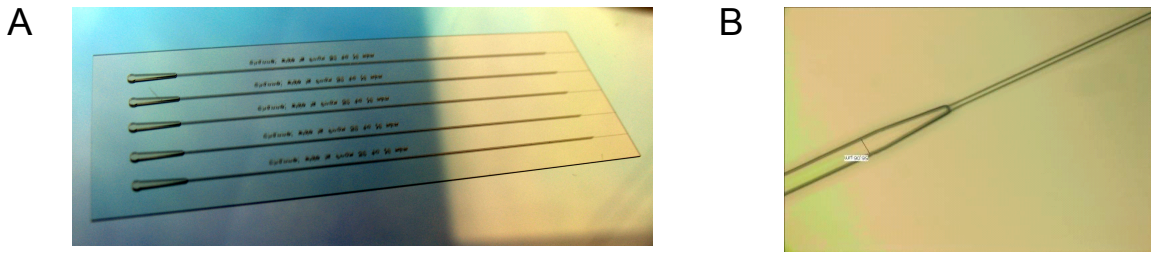

Figure 4.7 a) The overview of the created channels structure on the master wafer using the SU-8 negative photoresist: 5 parallel channels have 56 µm height and 50 µm width in the middle section, and 10.3 µm height and 8µm width at the tip; b) Magnification of the transition part in the channel: the main body channel (56 µm) connection to the channel tip (8 µm).

The x-y stylus based surface profile-meter "Alpha-Step 200" was used for the heights control of the structures. The displacement of the stylus from the local position during the scanning process is proportional to the structure heights on the wafer. The thickness of each layer was controlled after post backing procedure and after final developing as well. The resulting measured thickness for the first (thin nozzle) part of the channel (first layer) was 10.3 µm, and the thickness for the second part of the channel (second layer) was 56.0 µm.

4.3.5.3. Thin PDMS film as a dielectric barrier

The general idea of the DB ESI is the usage of a thin dielectric barrier to transfer the charge without direct contact of the electrode to the electrolyte. One of the important characteristics of this dielectric layer is the total capacitance of the electrode to electrolyte within the capillary. This capacitance is directly related to the geometry of the interface area and the inherent characteristic of the dielectric material, it's the dielectric constant.

The PDMS thin films were used as a dielectric barrier in the electrospray µ-Chip structure. The dielectric constant of the pure PDMS has the thermal stability and has a value of 2.8 at the room temperature. Heating of the sample to the 200 degrees will decrease this parameter to the 2.3 [64].

The thin films were manufactured with the spin-coating as described in the following section 4.3.5.4. The surfaces of both PDMS top structure and PDMS thin film were subdued to plasma activation as described in section 4.3.5.5. and assembled together with the top PDMS top structure.

4.3.5.4. Thin film manufacturing using the spin-coating procedure

Spin coating is a common microfabrication method for producing thin polymer films with controlled and uniform thickness. After the polymerization it is possible to remove the manufactured elastic membrane from the master surface and to attach it onto the other surfaces such as a plastic film or a glass.

The PDMS mixture (1:10) of 8 mL volume was deposited onto the 6 inch clean wafer surface. For the adhesion reduction between PDMS wafer surface, the wafer was treated by HMDS gas before the deposition. The setting of the thin film thickness was controlled with the rotation speed (angular velocity) of the spin-coater.

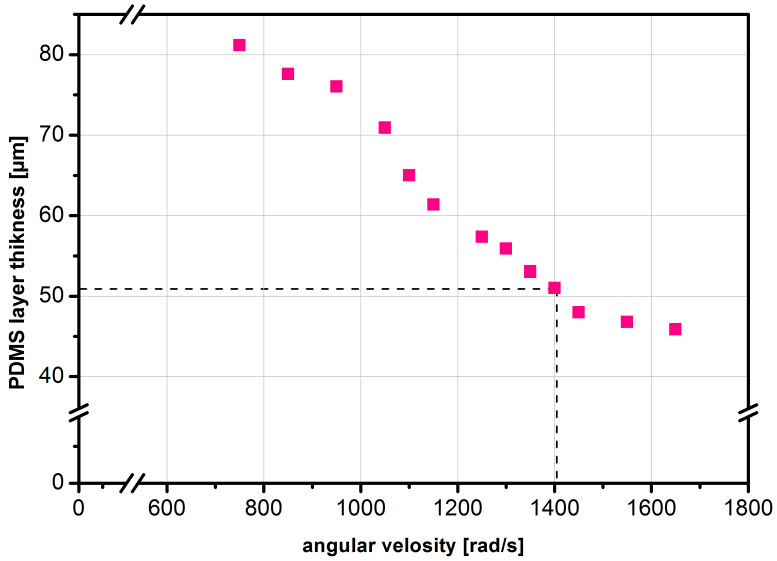

Figure 4.8 PDMS thin film thickness dependency on the angular velocity used during the spin-coating PDMS deposition. For the 50 µm layer thickness creation, the value of 1400 rad/s was used.

The spin coating procedure consists of 2 steps for better distribution over the surface. At the first step a fixed rotation speed of 500 rad/s during 10 s was used. During this first step the initial volume of deposited PDMS is spread half-uniformly over the wafer surface. During the second step rotation speed was increased with 1400 rad/s acceleration up to some predefined value, and the wafer was spinned at this angular velocity for 40 s (including acceleration time). During this second step a fine distribution of the PDMS over wafer surface with homogenous thickness was obtained.

Polymerization of the PDMS thin film takes approx. 10 min in the oven at 70 °C. After curing the thickness of the films was measured at 4 points of the wafer edges and in the

middle. Before the measurements the 2 cm of the PDMS film was removed from the edges of the wafer. The dependence of the thickness of the thin film on the angular velocity used during spin-coating is presented in the figure 4.8.

4.3.5.5. Plasma surface activation

Many various bonding methods for PDMS and glass surfaces are described in the literature. Among them is the bonding technique that relies on using a sticky layer with less cross linking agent that would be combined with a hard cross linked layer. Using an intermediate layer of uncured PDMS or UV-curable glue to bond the layers together was described by Satyanarayana et al. [65]. However, liquid adhesives are not suitable for microfluidic applications because the excess adhesive drains from the interface into the microfluidic channels and can block them upon setting. An alternative and more successful approach is the activation of the surface in the oxygen plasma.

Oxygen plasma treatment is advantageous because it enables the bonding of the PDMS with the glass surface. After curing, the PDMS surface is hydrophobic. In order to alter the surface properties, PDMS is exposed to an oxygen plasma. Reactive oxygen radicals are attacking the methyl groups (Si-CH3) from the PDMS surface and substitute them by silanol groups (Si-OH), which render the surface hydrophilic. However, the hydrophilic surface in air is unstable. Silanol groups are migrating into the PDMS bulk and condense to reduce the surface free energy. This process returns the surface to its hydrophobic state in roughly 30 min. The seal between two pieces of PDMS is significantly strong that the two substrates could not be peeled apart without failure in cohesion of the bulk PDMS.

4.3.5.6. Assembly of the top structure

The PDMS structure was manufactured further in the same way as the simple structure with mechanically-formed channels. A glass mold was placed on the wafer so, that it surrounds the created surface structures. The internal area surrounded by glass mold was filled with the liquid PDMS (Sylgard 184, mixed 10:1) and cured for 2 hours in the oven at 70 ºC.

After the curing procedure the PDMS structure was peeled off from the master wafer. The grooves in the PDMS structure surface now correspond precisely to the initial wafer relief.

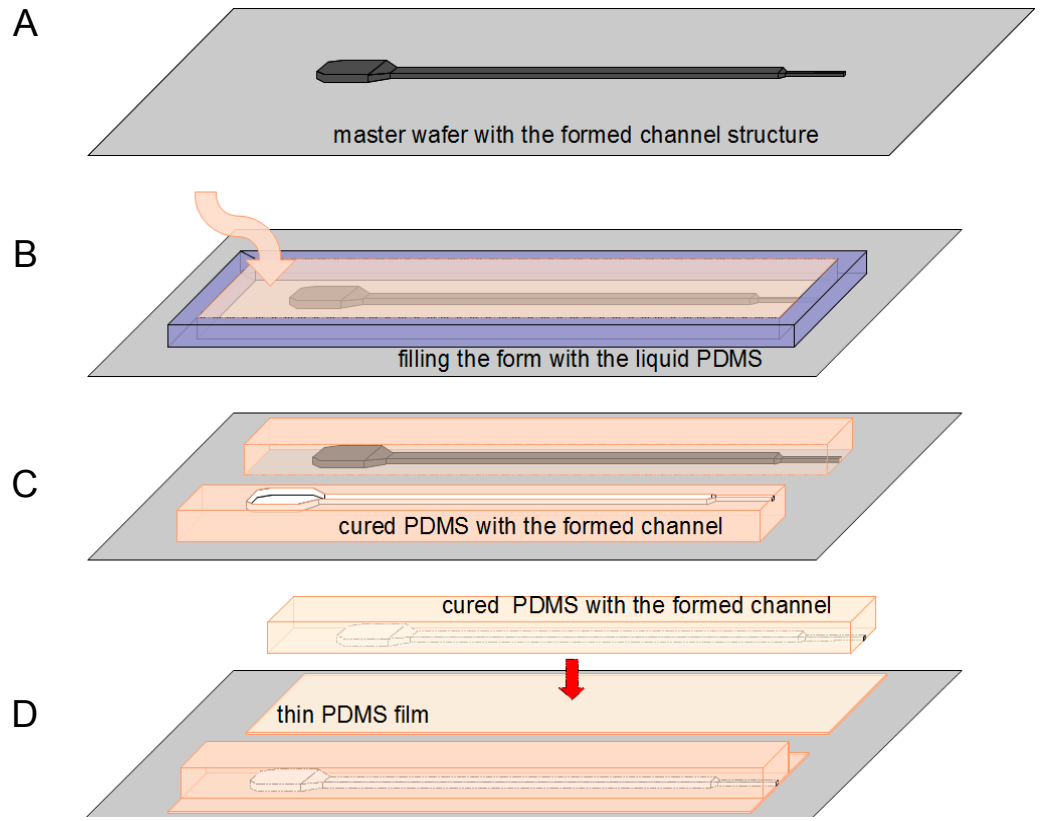

Figure 4.9 a) SU-8 structure of the channel on the master wafer; b) PDMS casting onto the wafer with capillary pattern within a glass mold; c) Hardened PDMS structure on the wafer pattern and detached for further use; d) Assembly of the PDMS bulk with the thin film (both surfaces are activated in plasma before the assembly) and the final the top structure of the µ-Chip.

A thin PDMS film of 50 µm thickness was manufactured as described in section 4.3.5.4. The surfaces of both thin film and PDMS structure are activated in the plasma as described in section 4.3.5.5. The PDMS structure was placed on the activated thin film and pressed together for 10 minutes. A good bonding of the surfaces was obtained. The thin film works as a lid for the capillary pattern on the PDMS bottom surface. The physical capillaries of rectangle cross-section were formed according to the pattern at the master wafer.

4.3.6. Final µ-Chip assembling procedure

The final view of the assembled µ-Chip is presented at the figure 4.10. The top µ-Chip part was manufactured with either one of two proposed approaches. The bottom glass base with coupling electrode is manufactured as described in section 4.3.2. Both surfaces were again subdued to plasma activation 4.3.5.5. By assembling the parts together as shown in figure 4.10 the final µ-Chip body was obtained.

In the case of simplified structure with mechanically-formed capillaries (section 4.3.4.) the inlet already contains a short capillary piece, which is hermetically sealed to the internal capillary. For the advanced top structure with wafer-casting-based capillary formation, the capillary must be connected in a separate step.

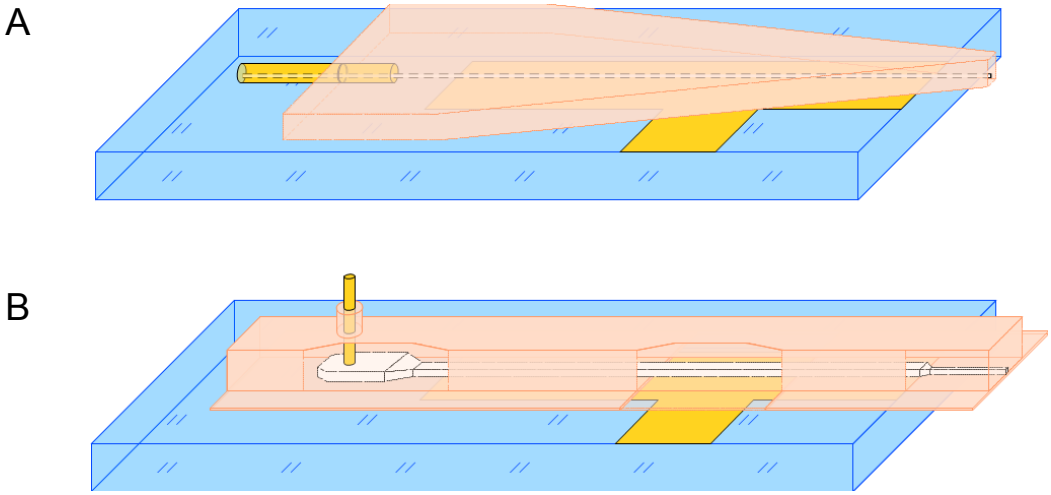

Figure 4.10 Overview of the µ-Chip with the DB-ES source. Bottom part includes the glass with the sputtered metal layer in both cases. The top part includes the PDMS bulk with the formed channel; a) Assembled µ-Chips with a) round channel outlet and triangle nozzle-type and b) with the rectangle capillary cross-section and flat-surface outlet type.

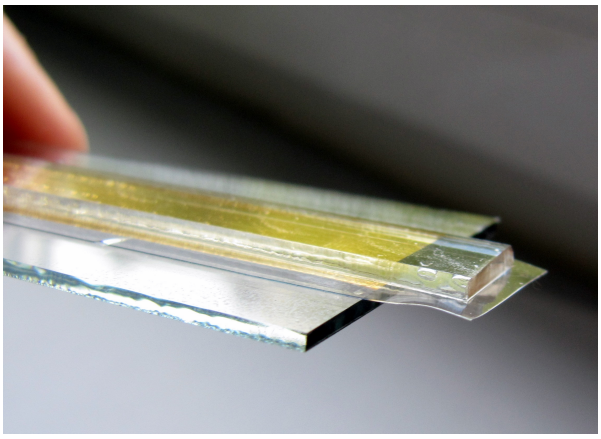

Figure 4.11 The photo of the assembled µ-Chip with the DB-ES source (before nozzle cutting).

4.3.6.1. Capillaries connection

The silica glass capillaries with 50 µm i.d. and 360 µm o.d. were used for connection to the pump system . Small connectors also made out of PDMS were used for finer connection of the glass capillary to the µ-Chip. These connectors had a cylinder form with dimensions of 2 mm in diameter and 2 mm in height. A tiny hole was made along the main cylinder axis. A glass capillary approx. 5 cm length was inserted through this connector. The tip of the

capillary should stick out out of the connector for 1-2 mm. This 1-2 mm capillary piece was inserted into the μ-Chip capillary inlet hole and hermetically sealed with the liquid PDMS.

The same PDMS Sylgard 184 mixed in the proportions of 3:5 and carefully degassed was used for sealing. Being mixed in this proportions, PDMS needs a very short time to harden, especially when the hardening process is accelerated with the heating process on the hot plate. The tip of the external capillary with PDMS connector was inserted into the μ-Chip inlet, and the structure was placed on the hot plate. The hot plate surface was heated to 100 ºC. A small droplet of PDMS was placed onto the surface of inserted glass capillary. The droplet slips down to the interface with the μ-Chip, flows over the connector, and after touching the hot PDMS bottom structure immediately hardens. The connector here plays the role of a lid to prevent the liquid PDMS dro pfrom flowing into the channel and sealing it from inside.

4.3.6.2. Nozzle formation

The first simplified structure requires no nozzle formation. Technically, the nozzle emitter type is already present due to the specific form of the μ-Chip body at the capillary outlet, which appears due to specific procedure of PDMS casting (see section 4.3.4.).

For the second structure two alternative solutions exist. The nozzles can be formed by shaping the structure manually with a cut procedure. This method however relies strongly on a human factor and thus return rather unstable and unreproducible results.

As a working solution, the μ-Chip can be cut once perpendicularly to the capillary to obtain a flat emitting surface with an outlet. The outlet surface can then processed as discussed in section 4.2.4.2. to obtain high surface hydrophobicity. In this case the stable electrospray can be expected from the flat-surface outlet and complex nozzle formation can be avoided.

4.4. DB-ESI μ-Chip characterization

Two possible structures of the DB-ESI PDMS μ-Chips were developed and manufactured. The functionality of both proposed structures was verified in the standard setup.

The first structure is the PDMS μ-Chip with the round channel and nozzle emitter type at the apex of the triangle outlet. The second structure is the μ-Chip with the rectangular channel shape and the square outlet at the flat cut outlet surface without any nozzle formation.

4.4.1. DB-ESI µ-Chip with the mechanically – formed channel

The first µ-Chip was tested in the setup similar to one, used in chapters 2 and 3. The supply pump was connected through the long capillary to the µ-Chip inlet, and the standard electrolyte was pumped into the system. The solution of water-methanol (1:1) with 1 % acetic acid was used as an electrolyte in following experiments.

The HV supply was connected to the µ-Chip coupling electrode. The voltage pulses were applied at 10 Hz frequency, and the amplitude was slowly increased. Starting with the amplitude of 4.0 kV the stable electrospray from the µ-Chip was observed.

In this experiment no counter electrode was used, so no measurements of the current curves were performed. The electrospray was monitored with small camera located close to the outlet. The photo of the electrospray is shown in figure 4.12.

The electrospray obtained from the round channel in the µ-Chip is a proof that the ionization of a fluid through a thin dielectric layer of PDMS is possible.

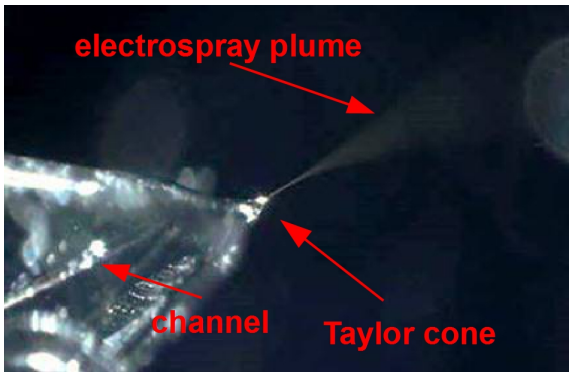

Figure 4.12 A photo of the electrospray obtained from the DB-ESI µ-Chip with round channel and nozzle-type capillary outlet at the emitter. Applied voltage is 4,0 kV, f=10 Hz.

Such simplified assembly process involving a metal wire for mechanical channel formation is unstable and strongly dependent on human factor. Moreover, the proposed structure is not applicable for manufacturing of the µ-Chip with multiple channels, located at equal distances from each other. Thus, the second structure, where the channels were manufactured using the master wafer, was used for the further analysis.

However, this experiment has shown that a simple polymer membrane with thickness of approx. 150 µm serves as a good dielectric for DB-ESI source purposes. Without any additional processing, the thin PDMS layer provided very good coupling of metal electrode

to the electrolyte within the channel, and allowed to obtain a stable electrospray. This assembly technology can be considered to be perspective for the local applications and will be upgraded in the future.

4.4.2. DB-ESI µ-Chip with wafer-casting based rectangle channels

In the DB-ES µ-Chip two factors influence are responsible for the stable electrospray formation process. The properties of the coupling electrode and dielectric barrier are responsible for the electrolyte ionization, while the surface properties of the emitter outlet affect the Taylor cone formation and corresponding electrospray stability. The second µ-Chip structure has both factors in it, and both are unknown. The experiment was set to verify each factor separately.

It was shown in chapters 2 and 3, that the process of ionization and charge separation in the DB-ES system depends on the coupling electrode shape and on the dielectric properties of the insulator material. The rest system properties affect the propagation of the charge through the system to the counter electrode (or to the MS inlet). The test setup with the counter electrode, which was used for the measurements of the output signal and the electrospray current, was described in the chapters 2 and 3 in more details. Figure 4.13 shows the modified setup, which was assembled in order to demonstrate the ionization properties of the DB-ESI µ-Chip. Figure 4.13 a demonstrates the initial capillary system with the 4 cm coupling electrode deposited directly onto the capillary. The capillaries used in the system had 75 µm i.d and 80 cm length. The distance to the emitter from the coupling electrode is 16 cm, the emitter has 75 µm i.d, 5.5 cm length and 8 µm i.d at the tip.

Figure 4.13 b demonstrates the modified setup. Instead of the coupling electrode the DB-ESI µ-Chip was connected between the supply capillary and the electrode capillary. In this setup, the ionization takes place in the DB-ESI µ-Chip. The coupling electrode also has the length of 4 cm and is located inside the µ-Chip under the capillary channel with rectangle cross-section of 70×56 µm. The coupling electrode was separated from the channel with 50 µm thin PDMS film. The distance from the coupling electrode in the µ-Chip to the emitter tip was fixed at the same 16 cm as in the reference setup. The same emitter with 75 µm i.d and 5.5 cm length was used. The supply and emitter capillaries were inserted into the DB-ESI µ-Chip in such a way, that the electrolyte from the syringe was flowing through

the chip, ionized with DB-ES coupling electrode, and followed the capillary to the emitter tip.

Altogether, the test setup with DB-ESI µ-Chip was assembled so, that the ionization takes place inside the channel using the built-in coupling electrode. In the same time the common emitter is used for spraying, thus the outlet surface properties of the µ-Chip are not involved in the electrospray formation process within this experiment.

The voltage pulses with 5.5 kV amplitude were applied to both systems at 10 Hz frequency. The obtained signal responses at the counter electrode were measured for both original coupling electrode and DB-ESI µ-Chip coupling electrode. The measurement results are shown in the figure 4.14.

The stable electrospray was observed in both cases. The same current components were observed at the response curve, both with ionization performed within the DB-ESI µ-Chip and in original capillary system. The EMT, ion current and electrospray peaks appear simultaneously in both setups. The ion current peak (marked with “b” letter) appears with the same 1.2 ms delay in both cases. The electrospray current (marked with “c” letter) reaches the maximum value at 7 ms in both cases. This is explained by the same test setup configuration. The time delay to the first two peaks (EMT and ion current) is determined by the test setup properties. According to the electric circuit model discussed in the chapter 3, the time delay until the second signal peak in the response is the time necessary for the ionized particles to reach the emitter tip and to form sufficient potential there.

The heights of the peaks are different for two discussed ionization types. The ion current peak in the case of normal capillary ionization has two times higher value than the one obtained with µ-Chip ionization. The electrospray current also shows visible deviation. The stable electrospray value of 0.11 µA was obtained in the case of DB-ESI µ-Chip ionization, while a less stable but initially higher current was observed with the original coupling electrode. This is explained by the lower electrode coupling capacitance in DB-ESI µ-Chip compared to the original electrode deposited directly onto the capillary.

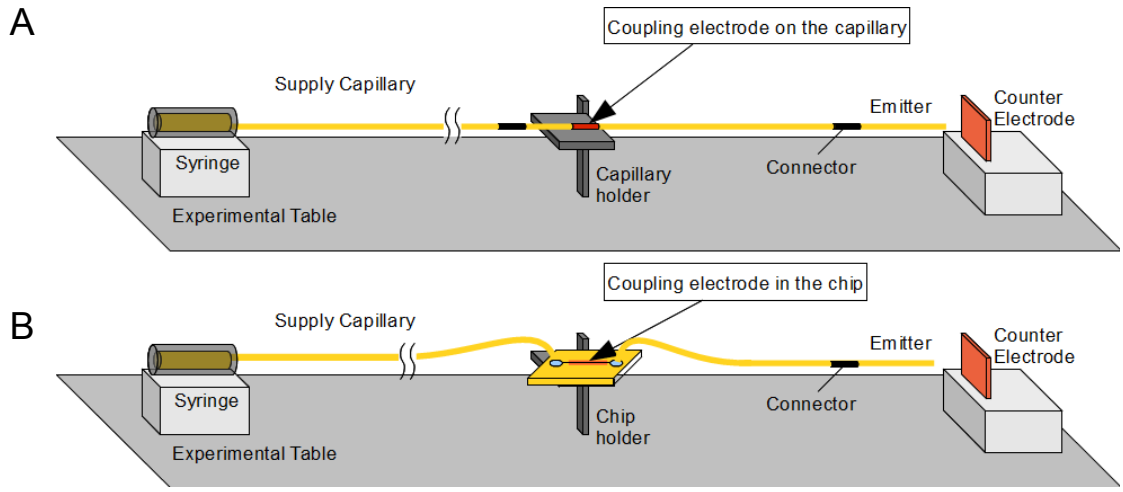

Figure 4.13 a) Schematic representation of the original DB-ES setup. Coupling electrode is sputtered on the the electrode capillary; b) Schematic representation of the setup with coupling electrode located inside the DB-ESI µ-Chip. The supply capillary and emitter are the same in both cases.

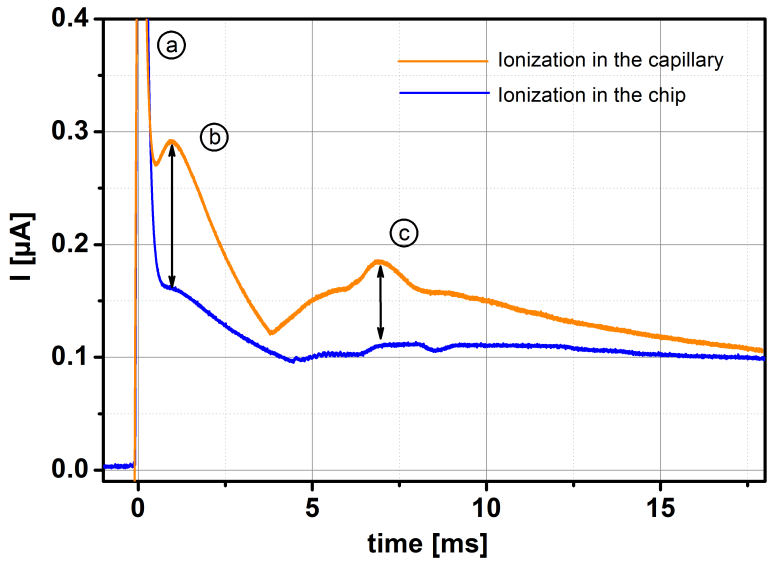

Figure 4.14 Total counter electrode current responses obtained at the 5.5kV applied voltage and 10 Hz frequency for the different types of the coupling electrode: red line shows the current response for the coupling electrode sputtered directly at the capillary, while the blue line shows the current response for the coupling electrode in the DB-ESI µ-Chip.

The experiment shows, that the ionization in DB-ESI µ-Chip functions properly and shows qualitatively same results as original ionization, while quantitatively smaller differences can still be observed.

In the second experiment the second unknown factor, the outlet influence on the electrospray characteristics, was verified. The DB-ES µ-Chip was manufactured according to the entire

procedure, including the outlet formation. The rectangular channel outlet was located at the flat PDMS surface. The surface was processed with high temperature as discussed in section 4.2.4.2. to obtain highly-hydrophobic properties. A DB-ES test setup was assembled.

The DB-ESI µ-Chip was located in 2 mm in front of the counter electrode in the same way as the standard emitter in the previous experiment. The voltage pulses of 6 kV and 33.3 Hz with the duty cycle of 80 % were applied, and the response signal at the counter electrode was measured. The measured response for flat-surface outlet is shown in figure4.15.

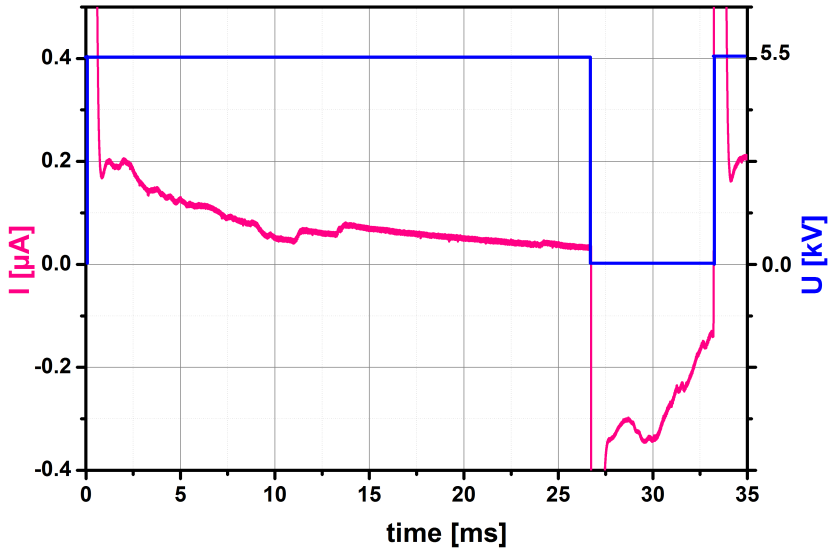

Figure 4.15 Total counter electrode current responses obtained from the µ-Chip with the square channel outlet and flat nozzle-type of the emitter at the the 6 kV applied voltage and 33 Hz frequency with duty cycle 80 %. The stable electrospray was obtained from the flat nozzle of the µ-Chip.

Under the applied voltage pulses, the current response of the expected shape was observed. At the response curve the same current components such as very short EMT signal, ion current peak at 1.6 ms and the electrospray current can be seen. The electrospray current has approx. value of 0.1 µA, which is comparable with the values obtained in the experiment with the standard emitter and µ-Chip combination. The 80 % duty cycle was used in order to obtain more positive ions for the MS investigation (see paragraph 3.7. for details).

After the presence of the electrospray current was confirmed with counter electrode measurement, the µ-Chip was placed in front of the MS inlet. A stable electrospray was again observed, both visually and on the MS screen in form of measured absolute intensity

of the signal. The absolute intensity of the electrospray signal and reserpine spectrum captured by MS in continuous operation mode is shown in figure 4.16.

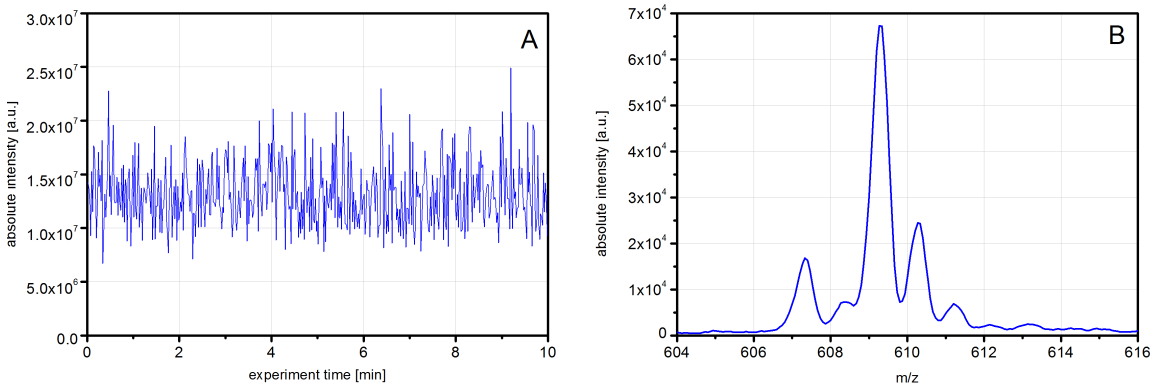

Figure 4.16 DB-ES μ-Chip – MS combination: a) the absolute intensity signal obtained from the μ-Chip; b) Reserpine spectrum. Parameters: 6 kV applied voltage, 33 Hz frequency, duty cycle 80 %.

The second experiment has confirmed, that the stable electrospray can be obtained also from the flat-surface emitter outlet without any complex nozzle formation. The significant condition is the high hydrophobicity of the surface surrounding the outlet.

4.5. Conclusions

In the current chapter the development procedure for the μ-Chips with dielectric barrier electrospray ionization was described. The dielectric barrier between the electrolyte in the capillary channel and the coupling electrode was created of the thin 50 μm PDMS film. The PDMS material and casting technique was used also for the main μ-Chip body and capillary channel formation. The coupling gold electrode was sputtered on the glass base surface.

The final μ-Chip has the sandwich structure and consists of the several component, namely the PDMS body with the channel, the PDMS thin layer (dielectric barrier) and the glass base with the sputtered coupling electrode. All these layers were assembled together using the surface activation in the plasma.

The μ-Chips with different geometries and channel cross-sections were manufactured in the work. The first developed μ-Chip had the channel with round cross-section and the sharp nozzle outlet. For the formation of channels with round cross-section, a thin metal wire was

used. The second μ-Chip had the rectangular channel shape and the flat nozzle outlet. The channel was manufactured using the soft lithography and following PDMS casting and hardening on the surface pattern.

The electrospray obtained from the round channel outlet is a proof that the ionization of a electrolyte through a thin dielectric layer of PDMS is possible. For the μ-Chip with the rectangular channel the ionization efficiency comparison with the capillary ionization was performed. The ionization in DB-ESI μ-Chip works properly and shows qualitatively same results as original ionization, while quantitatively smaller differences can still be observed.

The surface properties of the PDMS flat outlet were modified using the high temperature treatment in order to make the PDMS surface extremely hydrophobic. A stable Taylor cone was observed at the modified surface and good signal was detected with the MS instrument.

The proposed assembly procedure based on PDMS-casting onto the wafer with initially-manufactured channel relief opens vast opportunities for further structure development, including manufacturing of the μ-Chips with multiple channels and electrodes, or the formation of complex electrode shapes to obtain higher coupling. This also allows to combine the DB-ESI with any separation procedure which is realizable within a capillary system.

Chapter 5 DB-ESI application for multiple-emitter systems

5.1. Free-flow electrophoresis

Free flow electrophoresis (FFE) is a well known and established separation technique for the protein investigation. In the FFE the sample separation is performed continuously, hence FFE fits to the sample preparation in the large scale. This technology is based on difference in the masses and electrical charges of different components in the mixture. FFE system uses a chamber, where the analyte flow creates the hydrodynamic force. Electric field is applied to the chamber in such a way, that two emerging forces (hydrodynamic flow and electric field) create two orthogonally acting velocity vectors which are equal to the flow velocity and proportional to the electrophoretic mobility, respectively. The resulting velocity vector deviates by a specific angle from the flow direction. For different analytes with different size and charge and therefore different electrophoretic mobilities, the angles are different and thus the analytes are separated continuously in a two-dimensional manner at the outlet of the separation chamber. Hence, the time domain of separation is transferred to a local domain [66].

The hydrodynamic and the electrophoretic forces are in a steady-state when the applied pressure and voltage are constant. Thus the analyte will be always focused to the same outlet channel. Due to this FFE peculiarity, combination of the FFE separation system with the ESI source becomes attractive for the rapid components analysis using MS.

FFE and electrospray integration requires the development of the stable multiple electrospray clusters. A multiple-channel electrospray system can be connected directly to the FFE chamber outlets. In this case the number of the outlets corresponds to the electrospray numbers in the array.

Development and operation of such multiple-channel electrospray system is a technically complex process. However, multiple electrospray emitters have several advantages over single-spray emitters. The high sample throughput and improved mass spectrometry sensitivity makes the electrospray sources very attractive for these applications.

5.2. Multi-nozzle emitters

Investigations on multiple electrospray emitters have been performed in the last years by different research groups. In 1992 Rulison and Flagan [67] have reported about established Taylor cones at the outlets of the capillary array. Eight stainless capillaries with the squaring tips shapes were used. All capillaries were placed in one line. The same potential value was applied to all capillaries. Each capillary have sprayed approximately the same volumetric flow rate of the liquid. It was shown, that with the linear capillaries array the onset voltage should be higher, than for the single capillary operation mode. Influence of the capillary radius and spacing on the onset voltage was demonstrated. For the smallest diameter-to-spacing ratio (this corresponds to the case when only a single capillary is used) the voltage of 4.8 kV was required to obtain the Taylor cone. When the ratio was increased to 1.6, then 7.4 kV voltage was required to establish the stable Taylor cones.

In 1999 Almekinders and Jones [68] have reported about a multiple jet electrospray atomizer (length is 15 cm) with eight emitters. The emitters were placed in one line with an equal distance between emitter tips. A very high voltage (35 kV) was required to obtain the electrospray from this array.

Tatemoto [69] have investigated the multiple-nozzle emitters with a different number of nozzles. All nozzles had 210 μm diameter and were placed at the equal distances from each other in the circle shape (distance between nozzles was varied from 0.7 to 3 mm in the different experiments). The cone jet mode with the finest droplets formation for one nozzle was obtained at the 5.5 kV applied voltage. The cone-jet mode for the array of 7 emitters was established under the 8.0 kV. The operation voltage for the 19-emitter array cone-jet mode was 12.5 kV. A higher voltage in the multiple-nozzle case is required because the electric field intensity at the tip of the capillary nozzle decreases as a number of capillary nozzles increases in order to obtain a finest drop of uniform size for the multiple-nozzle emitter. The

authors have shown, that the voltage required for the steady cone-jet mode increases linearly with the number of capillary nozzles.

A micro fabricated electrospray array was established by Tang in 2001 [59]. A polycarbonate substrate was used for the multiple-nozzle system. An array of nine electrospray emitters was arranged in a 3×3 configuration using a laser ablation method. The emitters have 30 μm holes at the tip and were positioned 1.1 mm apart. The high voltage around 7.0 kV was required in order to establish the stable focused electrospray from all emitters.

5.3. Effects of nozzle interaction

In the multi-nozzle electrospray system the interaction between the capillary nozzles is the important factor for the fine droplets of uniform size formation. These fine droplets are obtained when only a small interaction between the capillary nozzles exists.

In order to show the possible interactions between electrospray capillaries, two fused silica capillaries (o.d. 360 μm, i.d. 50 μm) were placed close to each other in parallel (figure 5.1). Both capillaries were filled with a mixture of purified water and methanol 1:1 (v:v) with 1 % acetic acid using 1 μL/min liquid flow rate. The high voltage of 2.5 kV was applied to the capillaries, using the metal wires (direct contact to the liquid). Taylor cones were formed at the outlets of both capillaries.

Two effects, the Taylor cone repulsion and the Taylor cone confluence, have been observed during the experiment.

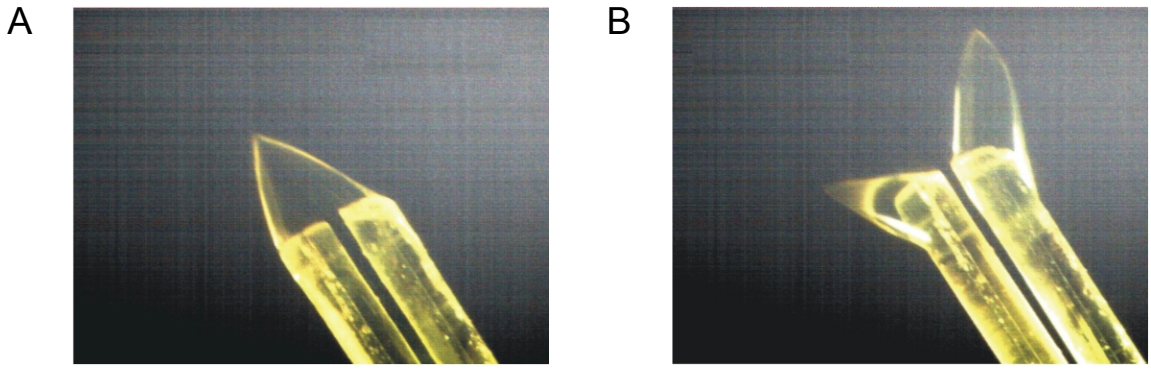

Figure 5.1 Two fused silica capillaries (1 and 2) are operated under the 2.5 kV. Observed Taylor cone formation effects: a) Taylor cone repulsion effect; b) Taylor cone confluence effect.

Figure 5.1 illustrates the repulsion effect (a) and the confluence effect (b). In the figure 5.1 a the formed Taylor cones are turned 90° away from each other. This repulsion effect is caused by electrical Coloumb repulsion force, caused by the potential of the same polarity applied to both capillaries. In figure 5.1 b the formed Taylor cones are overlapped and form a single large cone. The overlapping effect occurs at a high liquid flow rate when the outlet of the capillary is large.

The Taylor cone repulsion effect changes the cone apex position and hence, the direction of the formed electrospray is changed. In this case ionized substances will not reach the MS inlet. When the cones are overlapped, it is not possible to obtain the uniform droplets from the formed large cone. This leads to the a decreasing of the current signal. It was confirmed by a series of experiments, that the flow rate intensity can manage those effects. For higher flow rates the Taylor cones are becoming larger and hence, the interaction effects are stronger.

The interaction between the nozzles is an important factor for electrospray stability. The finest droplets could be obtained only when almost no interaction between capillaries exists. Smaller flow rate and surface outlets area helps to manage the interactions between capillaries, but can not solve the problem entirely.

5.4. Experimental validation of multiple-emitter DB-ES system

The finest operation of the multiple-nozzle system can be reached, when each working emitter is electrically insulated from the neighbouring one: the operated voltage is applied sequentially to each emitter. The facilities of the DB-ESI source can be successfully involved in such a multiple-nozzle system. The multiple-nozzle DB-ESI system facilitates high throughput MS measurements and avoids the direct physical contact between electrode and solvent.

Figure 5.2 shows a schematic representation of such DB-ESI system. The setup includes the holder with three emitters, the unique syringe for each emitter and a special constructed high voltage supplier for electrospray operation. Three fused silica emitters were used in the experiment. Each emitter has equal geometry: 5.5 cm length, 360 µm o.d., 50 µm i.d. and 8 µm i.d at the tip. The coupling electrode of 2.5 cm length was sputtered on each emitter in the middle. Emitters were placed in one horizontal plane using a holder. The angle between

two emitter tips were fixed at 30°. Each emitter was separately connected to the syringe using the supply capillary (20 cm length, o.d. 360 µm and i.d. 50 µm). For the applied voltage generation the positive high voltage generator (F.u.G. Electronic GmbH, Model HCN 7E 35000, Rosenheim, Deutchland) and the home made multi-DB-ES ISAS generator were involved. The DC generator generates the high positive voltage of 3 kV. The multiple DB-ES generator forms rectangular pulses for each emitter separately as shown at the figure 5.3 a.

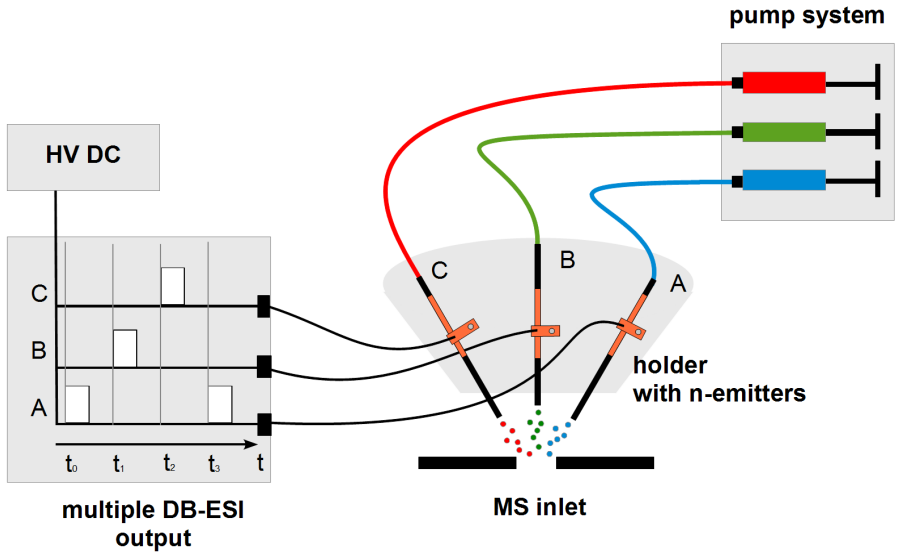

Figure 5.2 Scheme of the multiple-emitter DB-ESI system experimental arrangement

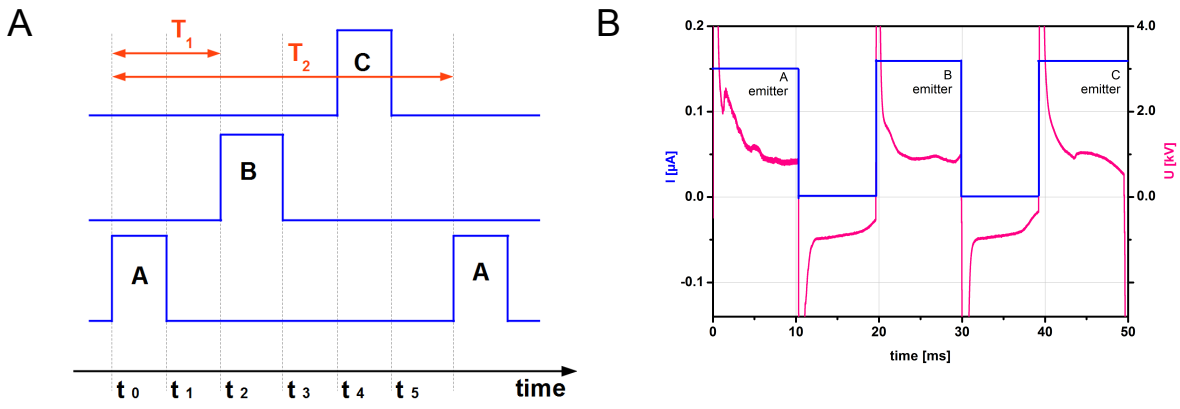

Figure 5.3 a) Time diagram of voltage: individual positive and negative pulse edges are applied sequentially to the A, B, C emitters using the multi-DB-ESI generator; b) Overview of the positive and negative current responses from individual emitters.
Parameters: flow rate: 0.3 µL/min; applied voltage: 3 kV.

Each emitter is operated with an individually applied voltage pulses, which are applied to the emitters one by one sequentially.

The HV signal generator produces the DC supply high voltage of 3 kV amplitude. The DB-ES generator distributes this high voltage with three separate pulses to three emitters. The internal DB-ES generator frequency was set to 50 Hz what corresponds to 20 ms time period for each emitter. In each time period both positive and negative edges are applied to one emitter with 10ms time delay. In three consequent time periods the pulses are applied to three emitters correspondingly.

For the electrical measurements the solution mixture of 1:1 water-methanol (v:v) + 1 % acetic acid was used. The electric current responses were measured at the counter electrode located at a distance of 3 mm in front of emitter tips. The current response from the electrode to ground was measured in the same way as described in section 2.2.1.

The current responses are shown at the figure 5.3 b with the blue lines. Red lines shows the applied voltage edges. Smaller differences in the shape of current responses can be observed due to the fact, that emitters in the setup could be not assembled completely symmetrically.

For clarity, the process is shown in figure 5.3 a. At the time t_0 = 0 ms the positive pulse edge is applied to emitter A. At t_1 = 10 ms the negative pulse edge is applied to emitter A, and the applied voltage at the emitter A returns to zero level. At t_2 = 20 ms the same positive edge, and at t_3 = 30 ms the same negative edge is applied to emitter B. At t_4 = 40 ms and t_5 = 50 ms the same occurs at emitter C. After the total time period of T = 60 ms the process starts again.

In such configuration the same time delay of 10 ms can be observed between any two consequent applied edges. When the signal at each emitter is observed separately, the duration of the positive and negative pulse component is 10 ms and 50 ms, which corresponds to 16.66 Hz frequency with 16.6 % duty cycle.

In this operation mode, the negative spray will discharge the capillary almost completely before the new positive edge is applied. Hence each new positive spray current will have the same height as the first positive current response. This electrospray phenomena was discussed in more details in sections 3.6.2. and 3.6.3.

The photo of electrospray plumes produces by multiple-nozzle DB-ESI system is presented in the figure 5.4. The fluorescein component was added in the solution of of 1:1 water-methanol (v:v) + 1 % acetic acid for better plume visibility. The Leica camera was used and the normal day light was focused to the emitter tips with a lens system. The photo of working electrospray system was made using 2 s exposure time.

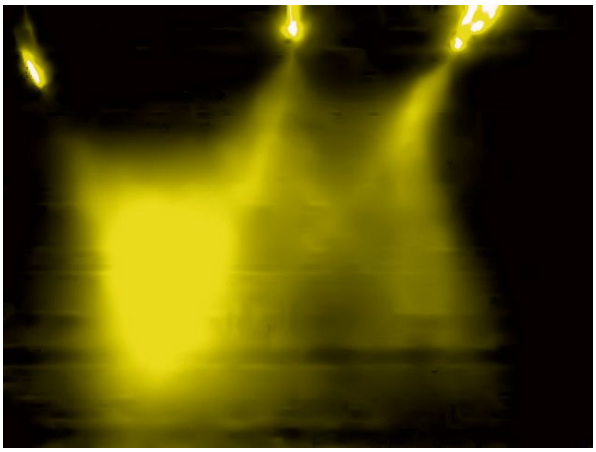

Figure 5.4 Photo of three electrosprays obtained from the multi-nozzle DB-ESI system operated at 3 kV with solution: methanol-water 1:1+1 % acetic acid + fluorescein. Exposure time 2 s.

5.5. Analytical application example

The multiple-nozzle DB-ES system was used in combination with a MS device to obtain the spectrum of amino acids mixture. Four amino acids in different concentrations were used in the experiment: Histidine (50 µmol/L), Arginin (50 µmol/L), Tryptophan (200 µmol/L) and Glutathion (200 µmol/L). For the calibration purposes, the normal ESI with the single emitter (o.d. 360 µm, i.d. 50 µm and 8 µm at the tip) was used. The amino acids mixture was placed into one syringe. The 2 kV high voltage was applied using a metal wire to the solution. MS was used in positive mode with automatic gate control (AGT) injection time and one micro-scan mode in MS preferences. The measured TIC for the amino acids mixture is presented in figure 5.5 a with the black line. The TIC absolute value of $6.1 \cdot 10^6$ was measured. For the multiple-nozzle DB-ESI system test, the amino acids Histidine, Arginin and Tryptophan were placed in three different syringes and Glutathion was added in each syringe as well. The same concentrations of all acids were used, as was mentioned above for the conventional electrospray. The flow rate in each emitter was fixed at 0.2 µL/min. The high voltage edges were applied to the emitters as was described before.

Table 5.1. - Amino acids concentrations for each emitter

Emitter A	Histidine (50 µmol/L) + Glutathion (200 µmol/L)
Emitter B	Arginin (50 µmol/L) + Glutathion (200 µmol/L)
Emitter C	Tryptophan (200 µmol/L) + Glutathion (200 µmol/L)

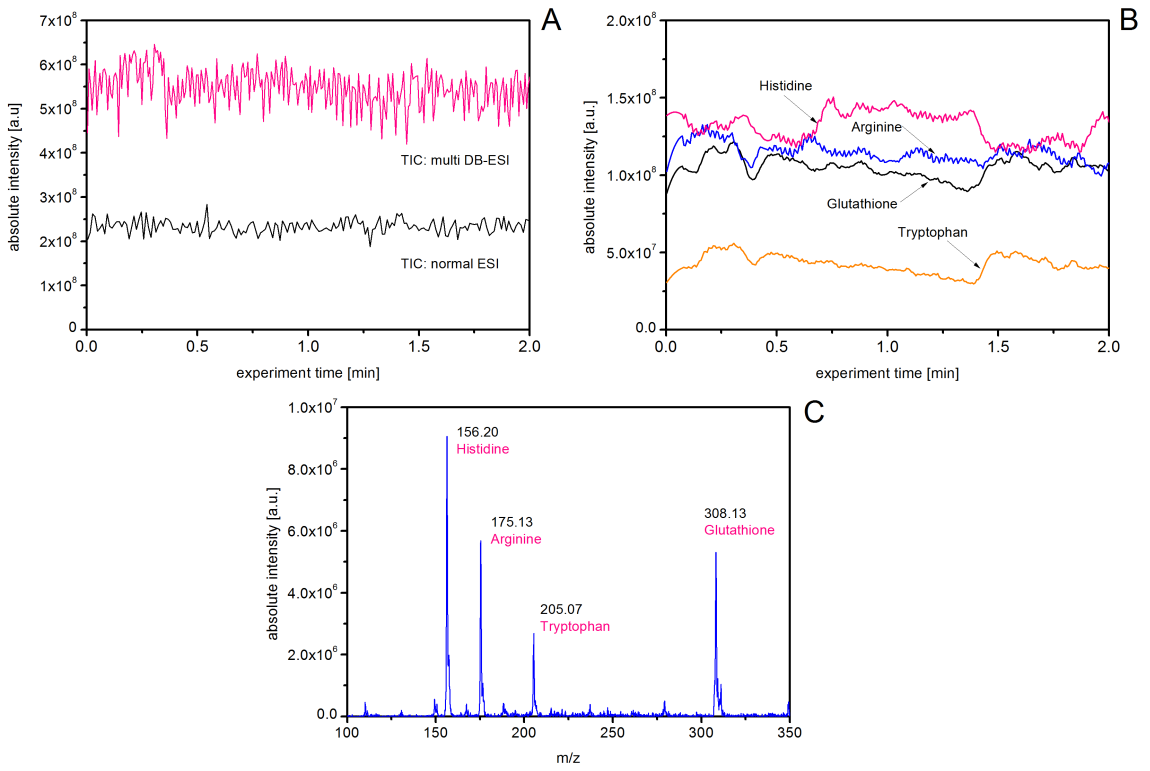

Figure 5.5 a) TICs obtained for amino acids mixture employing the normal ESI source (black line) and employing the multi-nozzle DB-ESI source (red line); b) Current intensities of the individual mixture components, obtained with the multiple-emitter DB-ESI source: tryptophan (blue line), glutathione (black line), arginine (green line) and histidine (red line); c) Amino acids mixtures mass spectra, obtained with the multiple-emitter DB-ESI source; Parameters: flow rate 0.2 µL/min, DB-ESI voltage 3 kV, normal ESI voltage 2 kV; Amino acids concentrations: Histidin - 50 µmol/L, Arginin - 50 µmol/L, Tryptophan - 100 µmol/L, Glutathion – 100 µmol/L.

The MS was used in positive detection mode with 35 ms injection time and one micro-scan mode in the preferences. The measured total intensity current for amino acids mixtures from three emitters is presented in figure 5.5 a with the red line. The TIC absolute value of $8.3 \cdot 10^6$ was registered for the multiple-emitter DB-ES system. Figure 5.5 b shows the absolute intensities of the individual components from different emitters, obtained with the same

scanning time. The absolute registered values of the amino acids were $7.5 \cdot 10^6$ for Histidine, $8.3 \cdot 10^6$ for Arginin (50 µmol/L), $6.0 \cdot 10^6$ for Tryptophan (200 µmol/L) and $2.3 \cdot 10^6$ for Glutathion (200 µmol/L). The mass spectrum of amino acids is presented in figure 5.5 c.

The experiment has shown, that the developed dielectric barrier ionization method can be successfully applied to multiple-emitter electrospray applications.

5.6. Conclusions

Multiple-emitter electrospray system makes it attractive in comparison with the single-spray for the MS analytical investigations. The DB-ESI technology can be successfully integrated in the multiple-emitter system. The first steps have been done in this direction.

It was shown, that efficiency of the DB-ESI multiple-emitter electrospray source is higher in comparison with the single electrospray source. The electrospray system based on the dielectric barrier technique have been successfully integrated with the multiple-emitter electrospray system using the special HV generator. The voltage pulses have been applied to each emitter one by one. In this system each working emitter was electrically insulated from the neighbor one: the operated voltage was applied sequentially to each emitter.

The finest operation of the multiple-emitter system have been reached for the three-emitter configuration. It was shown with the current measurements and proved by the mass spectrometry investigations, that usage of the non-contact DB-ESI technique in combination with the multiple-emitter system increases significantly the signal efficiency.

Conclusions

The soft electrospray ionization technique based on the dielectric barrier (DB-ESI) have been studied in detail in the current research. The physical mechanism of the electrospray ionization is based on ion generation under the atmospheric pressure using an external high electric field. Comparing to the commercial electrospray, no direct contact of the electrode to the electrolyte is used in the DB-ESI source. A dielectric barrier is present between the external electrode and the electrolyte. The displacement current in the dielectric barrier is utilized as an intermediate charge transfer mechanism from the external electrode to the analyte. DB-ESI technique prevents emitters from erosion process and hence increase their life times.

For the empirical investigations of the DB-ESI method, the experimental setup has been used. The physical mechanism of the charge transfer process in DB-ESI capillary system has been investigated. The electrospray current signal was measured and could be divided into several individual components, which correspond to different charge transfer mechanisms in the DB-ESI capillary system. The charge transfer from the coupling electrode, where the high potential was applied, to the emitter orifice and finally to the counter electrode was investigated. The electrospray current signal was analyzed for different geometrical setup configurations, various capillary, emitter and analyte properties.

The displacement current which is initiated in the dielectric barrier (fused silica capillary wall) transfers the charge from the sputtered coupling electrode to the electrolyte, when the square wave voltage is applied to it. When the positive or negative slope of the square wave signal is applied, the dipoles of the fused silica material change the orientation in the electric field direction. This rotation of dipoles is very fast and results in the small shifts of electrical charges. This is physically equivalent to the electric current directed from the external electrode surface to the inner surface of the capillary wall. After this displacement, the charge is transferred in electrolyte inside the capillary volume to the emitter tip. This current is called ion transfer current. The ion transfer current causes the increase of the potential at the emitter tip. The potential difference between the emitter tip and the counter electrode forms the Taylor cone at the emitter tip. Due

to the Taylor cone formation at the emitter tip, the electrospray appears and transfers the charges to the counter electrode, where they can be measured.

It was found, that the total current response measured at the counter electrode comprises several components in addition to main electrospray current. First, the electromagnetic transmission current component, i.e. the charge transfer with the electromagnetic field from the coupling electrode, was observed as a sharp and short current peak in the measurement. This peak have been registered at the beginning of the time scale. Next, the ion current peak which is responsible for the forming of the potential at the emitter tip, appears in the measured signal as a smoother (in comparison with the electromagnetic transfer signal) second peak. Finally, with a smaller time delay after ion current peak, the stable electrospray current was observed. It was shown, that the capillary system dimensions and the properties of the sputtered electrode have significant influence on the ion current formation and hence on the electrospray current component. The ion current peak can be detected when the distance between the coupling electrode and the emitter tip is significant. The position of the ion current peaks do not show the absolute time of movement from the counter electrode to the emitter tip for each ion type. The exchanging time of the cations and anions is resulting in the ion current peaks. The positive ion peak formation is impossible without negative ions movement and vice versa.

The electrolyte concentration and the ion properties, namely the ion size, the mobility and the ion concentration, summarized as the electrolyte specific conductance, have shown significant influence on the ion current peak formation and hence on the electrospray current starting time and its intensity.

The electric circuit for the DB-ESI capillary system was developed. The DB-ESI physical setup was separated into the different components with the unique properties. The main properties of each unique component and its contribution to the total current formation were discussed. All components of the experimental capillary setup were modeled with corresponding active and passive electrical circuit elements. The circuit includes the models for the coupling electrode, electrolyte in the both capillary types, air gap between emitter tip and counter electrode, counter electrode itself, electromagnetic signal transfer and electrospray current.

The modeling and simulation process was split in two parts. The “Closed Emitter Model” was used for the simulation of the charge transfer in the capillary system. In this model all system components were included except the electrospray itself. Physically this circuit corresponds to the configuration, where the capillary system is filled with the solution, but the emitter tip clogged. The main focus in this model part was made on the explanation of the potential formation under the coupling electrode and at the emitter tip. The analysis of all charge transfer processes in the system, except of the electrospray formation were performed. The modeling results have very high level of compliance with the results obtained during experimental measurements.

In the second simulation step the equivalent setup circuit “Closed Emitter Model” was extended with a model for the electrospray itself. In the “DB-ES Final Model” the influence of the additional electrospray element on the potential formation process in the capillary system has been shown and compared with the potential formation in the same nodes in “Closed Emitter Model”. Using the developed “DB-ES Final Model”, the simulation of the individual current components (electromagnetic transfer current, ion transfer current and electrospray current) were performed.

The extended model allowed to find and analyze the new effects in the DB-ESI system. It was shown, that electrospray current in the system depends on the number of the consequently applied voltage pulses (i.e. the response to the first pulse and to the n^{th} pulse are different under specific conditions) and that the negative electrospray current component has direct influence on the positive electrospray current component formation. The “DB-ES Final Model” has very good correlation with the results, obtained by current measurements during experiments. Based on the analyzed effects in the DB-ESI capillary system, the effective control of the mass spectrometer signal absolute intensity have been demonstrated.

DB-ESI technique allows to generate ions of both polarities (anions and cations). The mass spectrometry detection can be performed only for the ions of chosen polarity, e.g. positive. Since the DB-ESI technique requires square wave voltage pulses to be applied instead of constant DC voltage level, both negative and positive electrospray currents are produced sequentially after each other. The electrospray current of opposite polarity has shown to be necessary to obtain the

charge compensation in the capillary system, and thus a higher and more stable level of positive electrospray current.

Since both systems, the DB-ESI and the mass spectrometer, run independently, the initial points of the positive electrospray in DB-ESI system and the injection time of the ion trap are random. This leads to the TIC signal decreasing. Due to the technical reasons, the triggering procedure can not be achieved by triggering the mass spectrometer on the DB-ESI, the DB electrospray was triggered to the mass spectrometer.

Using the triggering procedure it was possible to always form the "first" electrospray current response, which has the highest value in comparison with the following pulses. Also with the mass spectrometer measurements the electrospray start times for the fixed geometrical conditions of the DB-ESI capillary system setup have been measured as an additional proof of the varying electrospray starting time discovered with the "DB-ES Final Model".

The μ-Chip with integrated DB-ESI source was developed and fabricated to assure that the discovered ionization method is also applicable in the μ-Chip. The main μ-Chip body with capillary channels was fabricated with PDMS polymer material. The dielectric contact between the liquid in the channel and the coupling electrode was created with a thin 50 μm PDMS film. The coupling electrode was sputtered on the glass substrate. The μ-Chip was assembled as a sandwich structure of PDMS body with capillary channel, thin PDMS layer (dielectric barrier) and the glass substrate with the sputtered coupling electrode. All layers were assembled together using the plasma surface activation.

The different channel geometries were employed. The channels with round cross-section and the sharp nozzle outlet were manufactured using the mechanical mold and thin 50 μm wire on the flat surface. The advanced μ-Chip with the rectangular channel cross-section and the flat nozzle outlet was manufactured by PDMS casting and following hardening on a wafer with capillary pattern created by soft lithography technique.

The electrospray obtained from the round channel outlet was a proof that the ionization of a electrolyte is also possible through a thin dielectric layer of PDMS in a μ-Chip structure. For the second μ-Chip with the rectangular channel cross-section the ionization efficiency was measured and compared with the common capillary DB-ESI. The ionization in the DB-ES μ-Chip functions properly and

shows qualitatively the same results as in the DB-ESI capillary system. Quantitatively smaller differences have been still observed, which might be explained by the lower coupling capacitance in DB-ESI μ-Chip compared to the electrode form in the capillary DB-ES system.

The surface properties of the PDMS μ-Chip flat outlet were modified using the high temperature treatment in order to make the PDMS surface extremely hydrophobic. The stable Taylor cone was observed at the flat-surface in such modified surface, and a good signal was detected with the mass spectrometer. With this experiment it was confirmed, that the sophisticated procedure of the nozzle fabrication is not necessary in the DB-ESI μ-Chip.

The proposed assembly procedure based on PDMS molding technology opens vast opportunities for further structure development, including the manufacturing of the μ-Chips with the multiple channels and hence multiple channels outlets to obtain higher signal efficiency and the possibility to use the DB-ESI technique in the separation systems, where the analysis procedure is transferred from the time domain to the local domain.

The first steps have been done in this direction. The electrospray system based on the dielectric barrier technique have been successfully integrated with the multiple-emitter electrospray system. Using a special generator, the voltage pulses have been applied to each emitter. Each working emitter was electrically insulated from the neighboring one, and the operation voltage was applied sequentially to each emitter one by one. It was shown with the current measurements and proved by the mass spectrometry investigations, that the usage of the non-contact DB-ESI technique in combination with the multiple-emitter system increases the signal efficiency significantly. The emitter interaction problem, when the voltage of one polarity had been applied was solved in the multiple-emitter DB-ESI system as well. The multiple-emitter DB-ESI system is more attractive for the analytical investigations, then the single-emitter electrospray system. The research on the multiple-emitter DB-ESI system is going on.

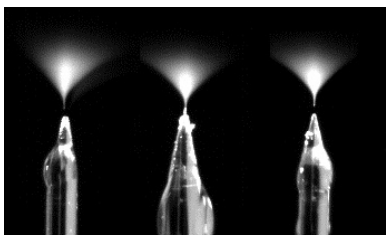

Literature

1 Wolf D. Lehmann, *Massenspektrometrie in der Biochemie*, Heidelberg; Berlin; Oxford: Spectrum, Akad. Verl. (1996)

2 Friedrich Lottespeich, Haralabos Zorbas, *Bioanalytic*, Heidelberg; Berlin: Spectrum, Akad. Verl. (1998)

3 William Gilbert, *De Magnete,* London (1600)

4 Bose, G. M. *Recherches Sur La Cause Et Sur La Veritable Theorie De L'Electricite* Wittembergae (1745)

5 Lord Rayleigh, *"On the Equilibrium of Liquid Conducting Masses charged with Electricity"*, Philosophical Magazine Series 5 Volume 14, Issue 87 (1882)

6 Burton, E. F. "*Effect of electricity on streams of water drops*", Philosophical Magazine 23(133-8): 148-165 (1912).

7 Zeleny, J. "*An apparatus for demonstrating the electrical properties of conducting gases*" Journal of the Optical Society of America and Review of Scientific Instruments 6(5): 521-523 (1922).

8 Sir Taylor, G.*, "Disintegation of water drops in an electric field. Proceed",* Royal Soc. London. Series A: Math. Phys.Sci., 280 (1382): p. 383-397 (1964)

9 Dole, M., et al. "*Molecular beams of macroions*", Journal of Chemical Physics 49(5): 2240-2249 (1968)

10 Iribarne, J. V. and B. A. Thomson "*Evaporation of small ions from charged droplet*s", Journal of Chemical Physics 64 (6): 2287-2294 (1976)

11 Thomson, B. A. and J. V. Iribarne "*Field-induced ion evaporation from liquid surfaces at atmospheric-pressure*", Journal of Chemical Physics 71 (11): 4451-4463 (1979)

12 Fenn, J. B., et al. *Electrospray ionization for mass-spectrometry of large biomolecules*, Science 246 (4926): 64-71 (1989)

13 Yamashita, M. and J. B. Fenn "*Electrospray ion-source - another variation on the free-jet theme*", Journal of Physical Chemistry 88(20): 4451-4459 (1984)

14 Bruins, A. P., et al. "*Ion spray interface for combined liquid chromatography/atmospheric pressure ionization mass-spectrometry*", Analytical Chemistry 59(22): 2642-2646 (1987)

15 Wong, S. F., et al. "*Multiple charging in electrospray ionization of poly(ethylene glycols)*" Journal of Physical Chemistry 92(2): 546-550 (1988)

16 Smith, P. D. H. “*The electrodynamic atomization of liquids*”, IEEE Trans. Ind. App., IA-22, 527 (1986)

17 Loeb, L. B., et al."*Pulses in negative point-to-plane corona*", Physical Review 60(10): 714-722 (1941)

18 Kebarle, P. and U. H. Verkerk "*Electrospray: from ions in solution to ions in the gas phase, what we know now*" Mass Spectrometry Reviews 28(6): 898-917 (2009)

19 Wilm, M., et al. "*Femtomole sequencing of proteins from polyacrylamide gels by nano-electrospray mass spectrometry*", Nature 379 (6564): 466-469 (1996)

20 Blades, A. T., et al. "*Mechanism of electrospray mass-spectrometry - electrospray as an electrolysis cell*", Analytical Chemistry 63(19): 2109-2114 (1991)

21 Tang, L. and P. Kebarle "*Dependence of ion intensity in electrospray mass-spectrometry on the concentration of the analytes in the electrosprayed solution*" Analytical Chemistry 65 (24): 3654-3668 (1993)

22 Jackson, G. S. and C. G. Enke "*Electrical equivalence of electrospray ionization with conducting and nonconducting needles*", Analytical Chemistry 71(17): 3777-3784 (1999)

23 Fang, L. L., et al. "O*nline time-of-flight mass-spectrometric analysis of peptides separated by capillary electrophoresis*", Analytical Chemistry 66(21): 3696-3701 (1994)

24 Cai, J. Y. and J. Henion "*Capillary electrophoresis mass-spectrometry*", Journal of Chromatography A 703(1-2): 667-692 (1995)

25 Valaskovic, G. A., et al. "A*ttomole-sensitivity electrospray source for large-molecule mass-spectrometry*", Analytical Chemistry 67(20): 3802-3805 (1995)

26 Nilsson, S., et al. "*Gold-coated fused-silica sheathless electrospray emitters based on vapor-deposited titanium adhesion layers*", Rapid Communications in Mass Spectrometry 17(14): 1535-1540 (2003)

27 Kriger, M. S., et al. "D*urable gold-coated fused-silica capillaries for use in electrospray mass-spectrometry*", Analytical Chemistry 67(2): 385-389 (1995)

28 Valaskovic, G. A. and F. W. McLafferty "*Long-lived metallized tips for nanoliter electrospray mass spectrometry*", Journal of the American Society for Mass Spectrometry 7(12): 1270-1272 (1996)

29 Zhu, X. F., et al. "*A colloidal graphite-coated emitter for sheathless capillary electrophoresis/nanoelectrospray ionization mass spectrometry*", Analytical Chemistry 74(20): 5405-5409 (2002)

30 Whitt, J. T. "*Capillary electrophoresis to mass spectrometry interface using a porous junction*", Analytical Chemistry 75(9): 2188-2191 (2003)

31 Gamby, J., et al. "*Supercapacitive admittance tomoscopy*", Journal of the American Chemical Society 127(38): 13300-13304 (2005).

32 Qiao, L., et al. "*Electrostatic-Spray Ionization Mass Spectrometry*", Analytical Chemistry 84(17): 7422-7430 (2012)

33 Wang, H. L. and M. Hackett "*Ionization within a cylindrical capacitor: Electrospray without an externally applied high voltage*", Analytical Chemistry 70(2): 205-212 (1998).

34 Schilling, M., et al. "E*lectrospray-ionization driven by dielectric polarization*", Analytical and Bioanalytical Chemistry 391(2): 555-561 (2008)

35 Stark, A. K., et al. "*Characterization of dielectric barrier electrospray ionization for mass spectrometric detection*", Analytical and Bioanalytical Chemistry 397(5): 1767-1772 (2010)

36 Stark, A. K., et al. "*Electronic coupling and scaling effects during dielectric barrier electrospray ionization*", Analytical and Bioanalytical Chemistry 400(2): 561-569 (2011)

37 Tipler, P.A. and G. Mosca "*Physics - For Scientist and Engineers*", W. H. Freeman and Company: New York (2008)

38 Charles E. Mortimer "*Chemie: das basiswissen der chemie in schwerpunkten*", Georg Thieme Verlag Stuttgard, New York, 1983

39 Kubota, H., et al. "*Specific volume and viscosity of methanol-water mixtures under high-pressure*", Review of Physical Chemistry of Japan 49(2): 59-69 (1979)

40 Paul A. Tipler "*Physik*", Heidelberg, Berlin, Oxford: Spektrum Akad. Verl. (1994)

41 Jackson, G. S. and C. G. Enke "*Electrical equivalence of electrospray ionization with conducting and nonconducting needles*", Analytical Chemistry 71(17): 3777-3784 (1999)

42 Desai, Y.C. Tai, M.T. Davis, and T.D. Lee, "*A MEMS Electrospray Nozzle for Mass Spectroscopy*", Technical Digest, 1997 International Conference on Solid State Sensors and Actuators (TRANSDUCERS'97), Chicago, IL, Vol. 2, pp. 927-930, June 16-19 (1997)

43 Licklider L, Wang, XQ, Desai A, Tai, YC and Lee TD, "*A micromachined chip-based electrospray source for mass spectrometry"*, Analytical Chemistry. Jan 15;72(2):367-75 (2000)

44 Schultz, G. A., et al. "*A fully integrated monolithic microchip electrospray device for mass spectrometry*", Analytical Chemistry 72(17): 4058-4063 (2000)

45 Gobry, V., et al.. "*Microfabricated polymer injector for direct mass spectrometry coupling*", Proteomics 2(4): 405-412 (2002)

46 Muck, A., et al. "*Fabrication of poly(methyl methacrylate) microfluidic chips by atmospheric molding*", Analytical Chemistry 76(8): 2290-2297 (2004)

47 Kim, J. S. and D. R. Knapp "*Microfabricated PDMS multichannel emitter for electrospray ionization mass spectrometry*", Journal of the American Society for Mass Spectrometry 12(4): 463-469 (2001)

48 Huikko, K., et al. "*Poly(dimethylsiloxane) electrospray devices fabricated with diamond-like carbon-poly(dimethylsiloxane) coated SU-8 masters*", Lab on a Chip 3(2): 67-72 (2003)

49 Kameoka, J., et al. "*An electrospray ionization source for integration with microfluidics*", Analytical Chemistry 74(22): 5897-5901 (2002)

50 Chen, Y.-T., et al. "*Fabrication and investigation of PDMS micro-diffuser/nozzle*", Journal of Materials Processing Technology 198(1-3): 478-484 (2008)

51 Sun, X., et al. "*Membrane-Based Emitter for Coupling Microfluidics with Ultrasensitive Nanoelectrospray Ionization-Mass Spectrometry*", Analytical Chemistry 83 (14): 5797-5803 (2011)

52 Svedberg, M., et al. "*Poly(dimethylsiloxane) microchip: microchannel with integrated open electrospray tip*", Lab on a Chip 4 (4): 322-327 (2004)

53 Chan, J. H., et al. "*Microfabricated polymer devices for automated sample delivery of peptides for analysis by electrospray ionization tandem mass spectrometry*", Analytical Chemistry 71 (20): 4437-4444 (1999)

54 Gao, J., et al. "*Integrated microfluidic system enabling protein digestion, peptide separation, and protein identification*", Analytical Chemistry 73(11): 2648-2655 (2001)

55 Chiou, C. H., et al. "*Micro devices integrated with microchannels and electrospray nozzles using PDMS casting techniques*" Sensors and Actuators B-Chemical 86 (2-3): 280-286 (2002)

56 Ramsey, R. S. and J. M. Ramsey "*Generating electrospray from microchip devices using electroosmotic pumping*", Analytical Chemistry 69 (6): 1174-1178 (1997)

57 Xue, Q. F., et al. "*Integrated multichannel microchip electrospray ionization mass spectrometry: Analysis of peptides from on-chip tryptic digestion of melittin*." Rapid Communications in Mass Spectrometry 11 (12): 1253-1256 (1997)

58 Zhang, B., et al. "*Microfabricated devices for capillary electrophoresis-electrospray mass spectrometry,*" Analytical Chemistry 71 (15): 3258-3264 (1999)

59 Tang, K. Q., et al. "*Generation of multiple electrosprays using microfabricated emitter arrays for improved mass spectrometric*

sensitivity", Analytical Chemistry 73 (8): 1658-1663 (2001)

60 Byun, D., et al. "*Electrospray on superhydrophobic nozzles treated with argon and oxygen plasma*." Applied Physics Letters 92(9) (2008)

61 Cassie, A. B. D. and S. Baxter "*Wettability of porous surfaces*" Transactions of the Faraday Society 40: 0546-0550 (1944)

62 Hunter, M. J., et al. "*Properties of polyorganosiloxane surfaces on glass*." Industrial and Engineering Chemistry 39(11): 1389-1395 (1947)

63 Chi-Han Chioua, Gwo-Bin Leea, Hui-Ting Hsua, Pang-Wei Chenb and Pao-Chi Liao "*Microdevices integrated with microchannels and electrospray nozzles using PDMS casting techniques*", Sensors and Actuators B: Chemical, Vol. 86, Iss. 2-3, 280-286 (2002)

64 Noll, W. "*Chemistry and Technology of Silicone*", Academic Press, New York (1968)

65 Satyanarayana, S., et al. "*Stamp-and-stick room-temperature bonding technique for microdevices*" Journal of Microelectromechanical Systems 14(2): 392-399 (2005)

66 Janasek, D., et al. "*Isotachophoresis in free-flow using a miniaturized device*" Analytical Chemistry 78(11): 3815-381 (2006)

67 Rulison, A. J. and R. C. Flagan "S*cale-up of electrospray atomization using linear arrays of taylor cones*", Review of Scientific Instruments 64(3): 683-686 (1993)

68 Almekinders, J. C. and C. Jones "*Multiple jet electrohydrodynamic spraying and applications*", Journal of Aerosol Science 30(7): 969-971 (1999)

69 Tatemoto, Y., et al. "*An electrospray method using a multi-capillary nozzle emitter*" Chemical Engineering & Technology 30(9): 1274-1279 (2007)

Acknowledgments

The current work was performed from 2009 to 2013 at Leibniz-Institute for Analytical Sciences ISAS, Dortmund. I would like to thank, first and foremost my adviser, ISAS Miniaturization Group leader P.D. Dr. J. Franzke for his commitment, wisdom and “open door policy”. The current research would not be possible without cooperation with the Microstructure Technology Lab of Technical University of Dortmund under the guidance of Prof. Dr-Ing. A. Neyer. For the financial support I would like to thank the International Leibniz Graduate School “Systems Biology Lab-on-a-Chip”.

I want to express my gratitude to all my colleagues at the Miniaturization group of ISAS, who have supported me during the research. I owe sincere and earnest thankfulness to Dr. Michael Shilling, Dr. Peter Jacob and Dr. Dirk Janasek for the great ideas and fruitful discussions

I am grateful to my colleagues from MST group of TU Dortmund. Thank you, Evi, Christian, Uli, Stephan, Florian for your help, support and “German lessons” especially in the really beginning of my project. Among all I am especially grateful to Uli Marggraf for teaching me during the work in the technology labs.

I would like to thank all my friends in Dortmund for the great out of work time. Special thanks should be sent to my parents, my family and my friends in Saint-Petersburg. Thank you, that you always believe in me! Without your support this thesis would not be never possible.

This thesis I want to dedicate to my husband Sergey. This dissertation would be simply impossible without your support. Thank you for your help, patience and love.